의학박사 학위논문

Comprehensive Transcriptome Analysis of Traumatic Brain Injury−Related Neurodegenerative Diseases

외상성 뇌손상과 관련된
신경퇴행성질환들의
종합적인 전사체 분석 연구

2020 년 7 월

서울대학교 대학원
의과학과 의과학 전공
조　혜　선

외상성 뇌손상과 관련된

신경퇴행성질환들의

종합적인 전사체 분석 연구

지도교수 김 종 일

이 논문을 의학박사 학위논문으로 제출함

2020년 5월

서울대학교 대학원

의과학과 의과학 전공

조 혜 선

조혜선의 의학박사 학위논문을 인준함

2020년 7월

위 원 장   문 인 희   (인)
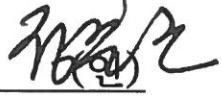
부위원장   김 종 일   (인)

위   원   서 정 선   (인)

위   원   정 준 호   (인)

위   원   류 훈   (인)

Comprehensive Transcriptome Analysis of Traumatic Brain Injury–Related Neurodegenerative Diseases

by

Hyesun Cho

A thesis submitted to the Department of Biomedical Science in partial fulfillment of the requirement of the Degree of Doctor of Philosophy in Biomedical Science at Seoul National University College of Medicine

July 2020

Approved by Thesis Committee:

Professor _Inhee Mook_ Chairman

Professor _JONG-IL KIM_ Vice chairman

Professor _SEO JEONG-SUN_

Professor _Junho Cheung_

Professor _HOON RYU_

ABSTRACT

Comprehensive Transcriptome Analysis of Traumatic Brain Injury-Related Neurodegenerative Diseases

Hyesun Cho

Major in Biomedical Science

Department of Biomedical Science

Seoul National University Graduate School

Chronic traumatic encephalopathy (CTE) is a progressive neurodegenerative disease caused by repetitive traumatic brain injury (TBI). CTE is mainly found in atheletes who have a history of repetitive blows to the head while playing contact sports such as boxing, American football and professional wrestling. The symptoms of CTE begin years or even decades following exposure to repetitive blows to the head and include changes in thinking, mood, and

behavior. The main symptoms of CTE are headaches, memory loss, aggression, depression and dementia. As with other neurodegenerative diseases, there is no specific treatment of CTE. The definitive diagnosis of CTE can only be dignosed from histology studies of brain tissue from those who are deceased. Moreover, the exact gene regulatory mechanisms of CTE are not fully elucidated until now. To better understand the molecular characteristics of CTE, we performed transcriptome sequencing analysis from the post-mortem human brain samples.

In the first part, we characterized common or unique transcriptome signatures of CTE, CTE/AD and AD. It is well known that CTE has common or unique neuropathological features with AD. The common neuropathological features of CTE and AD are deposition of hyperphosphorylated tau and presence of neurofibrillary tangles (NFTs). The distribution patterns of NFTs in CTE differs markedly from that in AD. Accordingly, the common or unique transcriptome signatures of CTE, CTE/AD and AD were illustrated by RNA sequencing analysis of post-mortem human brain samples. Interestingly, synaptic transmission- and memory function-related genes were commonly down-regulated in CTE, CTE/AD and AD. Especially, synaptotagmin family genes were markedly dysregulated in TBI-related disorders. Otherwise, cell adhesion molecules-related genes showed remarkable expression changes in CTE.

In the second part, we investigated the mechanism of how traumatic brain injury leads to tauopathy in TBI-related neurodegenerative diseases including CTE

and AD. Tauopathies are major pathological hallmarks of TBI-related neurodegenerative diseases including CTE and AD. In CTE, an irregular pattern of accumulation aberrantly phosphorylated tau presents in neurons and astroglia around small blood vessels at sulcal depths. In animal models, brain injury is sufficient to induce tau cleavage, acute and sustained aberrant tau phosphorylation and aggregation. In addition, tau-based PET indicates that the temporal neocortex of most individuals over the age of 65 contain pathogenic tau. However, the underlying molecular pathway which drives the tau mediated neurodegeneration is still enigmatic. We found down-regulation of protein phosphatases (PPs) such as PPP3CA, PPP3CB and PPP3R1 in CTE, CTE/AD and AD. We confirmed the elevation of p-tau is inversely correlated with PPs activity in CTE, CTE/AD and AD using *in vitro* cell lines and *in vivo* animal models.

The common transcriptome signature of CTE and AD was gene expression changes of synaptic transmission and memory loss. The unique transcriptome feature of CTE was upregulation of cell adhesion molecules (CAMs) -related genes. In addition, alteration of protein phosphatase expression contributes to tauopathy in CTE and AD. These studies provide a comprehensive transcriptional mechanism of TBI-related neurodegenerative diseases and lead to novel diagnostic and therapeutic approaches to the diseases.

CONTENTS

Part 2. Alteration of tauopathy-associated transcriptome signatures and molecular mechanisms in CTE and AD: Impaired protein phosphatase expression

LIST OF TABLES

Part 1

LIST OF FIGURES

Part 1

Part 2

LIST OF ABBREVIATIONS

GWAS : Genome-wide association sequencing

NGS : Next generation sequencing

WGS : Whole genome sequencing

RNA-seq : RNA sequencing

WES : Whole exome sequencing

MeS : Methylation sequencing

CDS : Coding domain sequence

SNPs : Single nucleotide polymorphisms

CTE : Chronic traumatic encephalopathy

NFTs : Neurofibrillary tangles

LBD : Lewy body disease

MND : Moter neuron disease

PD : Parkinson's disease

FTLD : Frontotemporal lobar degeneration

TBI : Traumatic brain injury

AD : Alzheimer's disease

CTE/AD : Chronic traumatic encephalopathy with Alzheimer's disease

APP : Amyloid precursor protein

RHI : Repetitive head injury

BUADC : Boston university Alzheimer's disease center

STAR : Spliced transcripts alignments to a reference

PCR : Polymerase chain reaction

BQSR : Base quality score recalibration

PCA : Principal component analysis

GATK : Genome analysis toolkit

DEGs : Differentially expressed genes

WGCNA : Weighted gene co-expression network analysis

MEs : Module eigengenes

GSEA : Gene Set Enrichment Analysis

MSigDB : Molecular Signatures Database

KEGG : Kyoto Encyclopedia of Genes and Genomes

FDR : False-positive rate

AT : Anterior temporal

PV : Posterior visual

SF : Superior frontal

SP : Superior parietal

shRNA : short hairpin RNA

AAV vector : Adeno-Associated Viral vector

qPCR : Quantitative real-time Polymerase Chain Reaction

MAPK pathway : Mitogen-activated protein kinase pathway

NINDS/NIBIB : National Institute of Neurological Disorders and Stroke/National Institute of Biomedical Engineering and Bioengineering

PPs : Protein phosphatases

CaMKII : Calcium/calmodulin-dependent protein kinase II

PKA : Protein kinase A

PKC : Protein kinase C

CAMs : Cell Adhesion Molecules

AMPA receptor : α-amino-3-hydroxy-5-methyl-4-isoxazolepropionic acid receptor

bp : base pair

Gb : Gigabase

FPKM : Fragment per kilobase of exon per million mapped reads

GO : Gene Ontology

α : alpha

δ : delta

APP : Amyloid precursor protein

TDP-43 : TAR DNA-binding protein 43

LTP : Long-term potentiation

General Introduction

Next generation sequencing: State-of-the-art method for genome study

Next generation sequencing (NGS) is known as massively parallel sequencing [3]. Sanger sequencing is a first generation sequencing and based on the use of chain-terminating dideoxy nucleotides by DNA polymerizing reaction [4, 5]. Sanger sequencing is relatively simple, so it takes less time to obtain results. However, it can only targeting smaller genomic regions of DNA [6].

The second generation sequencing is the most common sequencing technology. It is on the basis of generating millions of relatively short reads from a single amplified DNA fragments using a repeat cycle of nucleotide extensions [7]. Sanger sequencing depends on the individual analysis of DNA fragments (one fragment per capillary), but second generation sequencers can analyze millions of DNA templates in parallel. Amplified sequencing libraries is essential before sequencing of the amplified DNA clones. It generates large amounts of sequencing data at fast and relatively small costs

The third generation sequencing is a long-read sequencing that generates over 10,000 bp reads or map over 100,000 bp molecules. Third generation sequencing works by reading the nucleotide sequences at the single molecule level, in contrast to existing methods that require breaking long strands of DNA into small segments then inferring nucleotide sequences by amplification and

synthesis. Third generation sequencing data have much higher error rates than previous technologies, which can complicate downstream genome assembly and result data analysis.

The recently described fourth generation sequencing aims to perform longer reads and lower costs such as nanopore-based techology. Nanopore-based technology provide several advantages such as minimal sample preparation, elimination of the need for amplification or modification.

NGS has enabled researchers to collect large quantities of genomic sequencing data. This technology has a various applications such as whole genome sequencing (WGS), RNA sequencing (RNA-seq), whole exome sequencing (WES), and methylation sequencing (MeS). WGS provides a vast amount of data with high read coverage on disease-associated variants and reveals polymorphisms outside coding regions and genomic sequences [8]. RNA-seq is used to understand how altered expression of genetic variants affects an organism. It provides more accurate and sensitive measurement of gene expression levels than microarrays in the analysis of many samples [9]. WES provides coverage for more than 95% of human exons to investigate the protein-coding regions (CDS) of the genome and identify coding variants or single nucleotide polymorphisms (SNPs) [10]. MeS is used to determine the active methylation sites and the epigenetic markers that regulate gene expression, epi-structural base variations, imprinting, development, and the epigenetic state [11, 12]. NGS technology provides solutions to many different

problems in genetics and it impacts on many fields including medicine and biology.

Tauopathy: A hallmark of neuropathology

Tauopathy represents a group of human neurodegenerative diseases involving the deposition of abnormal tau protein. Tau is a microtubule-related protein that acts as a monomer and binds to the microtubule cytoskeleton in normal physiology [13]. In neurodegenerative disease, tau separated from the microtubules and accumulates in the cytoplasm, which leads to the formation of filament inclusions within the neuronal cell bodies [14]. Filamentous tau inclusions accumulates in the neuronal cells of the brain, causing neurotoxicity [15, 16].

Tau protein is one of the most common hallmarks associated with neurodegenerative diseases. Tauopathy is represented more than 20 different disorders such as corticobasal degeneration (CBD), Alzheimer's disease (AD), frontotemporal dementia (FTD) and Parkinson's disease (PD) etc. Interestingly, AD accounts for nearly 75% of the world's population suffering from dementia and represents the most widespread form of tau pathology [17]. Tauopathy mainly involves neuron dysfunction in the cortex and subcortical region of the brain, which it affects other anatomical areas including temporal and parietal lobes.

Tau phosphorylation is tightly regulated by the balance between protein kinases and protein phosphatases [18]. Tau kinases can be classified into three groups:

1) proline-directed serine/threonine-protein kinases such as mitogen-activated protein kinases (MAPKs), glycogen synthase kinase (GSK) 3α/β and cyclin-dependent kinase-5 (Cdk5); 2) non-proline-directed serine/threonine protein kinases including tau-tubulin kinase 1/2 (TTBK 1/2), microtubule affinity-regulating kinases (MARKs), casein kinase 1/2 (CK1/2), dual-specificity tyrosine phosphorylation regulated kinase 1A (DYRK1A), Akt/protein kinase B, cAMP-dependent protein kinase A (PKA), 5' adenosine monophosphate-activated protein kinase (AMPK), protein kinase C, calcium/calmodulin-dependent protein kinase II (CaMKII), and thousand and one amino acid protein kinases (TAOKs) 1 and 2; 3) protein kinases specific for tyrosine residues including Fyn, Src, Abl, and Syk [19]. Moreover, protein phosphatases 2A (PP2A) accounts for more than 70% of cellular phosphatase activity in the brain. PP2A activity is reduced by 50% in AD brain, which leads to increase tau phosphorylation [20]. PP5 (protein phosphatase 5) activity is also decreased by 20% in AD brain [21].

Chronic traumatic encephalopathy (CTE): Background and symptoms

Chronic traumatic encephalopathy (CTE) is a progressive neurodegenerative disease induced by repeated mild traumatic brain injury [22]. In 1928, it was first reported as "punch drunk" about chronic motor and psychiatric consequences that hit to the head in boxing [23]. It has long been known to appear only in boxers [24, 25]. However, CTE has recently been found in a people who have a history of repetitive brain injury as well as in athletes such as hockey, boxing, rugby, soccer, professional wrestling, and others.

The clinical symptoms of CTE are divided into 4 progressive stages. The first stage is most commonly found by headaches, loss of attentions and concentration. Some individuals experience short-term memory problems, depression, aggressive tendencies, explosivity and executive functional problems. In stage 2, the most common symptoms are depression, mood swings and short-term memory loss. A smaller percentage of patients experience executive dysfunction impulsivity, suicidal thoughts and language challenges. Stage 3 is characterized by memory loss, executive dysfunction, explosiveness, attention and concentration problems, depression, mood swings, visuospatial difficulties and aggression. The patients with final stage showed full-blown dementia. At this stage, there were many symptoms like paranoia, gait and visuospatial difficulties, and aggression.

The staging system for assessing the pathological severity of CTE was divided into four stages [26]. Neurofibrillary tangles (NFTs), aggregates of hyper-phosphorylated tau protein, around small vessels at the depths of cortical sulci are the most defining neuropathological biomarkers of CTE. In stage I, discrete foci of hyperphosphorylated tau are localized around cerebral bold vessels that are mostly found in the lateral and frontal cortices. In stage II, multiple foci of hyperphosphorylated tau are localized in the deep layer of the cerebral sulci and spread from epicenters to the superficial layers of cortex. In stage III, hyperphosphorylated tau is widespread to the frontal, temporal and parietal cortex. In stage IV, hyperphosphorylated tau pathology affects most area of the cerebral cortex and the medial temporal lobe.

CTE is related with other neurodegenerative disorders including AD, motor neuron disease (MND), Lewy body disease (LBD), or frontotemporal lobar degeneration (FTLD). Previous study reported that 37% of 142 CTE cases had CTE with other neuropathology [27]. 15 cases were diagnosed with AD. 15 cases had both CTE and MND. 10 CTE patients were diagnosed with LBD, 4 CTE cases were examined with FTLD and 7 CTE cases with two or more of these comorbidities.

Post-mortem assessments of CTE showed a different pattern from other proteinopathies including cavum septum pellucidum, substantia nigra and atrophy of the medial temporal lobes [28]. In particular, tau distribution pattern

and the presence of Aβ plaque are distinct from other tau pathology [29]. In AD, neurofibrillary tangles (NFTs) are more uniform and mainly in layer III and V of the cortex. Unlike AD, CTE has an irregular and patchy distribution and can be seen in the periventricular and superficial cortical layers. Also, AD has a lot of Aβ plaque deposition, while CTE has small amounts of Aβ plaque deposition [30, 31].

Alzheimer's disease and neuropathology

Alzheimer's disease (AD) is the most common neurodegenerative disorders in the world [32]. AD is pathologically defined by senile plaques containing Aβ deposition and neurofibrillary tangles (NFTs) in brain. Senile plaques contain a dense core of insoluble amyloid beta with neuritic structures and extracellular accumulations of amyloid deposition [33]. Generally, cells release soluble Aβ after amyloid precursor protein (APP) cleavage. In AD, abnormal division of APP causes precipitation of Aβ into dense beta sheets and formation of senile plaques. NFTs are intracellular aggregates of abnormally hyper-phosphorylated tau protein that serves as a microtubule stabilizing protein and plays a role in intracellular axonal and vesicular transport.

The symptoms of AD begin with short-term memory, which slowly progresses to profound memory functions. Initially, cognitive dysfunction occur such as difficulty recognizing familiar people and the inability to solve simple arithmetic problems [34]. The symptoms become more serious as the disease progresses. Patients are difficult to understand and learn new information. Patients aren't able to daily activities such as bathing and dressing up. In the later stages, hallucinations and psychosis can occur along with rigidity and bradykinesia. Patients become loss of mobility, speechless and complete loss of short- and long term memory. These symptoms usually develop over a period

of years. The progression of disease varies from person to person at different rates.

There are a few things that may make people more susceptible to Alzheimer's disease. Aging is the biggest risk factor for Alzheimer's disease. The risk of AD increases significantly after the age of 65, and the proportion of AD doubles every five years after the age of 65. The risk reaches nearly one-third after age 85. Women seem to be more likely to develop AD than men. According to the study, women are more likely to develop AD then men [35]. Many people with Down's syndrome are diagnosed with AD [36]. Signs and symptoms of AD tend to appear 10 to 20 years earlier in people with Down's syndrome than the general population. Traumatic brain injury (TBI) is an important risk factor for the development of Alzheimer's disease [37]. 30% of patients who die from TBI have Aβ plaques deposition, which are a characteristic of AD [38, 39] .

Objective of these studies

CTE is a progressive degenerative disease caused by repeated mild brain trauma. It is related with collision sport athletes, military personnel, domestic violence, and head banging behavior. A recent study examined the brains of 202 deceased people who had played football. They diagnosed CTE in 87% of the players. 110 out of 111 NFL players were found to have CTE [40]. CTE can only be definitively diagnosed in an autopsy after a person dies. There is no way to use MRI or other brain imaging methods to diagnose CTE. A specific pattern of tau protein in the brain can confirm the diagnosis [41].

In the first study, we describe a common or unique transcriptome signature of CTE by comparing AD. CTE and AD share various similarities including tau deposition and presence of neurofibrillary tangles. CTE and AD also have clinical and neuropathological distinctions delineating the two conditions. The signatures of AD are short-term memory deficiencies, whereas CTE patients diagnosed with autopsy are known to show depression, explosiveness, and substance abuse. Suicide is also often related with the cause of death for those suffering from CTE, while suicide is not common in those suffering from AD. CTE has a tau pathology that is distinguished from other neurodegenerative disorders including AD by a unique topographic and cellular pattern of tauopathy [42]. Moreover, CTE is generally large size of NFTs and more dot-

like neuritis than AD [43, 44]. Therefore, we tried to clarify genetic signatures of CTE, CTE/AD and AD through transcriptome analysis.

In the second study, we investigated the molecular pathogenesis towards the hyperphosphorylation of tau protein through transcriptome analysis of CTE and AD. The hyperphosphorylation of tau protein is a widely known phenomenon of neurodegenerative diseases and a key indicator of TBI-related neurodegenerative disorders. Microtubules act as a tracks along axonal projections of neurons. Tau phosphorylation leads to tau mutation or dysregulation of kinase/phosphatases. Phosphorylated tau causes destabilization of microtubules along with the aggregation of tau to paired helical filaments. Loss of tau contributes to neuronal dysfunction and eventually neuronal cell death. Thus, we performed transcriptome sequencing analysis of CTE, CTE/AD and AD.

It is expected that these studies will allow us to expand the molecular understanding of CTE, CTE/AD and AD and may lead to discover new diagnostic and therapeutic targets for neurodegenerative diseases.

Part 1

Characterization of transcriptome signatures in TBI-related neurodegenerative disorders (CTE, CTE/AD and AD)

Abstract

Chronic traumatic encephalopathy (CTE) is a neurodegenerative disorder found in athletes as well as in a people who have a history of repeated traumatic brain injury (TBI). CTE is known to share similar neuropathological features with AD, but little is known about the molecular properties in CTE. To better understand the molecular mechanisms of neuropathological changes in TBI-related disorders, we performed transcriptome sequencing analysis of CTE including AD and CTE with AD (CTE/AD) post-mortem human brain samples. We identified common or unique transcriptome signatures among CTE, CTE/AD and AD through the weighted gene co-expression network analysis (WGCNA) and principal component analysis (PCA). Interestingly, synapse signaling-associated genes (such as synaptotagmins) were commonly dysregulated in CTE, CTE/AD and AD. Quantitative real-time PCR (qPCR) and Western blot analyses confirmed that synaptotagmin 1 (SYT1) levels were significantly decreased in CTE and AD compared to normal brains. Moreover, calcium/calmodulin-dependent protein kinase II (CaMKII), protein kinase A (PKA), protein kinase C (PKC) and AMPA receptor genes that play a central role in memory function, were down regulated in head trauma-related disorders. Otherwise, the up-regulated genes of CTE were primarily involved in the cell adhesion molecules (CAMs) pathway. Our results suggest that dysregulation of synaptic transmission- and memory function-related genes are closely linked to

the pathology of head injury-related disorder and AD. Alteration of CAMs-related genes could be potential therapeutic markers for the CTE pathology.

* The first part was published in Scientific reports [1].

Student number: 2014-25074

Introduction

Chronic Traumatic Encephalopathy (CTE) is a progressive brain condition caused by a long-term consequence of repetitive closed head injuries [28, 45, 46]. It mostly happens in professional athletes who play contact sports like North American football, soccer, wrestling [47]. CTE results from cumulative damage and usually happens years later, and changes in cognitive, behavior, mood and motor occur.

Cognitive symptoms include learning and memory impairment as well as executive dysfunction and impaired attention. Behavioral changes are primarily seen as impulsivity, quick temper, verbal and physical violence, and rage [48]. Mood changes typically involve depression, hopelessness, anxiety, and apathy. Motor changes are parkinsonism, including ataxia, dysarthria, poor gait, tremor, and masked facies.

The clinical diagnosis of CTE can only be defined by post-mortem neuropathology with a complete autopsy, immunohistochemical analysis, and tau PET imaging. The pathognomonic lesion of CTE involves an irregular deposition of p-tau around small blood vessels at the base of the cortical sulci.

The stage of CTE was defined by the extent of tau pathology. In Stage I, CTE

has isolated perivascular foci of hyperphosphorylated tau and primarily seen in the superior, dorsolateral or lateral frontal cortices. In Stage II, the tau pathology extended to the superficial layers of adjacent cortex and involves multiple foci in the frontal and parietal lobe. In Stage III, hyperphosphorylated tau pathology is widespread to the temporal cortex. In Stage IV, most regions of the cerebral cortex were involved with serious hyperphosphorylated tau pathology [42].

CTE and AD have common characteristics in clinical and neuropathological aspects. Perivascular deposition of hyperphosphorylated tau and presence of NFTs are common neuropathological features of CTE and AD [49]. The tau isoform profile and phosphorylation state of CTE are similar to those of AD [50]. Widespread amyloid-β (Aβ) plaques are also known to be common features in CTE and AD.

Although there are some similarities between CTE and AD, significant differences exist. CTE symptoms generally appear earlier than the symptoms of AD. The symptoms of CTE present in one's 40s, while symptoms in most AD cases generally appear in one's 60s. The first and most important symptoms of AD are memory problems, while the first symptoms of CTE involve problems with judgement, reasoning, problem solving, impulse control, and aggression.

In addition, these diseases differ in postmortem neuropathological findings. Location of tangles and presence of Aβ plaque are the difference between CTE and AD. In CTE, tangles are predominantly in the superficial cortical layers and seen in Ammon's horn (CA1-CA4). In AD, tangles are seen in the deeper cortex and most commonly found within CA1 [23] Also, CTE lacks significant amounts of beta-amyloid plaque deposition unlike AD. AD has significant amounts of beta-amyloid plaque deposition. Moreover, In CTE, abnormal accumulation of hyperphosphorylated tau first appears in the neocortex and locus coeruleus (CTE Stage I), then involves the diencephalon (CTE Stage II). In CTE Stage III, abnormal accumulation of hyperphosphorylated tau appears in the medial temporal lobe, and finally widespread involvement of neocortical, brainstem, and cerebellar regions (CTE Stage IV). In contrast to CTE, tau pathology of AD occurs in the brainstem, next involves the entorhinal cortex, then more widespread involvement of the medial temporal lobe, and finally widespread involvement of the neocortex.

CTE is associated with other neurodegenerative diseases such as AD, motor neuron disease (MND), Parkinson's disease (PD), Lewy body disease (LBD), frontotemporal lobar degeneration (FTLD) and multiple system atrophy. Previous studies have shown that of the 142 cases with CTE, 37% had CTE with other neuropathology [27]. It is not known whether other pathological substrates contribute to clinical symptoms of CTE with other neuropathology.

Despite the neuropathological features of head trauma-related disorders were well documented, the definitive diagnosis of TBI-related diseases can't be diagnosed during lifetime and only depends on the medical history, mental status examination and brain imaging. In addition, the exact gene regulatory mechanisms and molecular pathways are not fully understood. In this study, we tried to identify the molecular properties and propose the biological markers of TBI-related diseases. Thus, we performed genome wide RNA sequencing analysis of post-mortem human brain tissues including CTE, CTE/AD and AD.

Materials and methods

Human tissues

We collected 34 postmortem human brain temporal cortex samples (10 normal, 8 CTE, 6 CTE/AD, 10 AD) from the Boston University Alzheimer's Disease Center (BUADC) and Boston University's CTE Center. Next of kin provided informed consent for participation and brain donation. Institutional review board approval for ethical permission was obtained through the BUADC and CTE center. This study was reviewed by the Institutional Review Board of the Boston University School of Medicine (Protocal H-28974) and was approved for exemption because it only included tissues collected from post-mortem subjects not classified as human subjects. This study was performed in accordance with institutional regulatory guidelines and principles of human subject protection in the Declaration of Helsinki. The clinical data were described in Table 1-1 including age, sex, exposure Hx, stage, age of symptom onset, tauopathy, TAR DNA-binding protein 43 (TDP-43) and regional pathology.

CTE is pathologically defined by frontal and temporal lobe atrophy. Especially, the temporal lobe, including the hippocampus and the surrounding hippocampus regions, is critical for memory function. The temporal lobe is also involved in the primary organization of sensory input. The most common symptoms of neurodegenerative disorders are memory probl

ems and sensory processing disorder. Moreover, hyperphosphorylated tau p

athology is found in most regions of the cerebral cortex and the temporal

lobe in CTE. Thus, temporal lobe dysfunction is highly associated with ne

urodegenerative processes and the neuropathology in CTE. In this context,

we selected the temporal lobe of post-mortem brain for the transcriptome

analysis.

Transcriptome sequencing and analysis

Total RNA was extracted using the Illumina TruSeq RNA sample preparation

kit and sequenced on the Illumina HiSeq 2000 platform (Illumina, San Diego,

CA, USA). The sequenced reads were aligned to the human genome

(GRCh37.p13) according to the STAR 2-pass method. STAR is an accurate

alignment of high-throughput RNA-seq data. STAR is a two-step process that

generates genome indexes files and maps the reads to the genome [51]. We

marked duplicated reads using Picard's Markduplicate and filtered reads were

further processed for variant calling using the GATK, including

insertion/deletion realignment, base quality score recalibration and

haplotypecaller. According to Ensembl gene set, we used HTSeq to count the

reads aligned to each gene [52].

Cell-type specific genes analysis

Cell-type specific genes (neurons, astrocytes, oligodendrocytes, endothelial

and microglia) were computed by making use of a large scale human brain

single-cell RNA-seq dataset [53]. Cell-type specific genes were filtered by several criteria [54]. Genes with less than 50 reads across all samples were discarded. The remaining gene count data were analyzed by a Bayesian negative binomial regression model. Using numerical samples obtained by Markov chain Monte Carlo (MCMC), posterior probability was calculated and gene expression was enriched in one cell type compared to basal expression given by the regression. It was considered cell-type specific if the gene met two criteria: 1) abundant with 99.9% posterior probability in one cell and not in another, and 2) its expression in the enriched cells on average was fivefold greater than basal expression in numerical samples. We used filtered cell-type specific genes (1,032 neurons, 191 astrocytes, 111 oligodendrocytes, 76 endothelial, 118 microglia) and applied to gene expression data.

Differential gene expression analysis

For the gene expression profiling, we normalized read counts by using regularized log transformation method of DESeq2 [55]. The calculated p-values were adjusted to q-values for multiple testing using the Benjamini-Hochberg correction. Genes with a |Log2foldchange| ≥ 0.6 and p-value < 0.05 were classified as significantly differentially regulated. The normalized gene expression values were applied to PCA using the most variable 500 genes. The median subtracted regularized log (rlog) values were also used for hierarchical clustering analysis. Heatmaps were constructed using the dnet R package. FPKM (fragments per kilo base of exon per million mapped reads)

for each gene was calculated with edgeR and used for analyses. To identify the significantly regulated pathways, we applied DEGs to the Molecular Signatures Database (MSigDB) of Gene Set Enrichment Analysis (GSEA) [56]. Kyoto Encyclopedia of Genes and Genomes (KEGG) gene set of MSigDB was selected to be analyzed.

Weighted Gene Co-expression Network Analysis (WGCNA)

We constructed unsigned co-expression networks of WGCNA package in R package by using the normalized read counts [57]. 10,467 genes were used to construct each network. The step-by-step network construction and module detection method were used. Networks were constructed by obtaining a dissimilarity matrix based on the topological overlap. The adjacency matrix was calculated by raising the correlation matrix to a soft thresholding power of 14, chosen so as to attain scale-free topology. Gene dendrogram was generated and module colors were assigned. We calculated the module eigengene (ME) value, which was defined as the first principal component of a given module. Dendrogram cut height for module merging was 0.8. Merged module eigengenes were used to test the association of modules with diseases. Module membership (MM) was calculated as the correlation between gene expression levels and the module eigengene. Gene significance (GS) was also calculated as the correlation between gene and external traits. We defined hub genes using MM and GS values. If the module was positively correlated with the trait, we selected hub genes with positive GS and high positive MM (MM>0.5). If the

module was negatively correlated with the trait, we defined hub genes with negative GS and high positive MM (MM>0.5). To facilitate biological interpretation, we applied DEGs of hub genes to the Molecular Signatures Database (MSigDB) of Gene Set Enrichment Analysis (GSEA) [55]. Gene Ontology (GO) gene set of MSigDB was selected to be analyzed. For network analysis, we used the WGCNA algorithm to calculate gene-gene interaction level. Based on gene-gene interaction level, the top 10 hub genes were visualized with VisANT (weight cut off >0.22).

Western blot analysis

Western blot analysis was performed as previously described [2, 58]. For the detection of SYT1 proteins, the blots were probed with anti-synaptotagmin 1 (1:100 dilution; Abcam, ab131551) and anti-β-actin (1:10 000; Sigma Aldrich, St Louis, MO, USA) antibodies, followed by treatment with the appropriate secondary antibodies conjugated to horseradish peroxidase (Pierce, 170-6515 and 170-6516). Immunoreactivity was detected using an enhanced chemiluminescence (ECL) kit (Thermo Scientific).

 Quantitative real-time PCR

Total RNA was extracted from the frozen brain tissues using TRIzol reagent (MRC, TR118) as previously described [2, 58]. Fifty nanograms of RNA was used as a template for quantitative RT-PCR amplification, using SYBR Green Real-time PCR Master Mix (Toyobo, QPK-201, Osaka, Japan). Primers were

standardized in the linear range of the cycle before the onset of the plateau. GAPDH was used as an internal control. Real-time data acquisition was performed using an LightCyler96 Real-Time PCR System (Roche Diagnostics, Indianapolis, IN, USA) under the following cycling conditions: 95 °C for 1 min× 1 cycle, and 95 °C for 15 s, followed by 60 °C for 1 min × 45 cycles. The relative gene expression was analyzed using the LightCyler96 software and expressed as Ct the number of cycles needed to generate a fluorescent signal above a predefined threshold.

Immunohistochemistry analysis

To detect SYT1 in human postmortem brain tissues, we performed immunohistochemistry as described previously [59]. Coronal plane of paraffin-embedded tissue sections (10 μm) were incubated with blocking solution after 3% H_2O_2 reaction for 1hr. The tissue sections were incubated with anti-synaptotagmin 1 antibody (1:100 dilution; Abcam, ab131551) for 24 h. After secondary antibody reaction, the tissue slides were further processed with Vector ABC Kit (Vector Lab PK-6100). DAB chromogen (Sigma D5637) was used to develop the immunoreactive signals. The nuclei were counterstained with hematoxylin. The tissue slides were examined under a bright field microscope and the intensity of immunoreactivity was analyzed using Multi-Gauge Software (Fuji photo film Co, Ltd. Japan).

Results

Transcriptome analysis of CTE, CTE/AD and AD

We collected 34 samples from the anterior temporal lobe of the human brain (Figure 1-1). The samples consist of 8 individuals with CTE, 10 individuals with AD, 6 individuals with CTE/AD, and 10 individuals as normal. For each samples, we recorded diagnosis, gender, stage, age of symptom onset (Table 1-1). Among the 24 disease samples, most of samples were verified stage Ⅲ or Ⅳ.

Paired-end RNA-Seq was performed using the Illumina Hiseq 2000 platform, and sequencing reads were aligned to the human reference (GRCh37.p13). From RNA sequencing, we obtained 9.24Gb of RNA sequencing throughput on average and 84.17% of reads aligned to reference genome (Table 1-2). To compute distances between samples, we conducted principal component analysis (PCA). The expression pattern of CTE, CTE/AD and AD was distinct from normal, with 26% of the sample variance (Figure 1-2). Consistent with the PCA, unsupervised hierarchical clustering analysis of 10,467 genes showed that a significant similarity of gene expression between CTE, CTE/AD and AD (Figure 1-3).

The expression patterns of cell-type specific genes were similar to PCA and hierarchical clustering analysis. 543 neurons-specific genes were commonly down-regulated in CTE, CTE/AD and AD (Figure 1-4). Up-regulation of 120 astrocytes-, 61 oligodendrocytes-, 59 microglia- and 48 endothelial- specific genes was shown in CTE, CTE/AD and AD (Figure 1-5~1-8). We performed WGCNA analysis of cell-type specific genes (neurons, astrocytes, microglia) enriched in CTE, CTE/AD and AD.

Differentially expressed genes (DEGs) were determined based on p-value < 0.05 and |Log2foldchange| > 0.6. We found 4,083 up-regulated and 3,400 down-regulated DEGs in CTE. 3,445 DEGs were up-regulated and 3,883 DEGs were down-regulated in CTE/AD. The number of up-regulated DEGs is 3,706 and down-regulated DEGs are 3,069 in AD. The FPKM levels were calculated to compare the expression levels of each sample.

Weighted gene co-expression network analysis of CTE, CTE/AD and AD

 To explore the neuropathological features of TBI-related human brain disorders, we performed weighed correlation network analysis (WGCNA). 10,467 genes between CTE, CTE/AD and AD were used to construct gene co-expression networks. Based on topological overlap of genes, modules of co-expressed genes were identified by step-by-step network construction. The modules labeled by colors are depicted in the hierarchical clustering

dendrogram (Figure 1-9). We identified 4 modules, with a range in size from 1,716 genes in the blue module to 3,596 genes in the grey module. The grey module was excluded in the analysis because it was a collection of genes that could not be aggregated to other modules. We condensed the gene expression pattern within a module to a module eigengenes (MEs), which is the first principal component of a module and is representative for the gene expression profiles of a module. To test if MEs are associated with diseases, we correlated the modules with 3 clinical traits including CTE, CTE/AD and AD (Figure 1-10). Based on the PCA and hierarchical clustering analysis, we found a similar expression pattern between CTE, CTE/AD, and AD. As a result, we added a trait named CTE_CTE/AD_AD which is a trait including CTE, CTE/AD and AD.

We obtained the relationships between the module eigengenes and the 4 traits. The results revealed that the brown module was positively correlated with the CTE_CTE/AD_AD trait. The turquoise module had the strongest negative correlation with CTE_CTE/AD_AD (R= -0.8, $p<2\times10^{-8}$). We plotted a scatter plot of gene significance for CTE_CTE/AD_AD and module membership of genes in the turquoise module (Figure 1-11). We identified a number of genes of high significance for CTE_CTE/AD_AD as well as high module membership in the module. Through topological overlap matrix, we also discovered that the turquoise module was the most highly interconnected module (Figure 1-12).

Gene set enrichment analysis in CTE, CTE/AD, and AD

For modules with a strong negative correlation with the trait, the hub genes in the module should have negative GS and high positive MM. We defined the 1,603 hub genes of the turquoise module as GS < 0 and MM > 0.5 because turquoise module was negatively correlated with CTE_CTE/AD_AD trait. In case of the brown module, we identified 896 hub genes with positive GS and high positive MM (MM > 0.5) because brown module was positively correlated with CTE_CTE/AD_AD trait.

To identify the biological function associated with the modules, we performed GO enrichment analysis using up- and down-regulated genes in each module. In the turquoise module, 622 hub genes were commonly dysregulated in CTE, CTE/AD, and AD. Neuron part, synapse, and synapse part pathways were remarkably enriched in 622 down-regulated genes (Figure 1-13). Moreover, the number of genes belonging to the neuron pathway was the greatest in the turquoise module. In the brown module, 17 hub genes were commonly up-regulated in CTE, CTE/AD, and AD, and were not enriched in any pathways.

Synaptic transmission-related genes were down-regulated in CTE, CTE/AD and AD

To visualize gene-gene interactions, we obtained gene-gene connection scores from WGCNA. We selected 622 commonly down-regulated genes in CTE, CTE/AD, and AD. We filtered gene-gene connection scores as weight cutoff value > 0.22. We selected the top 10 hub genes that were highly connected to

other genes in the turquoise module, including *GABRA1, PTPN5, RAB3A, KIAA1549L, SLC12A5, PLK2, SYT7, AP3B2, STXBP1,* and *PCSK2*. We represented 266 genes that were connected with the top 10 hub genes (Figure 1-14). Among the 266 genes, 67 genes belonged to neuron part, synapse, and synapse part pathways and were shown in red. In particular, *SYT7* was involved in the top 10 hub genes and were significantly down-regulated in CTE, CTE/AD, and AD. Other synaptotagmin family genes (*SYT1, SYT4,* and *SYT5*) were also involved in neuron, synapse, and synapse part pathways. Synaptotagmin family genes (*SYT1, SYT4, SYT5, SYT7,* and *SYT13*) were remarkably down-regulated in CTE, CTE/AD, and AD (Figure 1-15).

In order to verify whether SYT1 immunoreactivity is altered in CTE and AD brains, we performed immunohistochemistry. SYT1 immunoreactivity was intensely found within the cytosolic compartment of neurons in normal subjects. However, the SYT1 immunoreactivity was markedly reduced in the neuronal cell body and dendrites of CTE and AD patients (Figure 1-16). Densitometry analysis exhibited that SYT1 immunoreactivity is significantly decreased in the neuronal cell body of CTE and AD patients compared to normal subjects (Figure 1-17). To validate our transcriptomic results, we performed quantitative real-time PCR (qPCR) analysis from the postmortem brain tissue of CTE, AD and normal subjects (Figure 1-18). In concordance with the transcriptome data, we found that *SYT1* mRNA level was significantly decreased in both CTE and AD patients compared to normal subjects (Figure 1-19). Moreover, Western blot and densitometry analyses showed that the protein level of SYT1 was

decreased in both CTE and AD patients compared to normal subjects (Figure 1-20).

Memory function-related genes were down-regulated in CTE, CTE/AD and AD

From the above mentioned genes, SYT1 and SYT7 were reported to play a critical role in memory function. Thus, we also looked at the expression of other genes related to memory function. The genes that play an important role in long term potentiation (LTP) process were prominently dysregulated in CTE, CTE/AD and AD; AMPA receptors, CaMKII, PKA, and PKC (Figure 1-21).

AMPA receptors contain four subunits, designated as GluA1 (GRIA1), GluA2 (GRIA2), GluA3 (GRIA3) and GluA4 (GRIA4). Among them, GRIA2, GRIA3 and GRIA4 were strikingly down-regulated in all three disease groups (Figure 1-22). CaMKII subfamily genes (CAMK2A, CAMK2D) were remarkably dysregulated in CTE, CTE/AD and AD (Figure 1-23). PKA catalytic subunits (PRKACA, PRKACB) were also down-regulated in CTE, CTE/AD and AD (Figure 1-24). PRKCG, one of the major forms of PKC, was commonly down-regulated in all three disease groups (Figure 1-25).

Cell adhesion molecules (CAMs) – related genes were up-regulated only in CTE

32

Based on differentially expressed genes (DEGs) derived from each of the diseases, we identified the number of common and distinct DEGs in CTE, CTE/AD, and AD (Figure 1-26 and Figure 1-27). Among them, we focused on 964 up-regulated and 455 down-regulated genes in CTE for investigating unique transcriptome signatures. In KEGG enrichment analysis of CTE, cell adhesion molecules (CAMs) pathway was shown to be highly enriched in up-regulated genes in CTE (Figure 1-28). Down-regulated genes were not enriched in any pathways. In CAMs pathway, MHC class I- related genes like *HLA-B, HLA-C,* and *HLA-E* were notably up-regulated in CTE (Figure 1-29).

Table 1-1. Clinical information on cases included in this study

Samples	Age/Sex	Exposure Hx	Stage	Age of Symptom Onset
CTE1	84/M	NFL	CTE (Stage 4)	59
CTE2	73/M	?	CTE (Stage 4)	?
CTE3	80/M	?	CTE (Stage 4)	?
CTE4	76/M	NFL	CTE (Stage 4)	25
CTE5	93/M	NFL	CTE (Stage 4)	76
CTE6	82/M	NFL	CTE (Stage 4 – Thal 4, Braak III, severe CAA)	67
CTE7	66/M	NFL, NCAA	CTE (Stage 4)	56
CTE8	69/M	NFL, NCAA	CTE (Stage 3 – No Aβ)	35

Table 1-1. continued

Samples	Age/Sex	Exposure Hx	Stage	Age of Symptom Onset
CTE/AD1	69/M	HS/College Football	CTE (Stage 4) and AD (Braak stage VI)	62
CTE/AD2	91/M	College Football	CTE (No stage given) and AD (Braak stage V)	83
CTE/AD3	63/M	College Football	CTE (suggestive) and AD (AD: Atypical: NIA Reagan High Likelihood, CERAD Frequent, Braak VI/VI)	NA
CTE/AD4	61/M	NCAA Football	CTE and AD (No stage given)	53
CTE/AD5	64/M	NFL	CTE and AD (No stage given)	59
CTE/AD6	69/M	NFL	CTE (Stage 4 with glial predominant tangles) and AD (No stage given)	52

Table 1-1. continued

Samples	Age/Sex	Exposure Hx	Stage	Age of Symptom Onset
AD1	80/F	Head injury during HS r/t sport or bicycle injury requiring hospitalization	AD : NIA Reagan High Likelihood, CERAD Frequent, Braak V/VI	Unknown
AD2	57/F	None	AD: NP Change: High (A3,B3,C3), Braak Vl/VI	Unknown
AD3	77/M	Not reported	AD : NP Change: Intermediate (A2, B3, C3), Braak Vl/Vl	Unknown
AD4	87/F	Not reported	AD : NP Change: Intermediate (A2, B3, C3), Braak Vl/Vl	Unknown
AD5	90/M	Not reported	AD : NIA Reagan: High Likelihood, CERAD Frequent, Braak Vl/VI	Unknown
AD6	95/F	None	AD : NP Change: Intermediate (A1, B3, C2), Braak V/Vl	Unknown
AD7	77/M	Concussion with LOC during HS	AD : NP Change: Intermediate (A2, B3, C3), Braak Vl/Vl	Unknown
AD8	89/F	Head injury without LOC due to fall at age 11	AD : NP Change: Intermediate (A2, B3, C3), Braak V/Vl	Unknown
AD9	80/F	None	AD : NP Change: High (A3,B3,C3), Braak Vl/VI	Unknown
AD10	96/M	Not reported	AD : NP Change: Intermediate (A1, B3, C3), Braak V/Vl	Unknown

Table 1-1. continued

Samples	Age/Sex	Exposure Hx
NORMAL1	82/M	Not reported
NORMAL2	74/M	Not reported
NORMAL3	87/F	Not reported
NORMAL4	63/M	Not reported
NORMAL5	83/M	Hx of horseback riding and repair of deviated septum
NORMAL6	83/F	Not reported
NORMAL7	89/M	Not reported
NORMAL8	73/F	Not reported
NORMAL9	81/F	Not reported
NORMAL10	69/M	Not reported

Table 1-2. Sequencing throughput summary

| Sample	Number of Input reads	Uniquely mapped reads number	Uniquely mapped reads %	Average mapped length
CTE1	41487409	30269963	72.96%	199.33
CTE2	38146269	29515356	77.37%	199.26
CTE3	44124873	35757623	81.04%	180.32
CTE4	47111652	34880165	74.04%	188.84
CTE5	40703506	26917471	66.13%	189.15
CTE6	49954950	46723660	93.53%	200.56
CTE7	52824172	46809244	88.61%	200.45
CTE8	55370370	49871328	90.07%	200.4
CTE/AD1	46752382	40877664	87.43%	200.04
CTE/AD2	46232640	41691307	90.18%	199.86
CTE/AD3	50473054	43078724	85.35%	200.01
CTE/AD4	61886381	55406750	89.53%	200.21
CTE/AD5	54655605	50575164	92.53%	200.47
CTE/AD6	61671568	55332941	89.72%	200.24
AD1	36882585	27492695	74.54%	198.37
AD2	41996015	33524994	79.83%	198.66
AD3	25942812	19992772	77.06%	198.37
AD4	23324742	12318777	52.81%	198.9
AD5	45096435	41782826	92.65%	200.24
AD6	60643775	55742151	91.92%	200.4
AD7	58715584	54329009	92.53%	200.34
AD8	67911469	61842078	91.06%	200.56
AD9	45347879	41343905	91.17%	200.26
AD10	48903014	44975602	91.97%	200.36
NORMAL1	42768325	31618770	73.93%	189.36
NORMAL2	49725360	40355942	81.16%	188.51
NORMAL3	30726584	27138658	88.32%	198.35
NORMAL4	21645208	18577292	85.83%	198.1
NORMAL5	43280418	36430378	84.17%	199.64
NORMAL6	53452381	44815585	83.84%	199.72
NORMAL7	44233097	37439524	84.64%	199.8
NORMAL8	33868806	28017442	82.72%	199.7
NORMAL9	44203951	41009945	92.77%	200.18
NORMAL10	45956924	41511034	90.33%	199.75
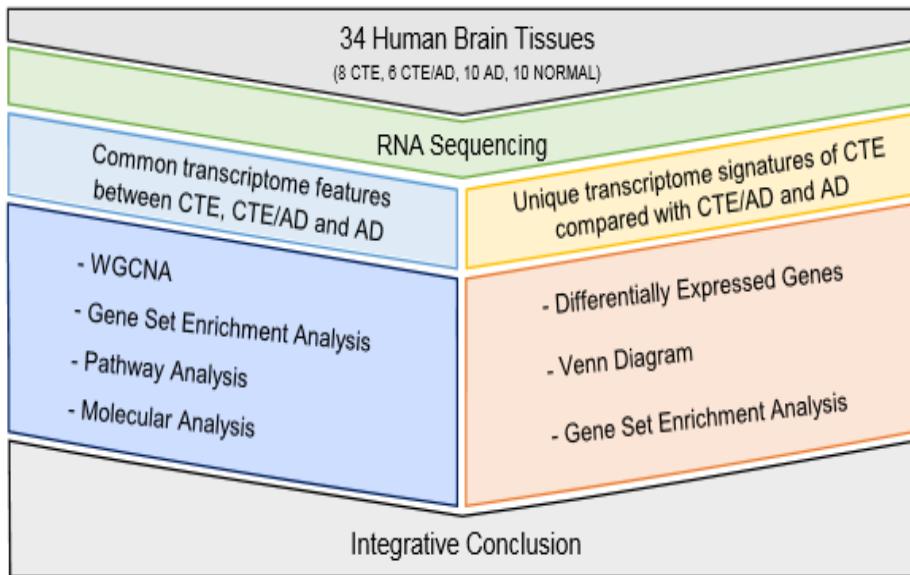
Figure 1-1. Workflow of transcriptome analysis
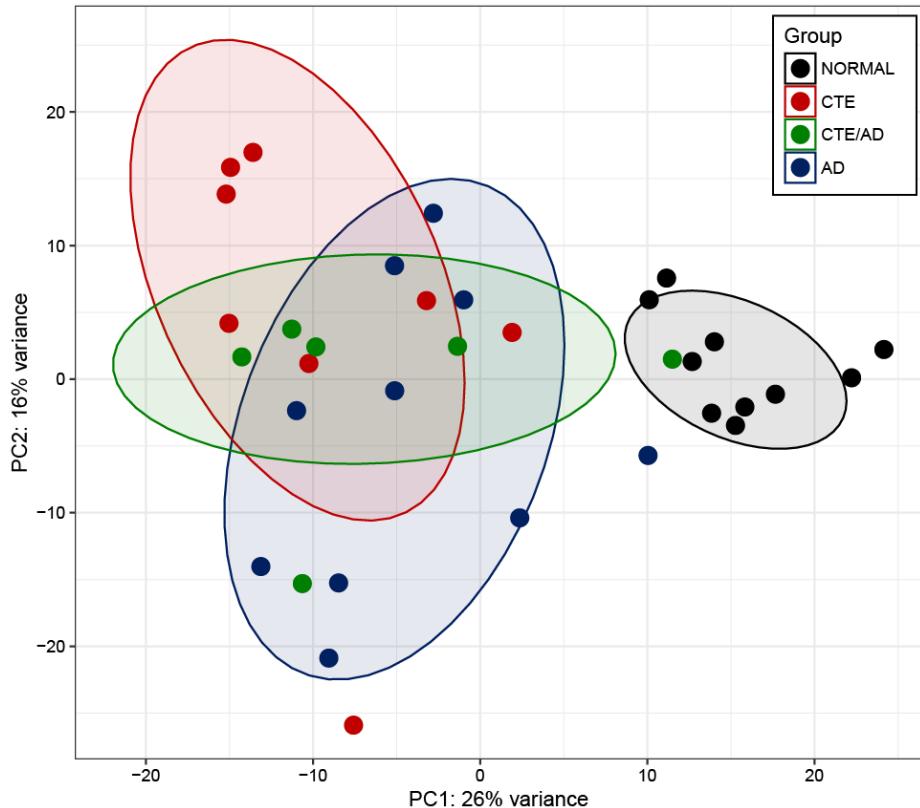
Figure 1-2. Principal component analysis of gene expression profiles of all samples

CTE samples shown in red colors, and CTE/AD samples shown in green colors and AD samples shown in blue colors, and normal samples were in grey colors. Diseases (CTE, CTE/AD, and AD) and normal samples were separated well in PC1 and PC2 axes.
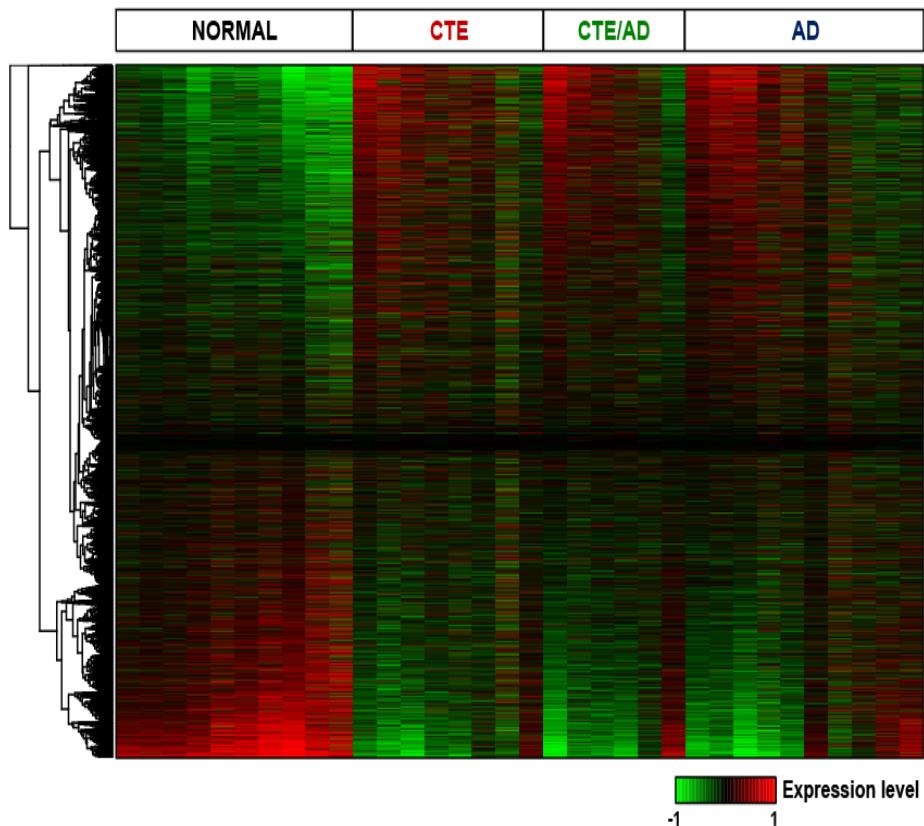
Figure 1-3. Hierarchical clustering analysis of all samples

CTE, CTE/AD and AD showed a similar expression pattern in heatmap.
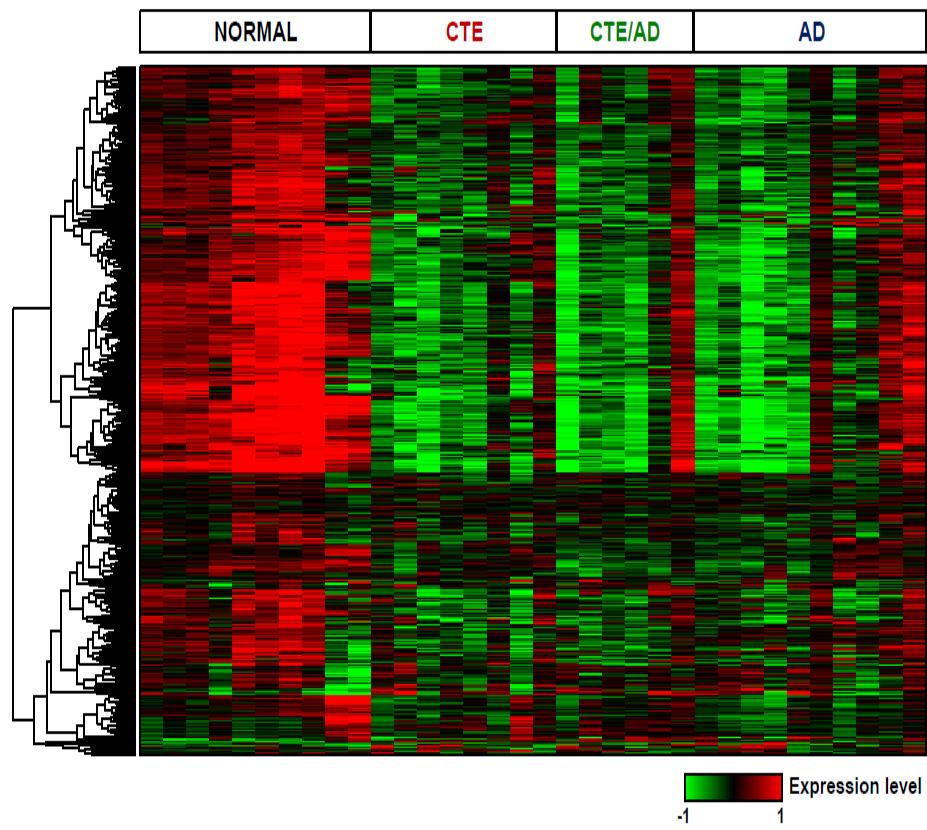
Figure 1-4. The expression patterns of neurons-specific genes

543 neurons-specific genes were mostly down-regulated in CTE, CTE/AD and AD.
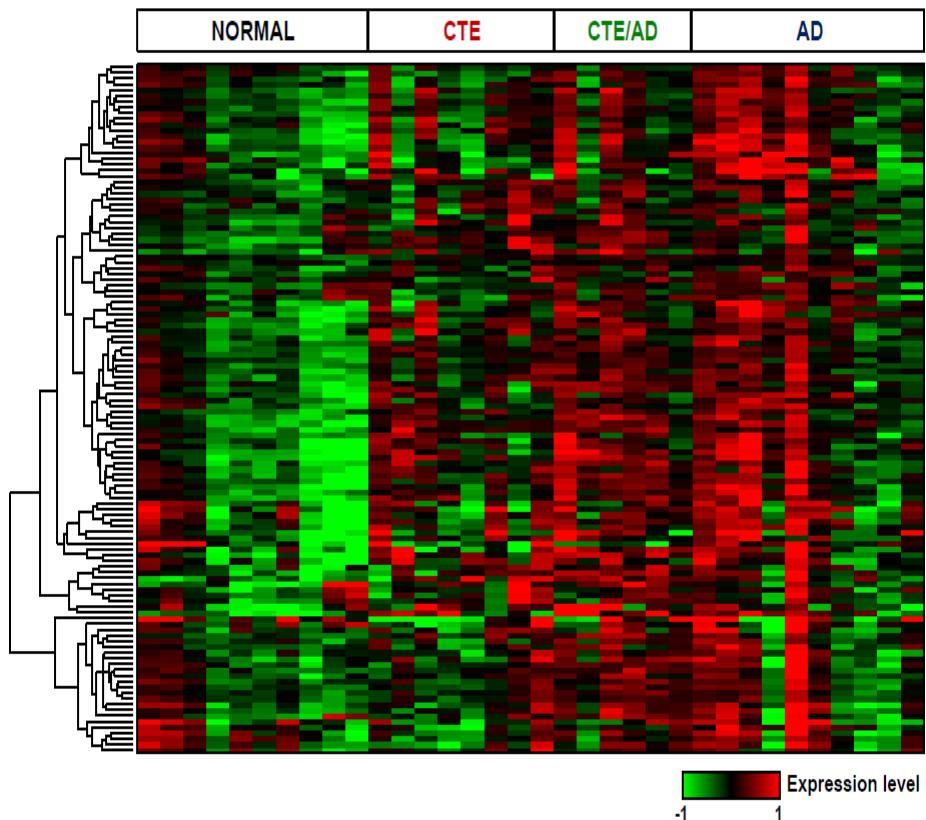
Figure 1-5. The expression patterns of astrocytes-specific genes

120 astrocyte-specific genes were up-regulated in CTE, CTE/AD and AD.
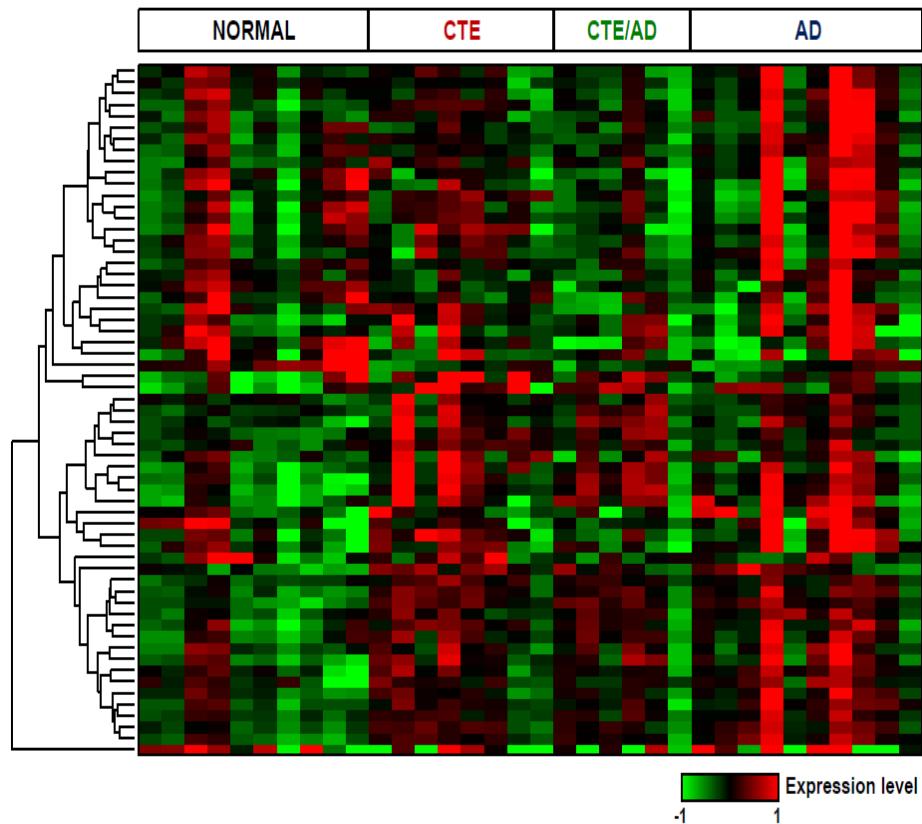
Figure 1-6. The expression patterns of oligodendrocytes-specific genes

61 oligodendrocyte-specific genes were shown to be higher expression in CTE, CTE/AD and AD.
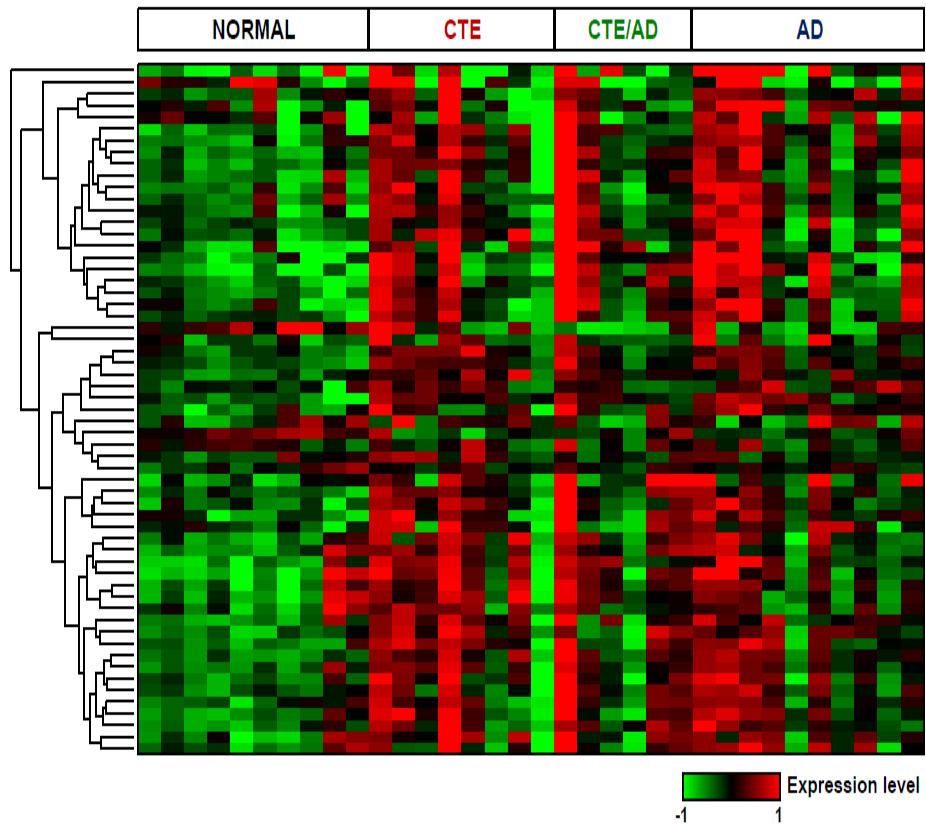
Figure 1-7. The expression patterns of microglia-specific genes

59 microglia-specific genes showed higher expression in CTE, CTE/AD and AD.
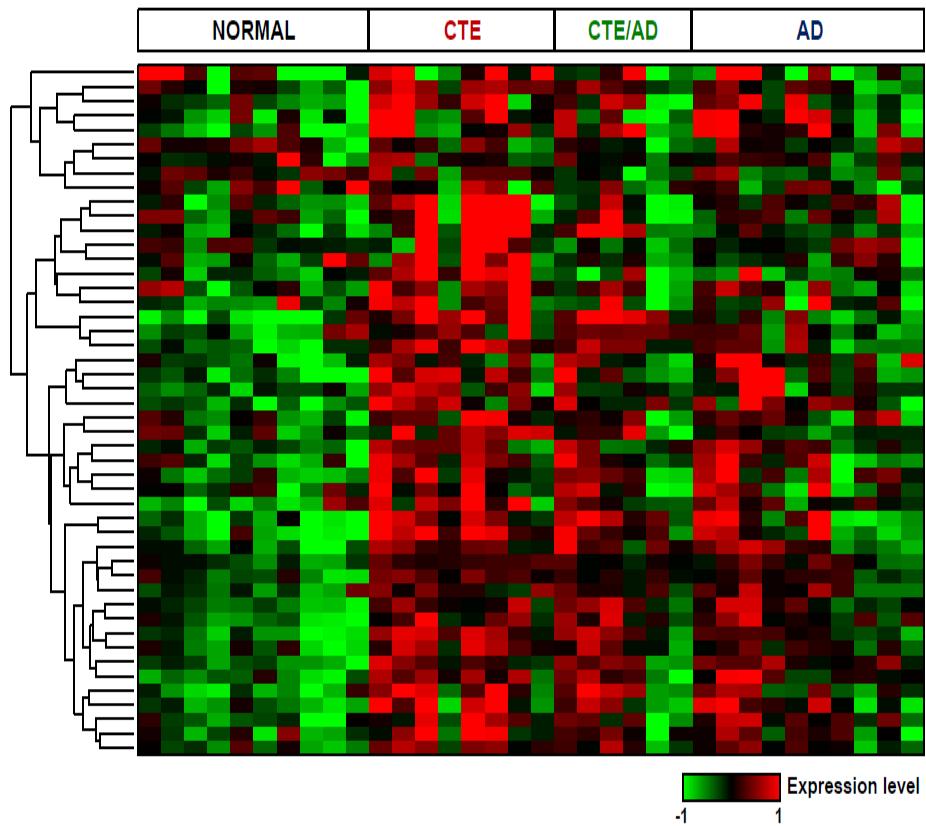
Figure 1-8. The expression patterns of endothelial-specific genes

58 endothelial-specific genes were highly enriched in CTE, CTE/AD and AD.
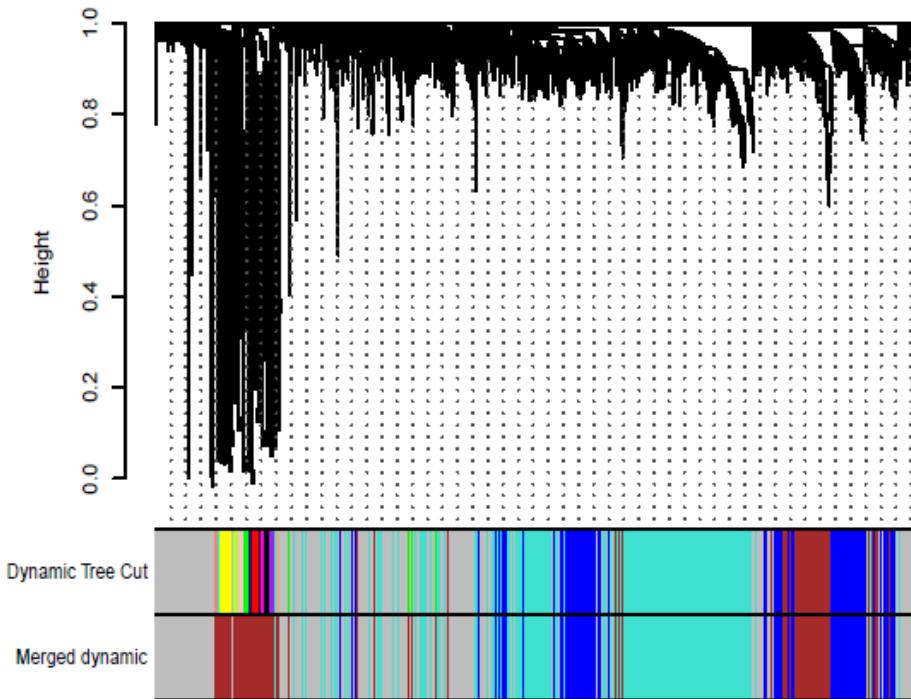
Figure 1-9. Gene cluster dendrogram

Gene dendrogram obtained by clustering the dissimilarity based on topological overlap with the corresponding module colors indicated by the color row. Dynamic tree cut indicates an original color-coded module and merged dynamic represents merged module colors, which each contain a group of highly connected genes. A total of 4 modules were identified (blue, brown, turquoise and grey).

	Brown	Blue	Turquoise	Grey
CTE_CTE/AD_AD	0.37 (0.03)	0.34 (0.05)	-0.81 (7e-09)	0.16 (0.4)
CTE	0.44 (0.01)	-0.013 (0.9)	-0.35 (0.04)	-0.046 (0.8)
CTE/AD	0.17 (0.3)	0.029 (0.9)	-0.28 (0.1)	0.33 (0.06)
AD	-0.18 (0.3)	0.33 (0.06)	-0.25 (0.2)	-0.072 (0.7)
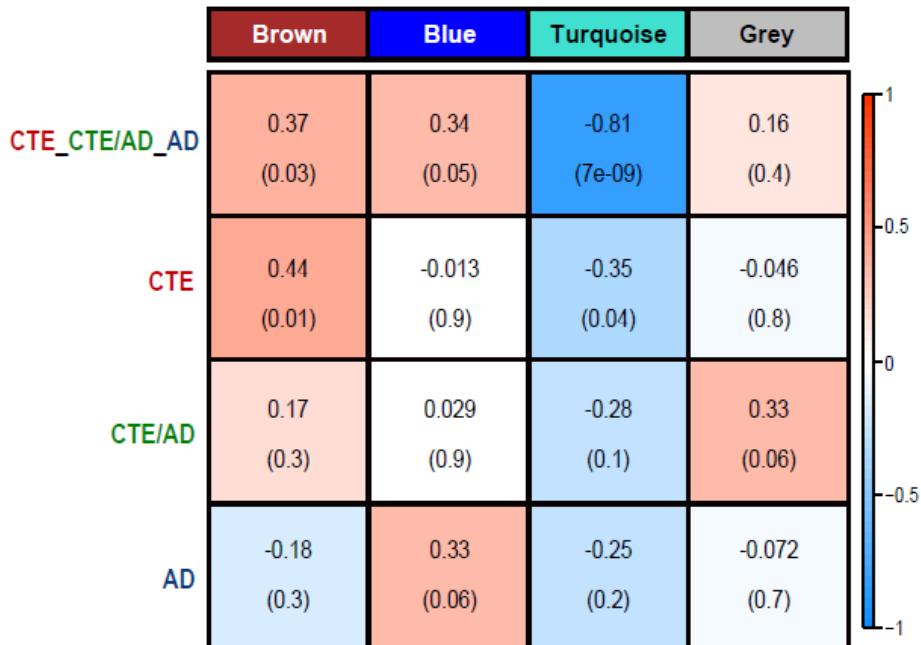
Figure 1-10. Module-trait relationships

Matrix with the module-trait relationships and corresponding p-values between the detected modules on the x axis and selected CTE_CTE/AD_AD and each disease (CTE, CTE/AD, AD) on the y axis. The pearson's correlation coefficient (PCC) values range from -1 (blue) to +1 (red) depending on the strength of the relationships. Each PCC values is accompanied by the corresponding p-value in brackets. Among the modules, turquoise module was highly correlated in CTE_CTE/AD_AD (3,417 genes).
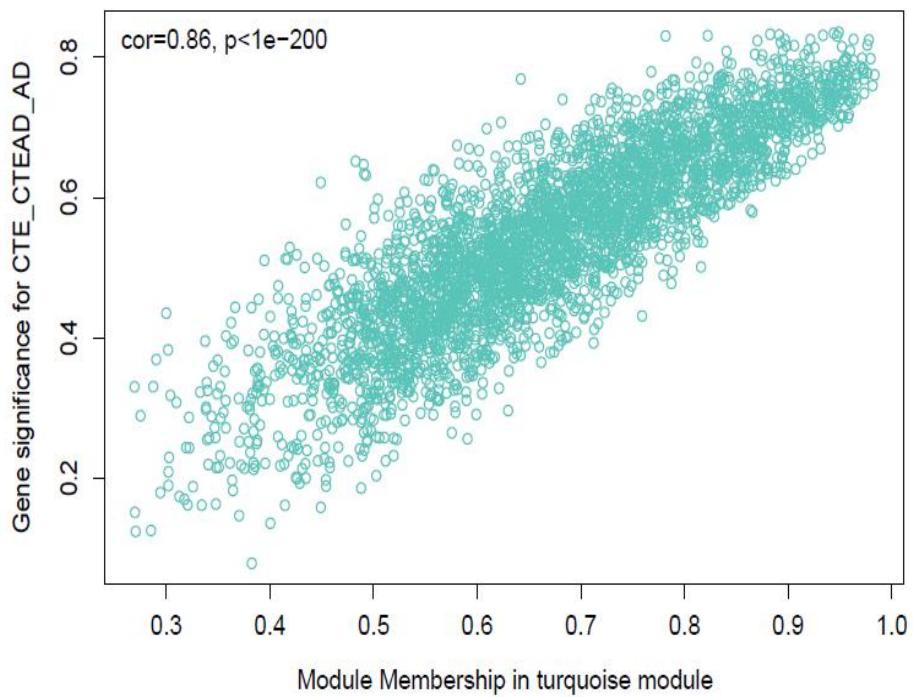
Figure 1-11. The correlation between gene significance for CTE_CTE/AD_AD and module membership in turquoise module

Gene significance for CTE_CTE/AD_AD status and module membership in turquoise module was significantly correlated.
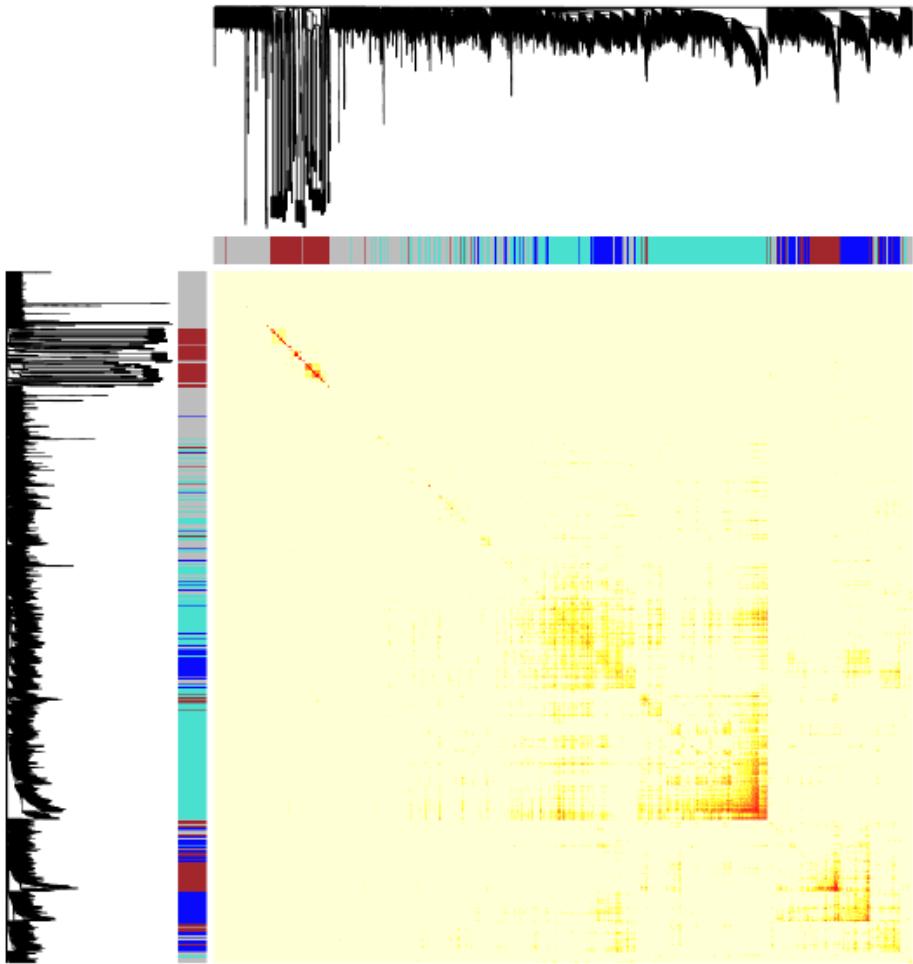
Figure 1-12. Topological overlap matrix plot

The heatmap indicates the topological overlap matrix (TOM) among all genes in 34 samples (8 CTE, 6 CTE/AD, 10 AD and 10 normal). Each row/column corresponds to genes. Left side and top indicate hierarchical clustering dendrogram and modules. Light colors represent lower topological overlap and a darker colors indicate higher topological overlap.

Module	DEG	Gene set name	#Genes	-log10(q-value)
				0 20 40 60 80 100 120
Turquoise	Down	Neuron part	203	
		Synapse	162	
		Synapse part	140	
		Neuron projection	148	
		Synaptic signaling	107	
		Cell cell signaling	138	
		Somatodendritic compartment	101	
		Presynapse	81	
		Postsynapse	87	
		Cell projection part	123	
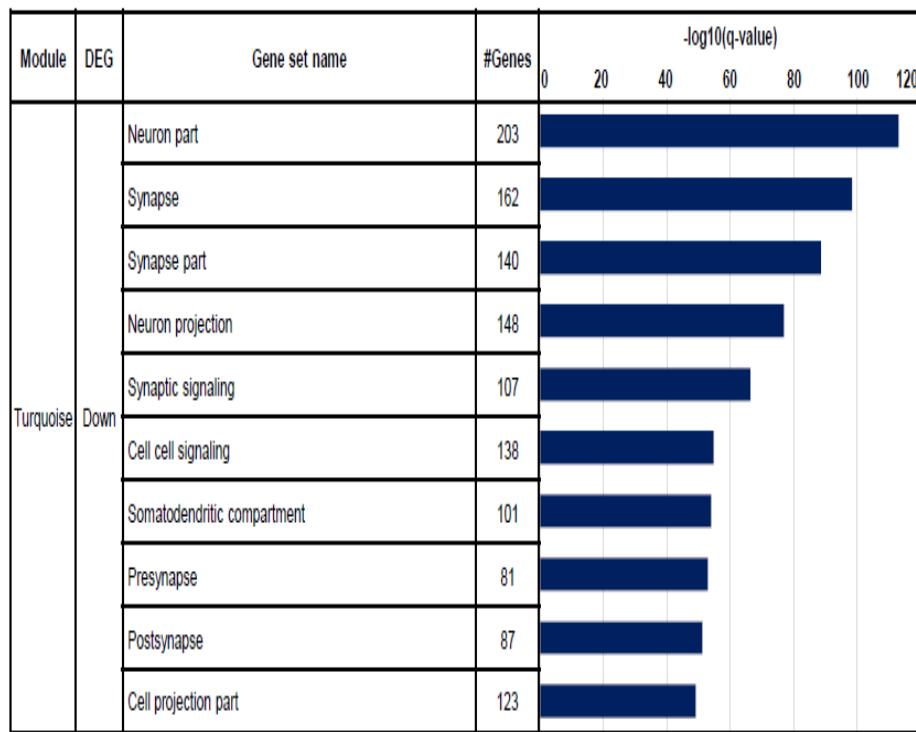
Figure 1-13. The result of top 10 gene set enrichment analysis of turquoise module

Among the gene sets of GO, neuron part, synapse and synapse part pathways were shown to be highly enriched in turquoise module.
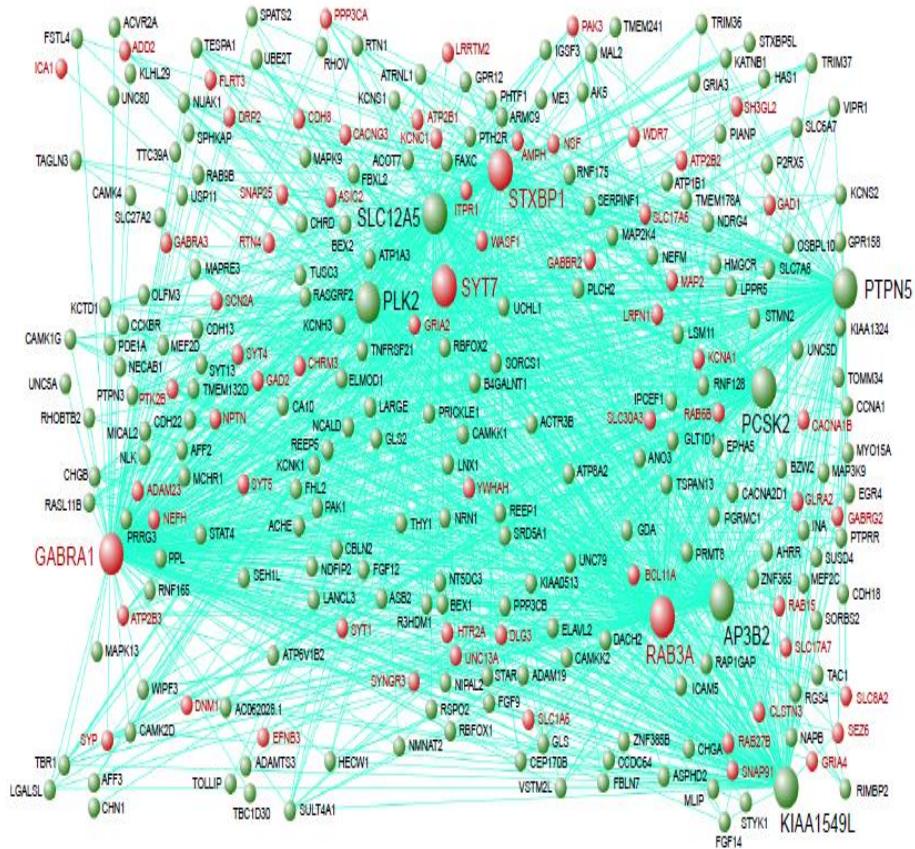
Figure 1-14. Network analysis of turquoise module

Each node indicates a gene. The genes with at least one connection when weighted cutoff value of > 0.22 are shown. Among the 266 genes, 67 genes belonged to neuron part, synapse and synapse part pathways and were shown in red. The 10 hub genes had higher connections with other genes and were represented with bigger nodes.
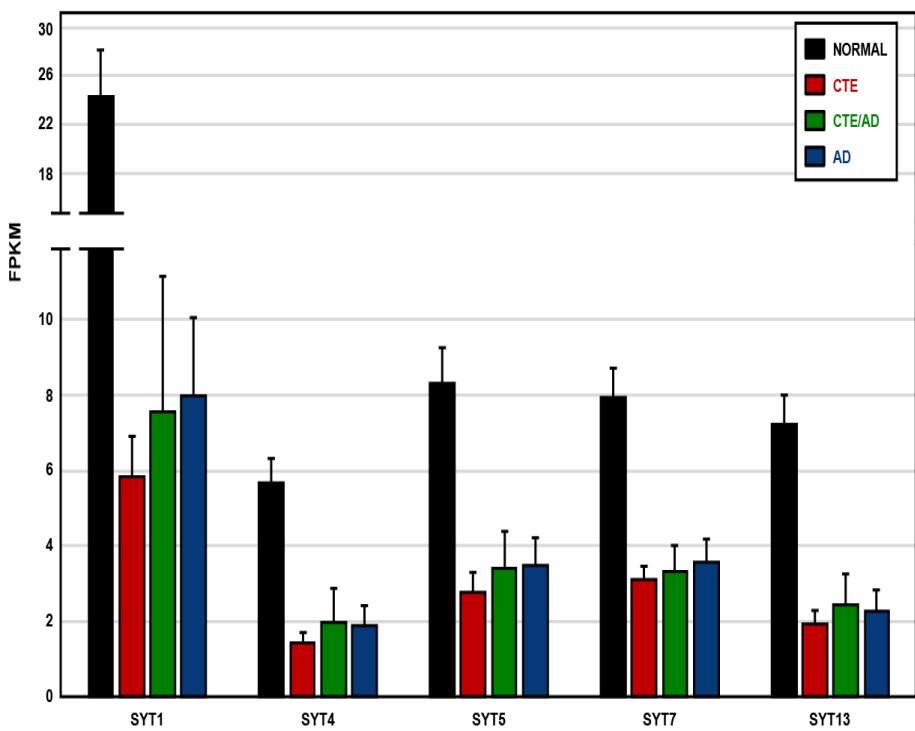
Figure 1-15. The expression levels of synaptotagmins (SYT1, SYT4, SYT5, SYT7 and SYT13)

NORMAL   **CTE**   **AD**

Synaptotagmin 1

Black bar = 20 µm
White bar = 10 µm
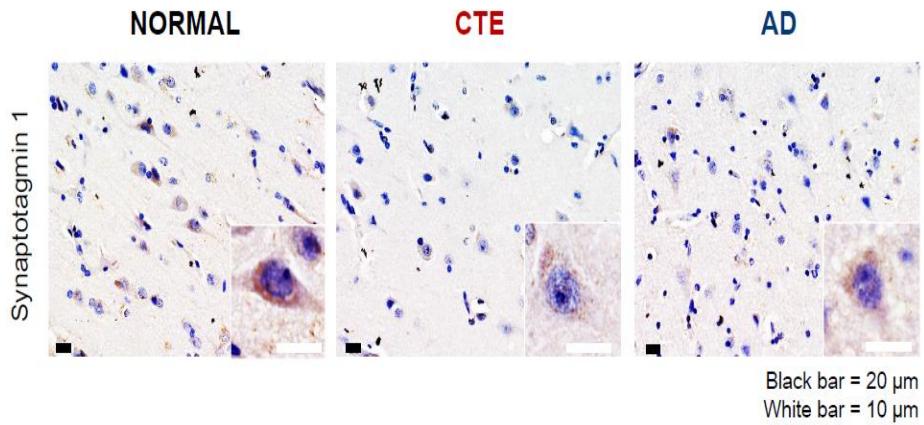
Figure 1-16. The immunoreactivity of SYT1 in CTE and AD

The SYT1 immunoreactivity was markedly reduced in the cytosolic compartment of cortical neurons in CTE and AD postmortem brain compared to normal subject. The nuclei were counter stained with hematoxylin (blue).

Scale bar : black, 20 µm; white, 10 µm.
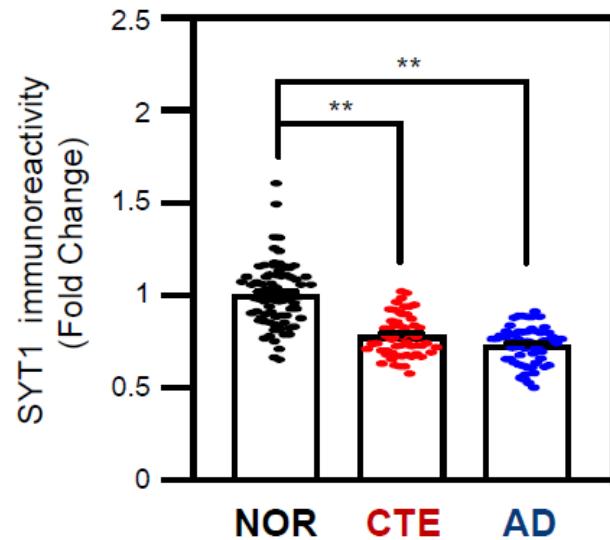
Figure 1-17. Foldchange level of SYT1 immunoreactivity in CTE and AD

Densitometry analysis showed that the intensity of SYT1 is significantly decreased the cortical neurons in CTE and AD postmortem brain compared to normal postmortem brain. The Student's t-test (unpaired) was performed for statistical analysis. **Significantly different at $p<0.001$.
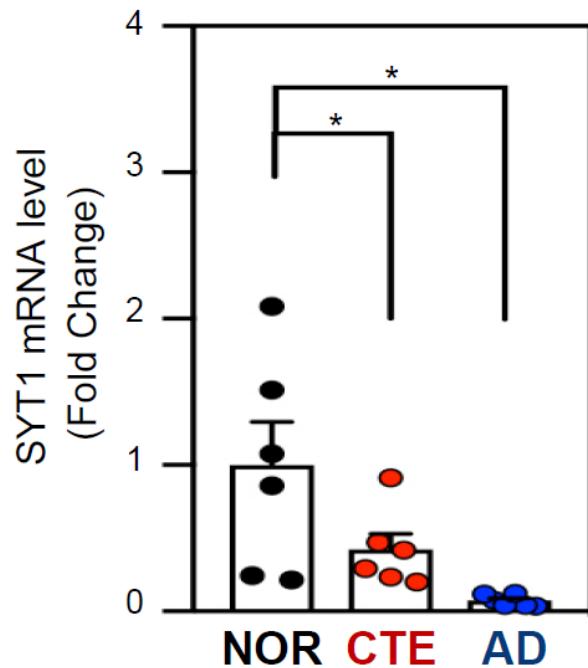
Figure 1-18. The mRNA levels of SYT1 in CTE and AD

The mRNA level of SYT1 was significantly reduced in CTE and AD patients

compared to normal subjects.
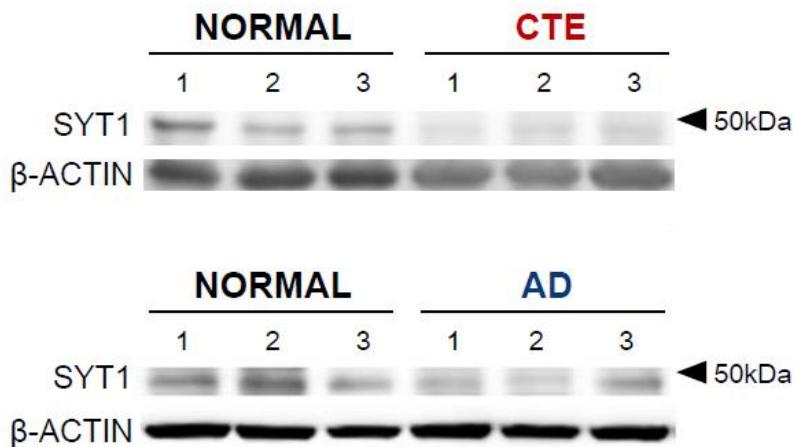
Figure 1-19. Western blot analysis of SYT1 in CTE and AD

Synaptotagmin 1 (SYT1) protein was downregulated in the cortex of postmortem brain of CTE and AD patients compared to normal subjects. Western blot data represent three cases of normal subjects, CTE and AD patients, respectively.
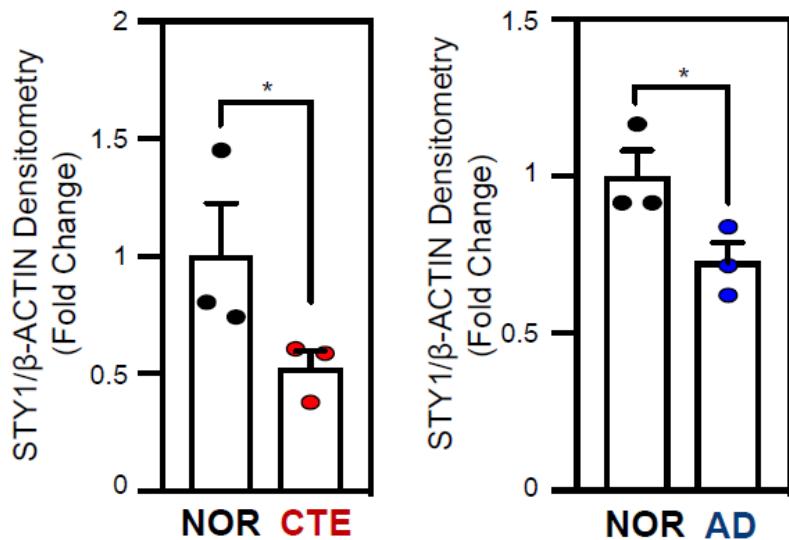
Figure 1-20. Densitometry analysis of SYT1 in CTE and AD

Densitometry analysis showed that SYT1 protein level was significantly reduced in the postmortem brain of CTE and AD patients. *Significantly different from the normal subject at $p < 0.05$.
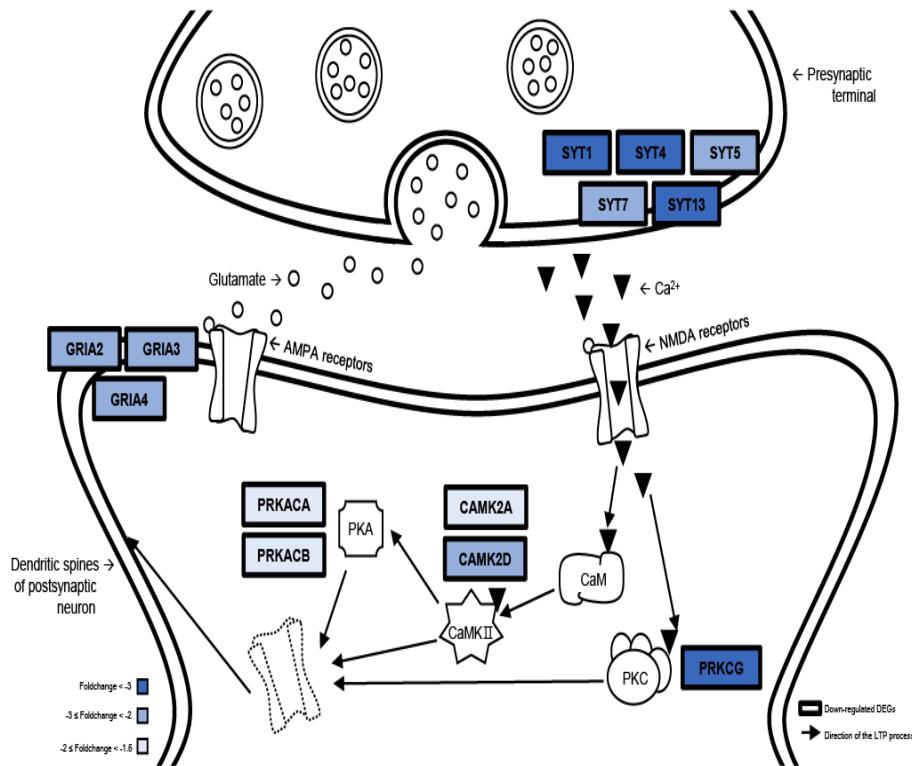
Figure 1-21. The schemes of long-term potentiation process

Memory function-related genes were significantly down-regulated in CTE, CTE/AD and AD. The common DEGs of CTE, CTE/AD and AD were shown in the scheme. The average foldchange levels of DEGs in CTE, CTE/AD and AD represented blue colors. The arrows describe the long term potentiation (LTP) process. (CaM = calmodulin, CAMKII = Ca2+/calmodulin-dependent protein kinase II, PKA = protein kinase A, PKC = protein kinase C)
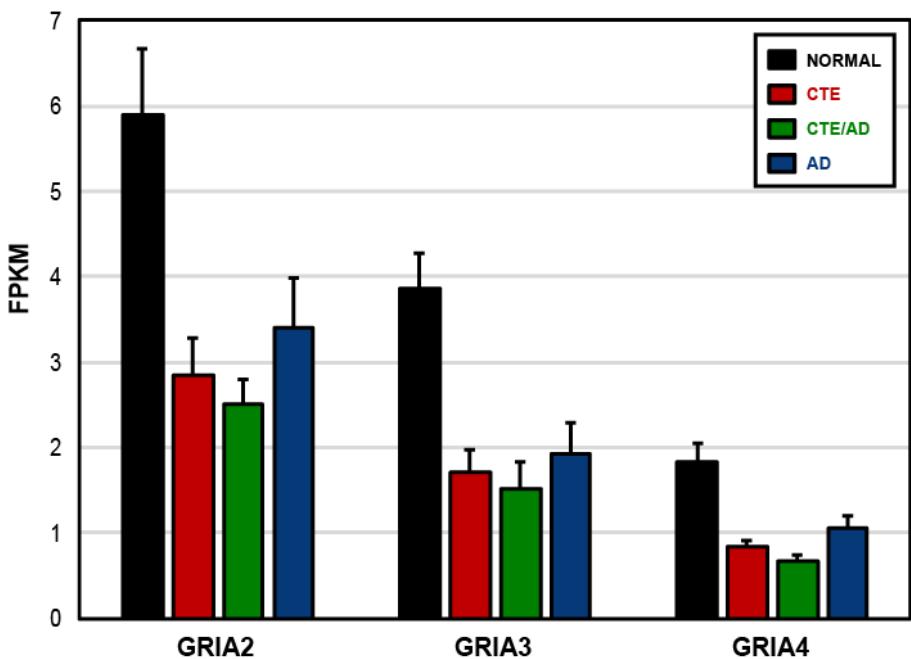
Figure 1-22. The expression levels of AMPA receptors

3 subunits (GRIA2, GRIA3 and GRIA4) of AMPA receptors were down-regulated in CTE, CTE/AD and AD
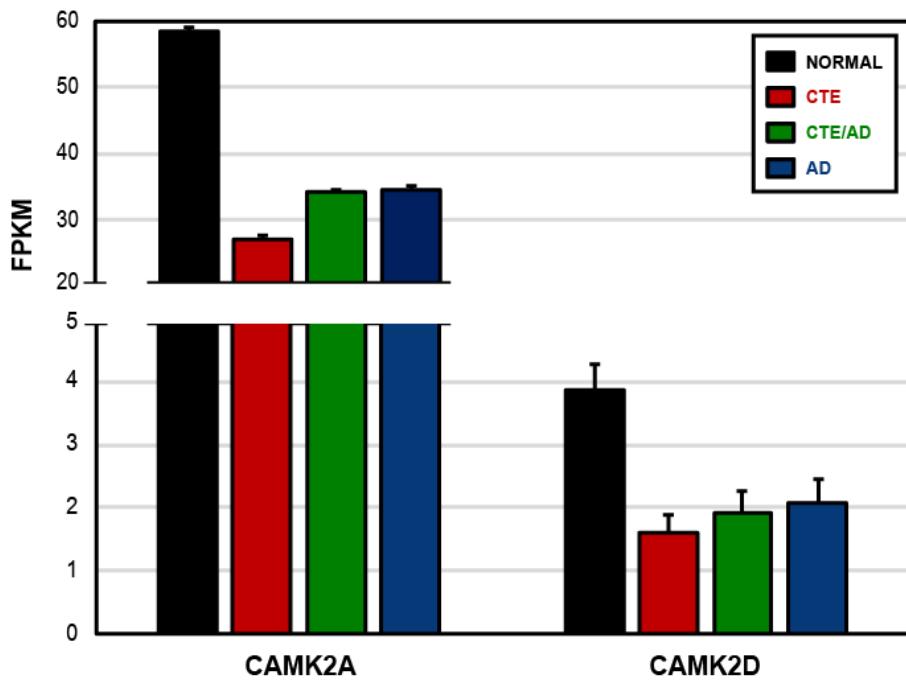
Figure 1-23. The expression levels of CaMKII subfamily genes (CAMK2A, CAMK2D)
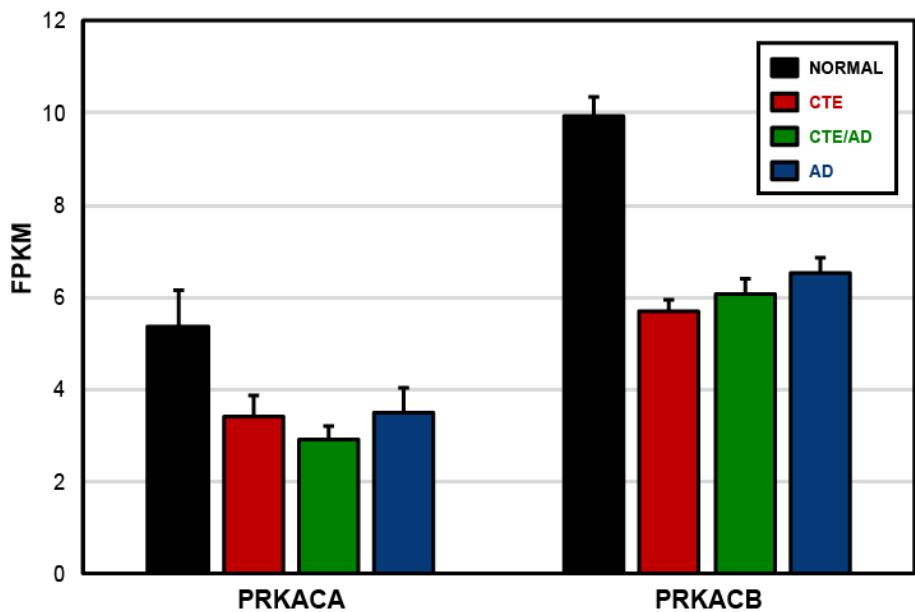
Figure 1-24. The expression levels of PKA catalytic subunits (PRKACA, PRKACB)
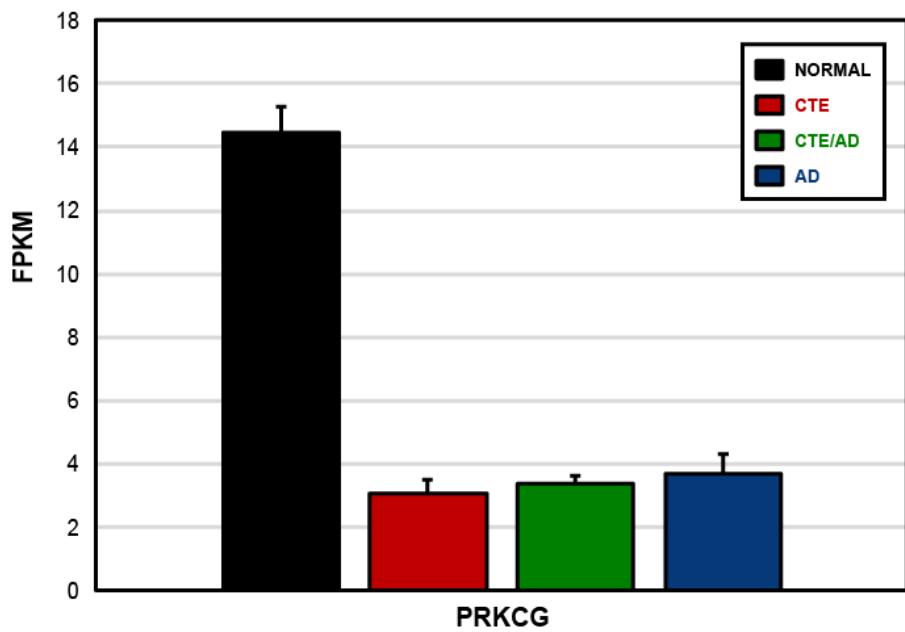
Figure 1-25. The expression levels of protein kinase C (PRKCG)
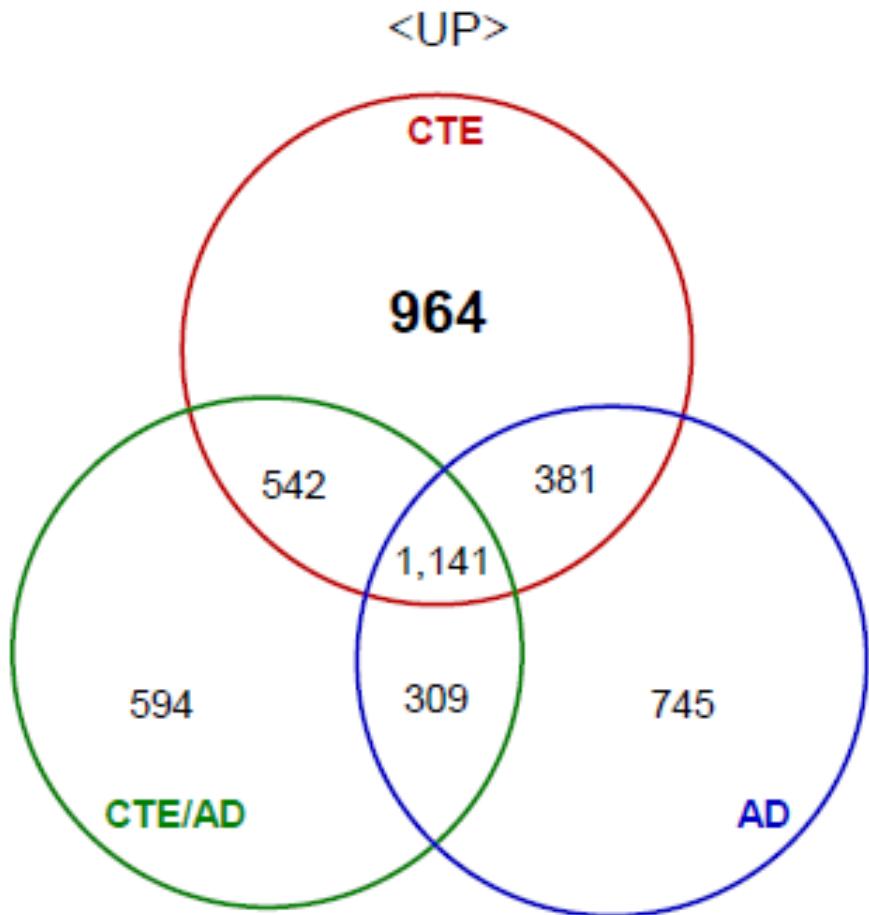
Figure 1-26. Comparison of the number of up-regulated genes in CTE, CTE/AD and AD

964 genes were uniquely up-regulated in CTE.
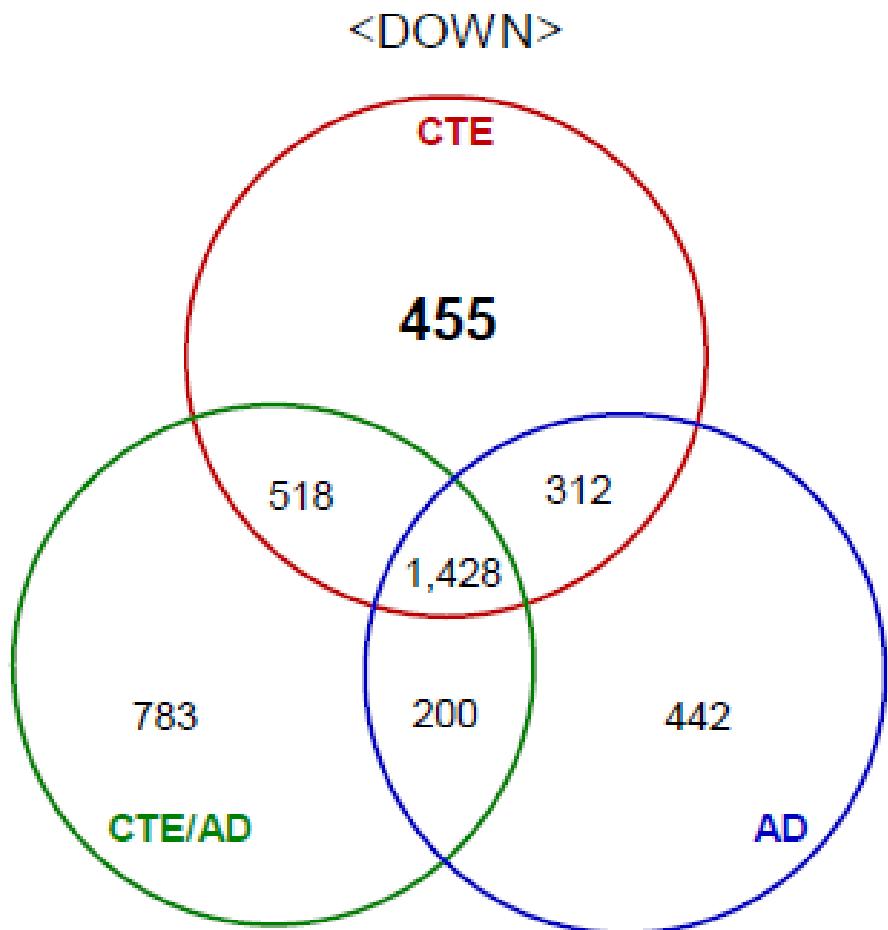
Figure 1-27. Comparison of the number of down-regulated genes in CTE, CTE/AD and AD

455 gene were uniquely down-regulated in CTE.

Gene set name	#Genes	-log10(q-value) 0 1 2 3 4 5
Cell adhesion molecules (CAMs)	14	
Pathways in cancer	22	
Allograft rejection	8	
Autoimmune thyroid disease	9	
Focal adhesion	15	
Graft-versus-host disease	7	
Type I diabetes mellitus	7	
ECM-receptor interaction	9	
Viral myocarditis	8	
Natural killer cell mediated cyto-toxicity	11	
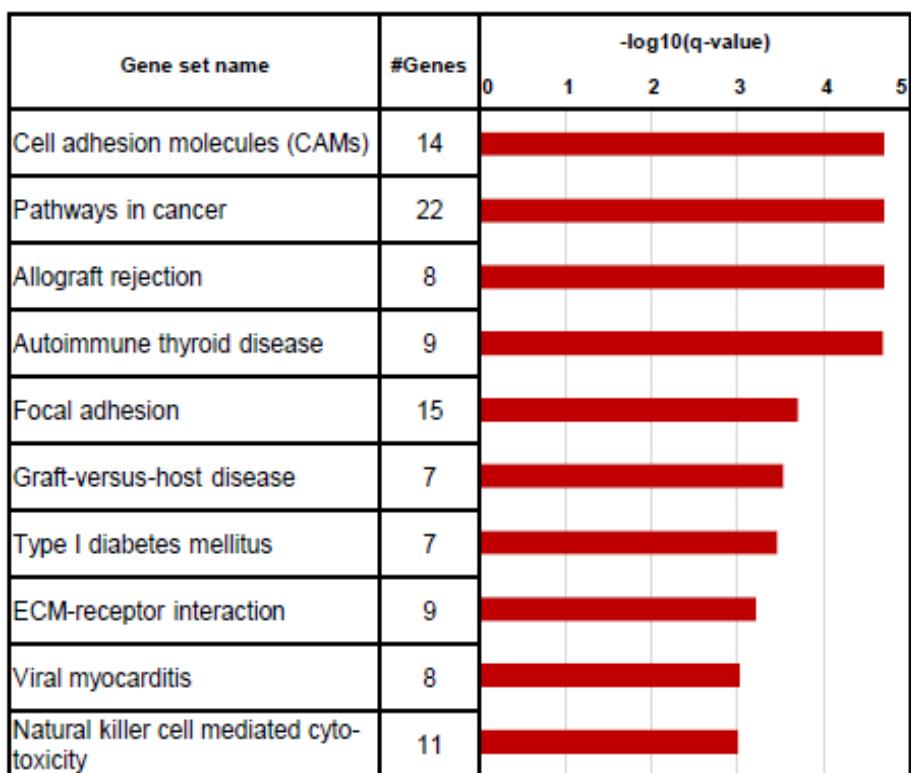
Figure 1-28. Top 10 KEGG pathway analysis of up-regulated genes in CTE

Among the top 10 KEGG enriched pathways, cell adhesion molecules (CAMs)

pathway was highly enriched in CTE.
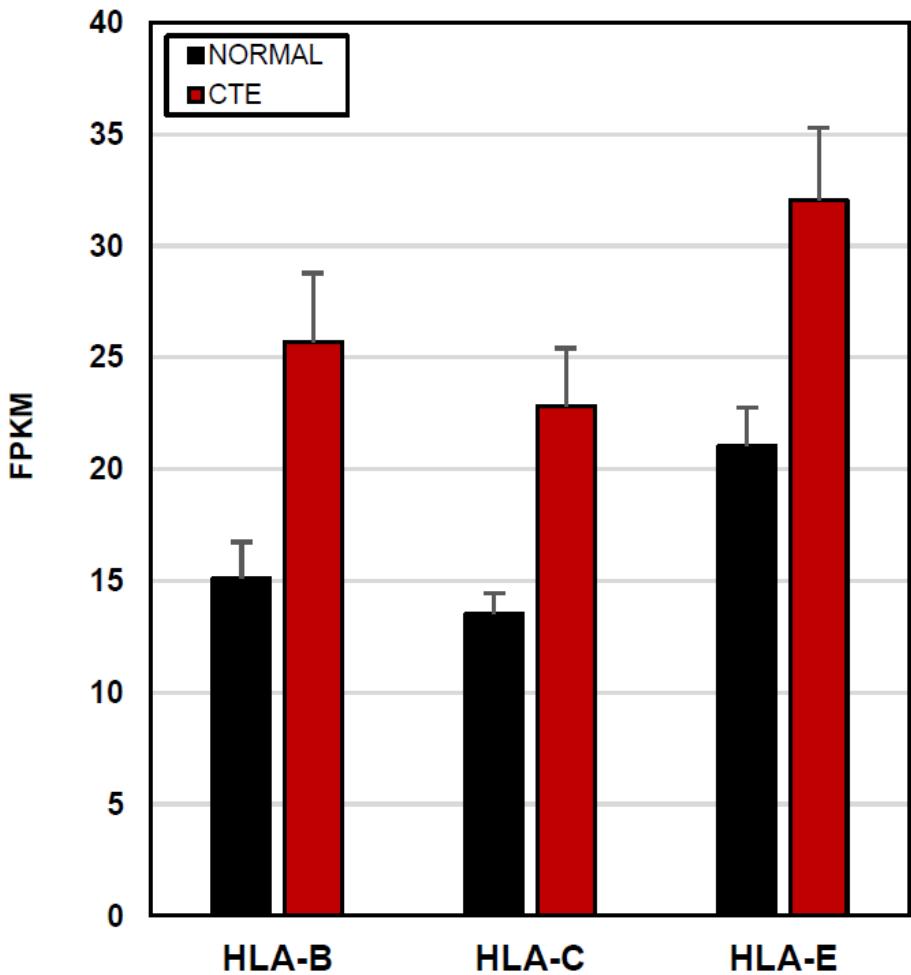
Figure 1-29. The expression levels of HLA genes (HLA-B, HLA-C and HLA-E)

Figure 1-30. Schematic table of findings

Discussion

CTE is a progressive neurodegenerative disease which affics the brain of people who have suffered repetitive concussions. Although the neuropathological features of CTE are fully demonstrated, the fundamental gene regulatory mechanisms and biological pathways of TBI-related diseases are still unclear. Previous our study revealed the mechanisms of how TBI causes neuropathological sequelae of tauopathy in CTE. In this study, we focused on common and unique transcriptome signatures of traumatic brain injury-related neurodegenerative diseases. We investigated how the gene expression changes associated with TBI-related diseases are associated with synaptic transmission and memory function through transcriptomes of CTE, CTE/AD, AD brain samples.

CTE, CTE/AD and AD showed common gene expression changes by cell-type. Neuronal genes were dysregulated in CTE, CTE/AD and AD. Neuron loss is known to be found in normal aging and in the early stage of disease development [60]. Neuron death correlates with the severity of memory impairments. Neuron loss leads to loss of ability to relocate neuronal organization of cerebral structures and add new neurons to them. Therefore, down-regulation of neuron prevents normal memory function and learning process in CTE, CTE/AD and AD.

Up-regulation of astrocytes-, oligodendrocytes-, endothelial-, microglia-genes was shown in CTE, CTE/AD and AD. Atrophy of astrocytes causes loss of synaptic connectivity, imbalance of neurotransmitter homeostasis, and neuronal death [61]. Oligodendrocytes are necessary for nerve repair after injury by preventing their cell death and maintaining myelin restoration [62]. Microglia is recognized as an essential players for preserving brain homeostasis and protecting the brain from infections and insults [63, 64]. Microglia also exert a neuroprotective role to phagocytose and clear Aβ aggregates in AD [65, 66]. Endothelial cells play an important role in maintaining cardiovascular homeostasis [67]. Based on these results, we assumed that the altered gene expression of astrocytes, oligodendrocytes, microglia and endothelial cells are a great impact on various biological mechanisms in CTE, CTE/AD and AD.

Changes in expression of synapse- and synaptic transmission- related genes represented the common transcriptome features of CTE, CTE/AD and AD. Synapse is essential for neuronal function and communication. Synapse connects the neurons in the brain by passing an electrical or chemical signal from neurons to other neurons. Previous studies have shown that synaptic dysfunction triggers cognitive decline in AD and other dementias [68, 69]. Our result suggests that dysregulation of synaptic transmission correlates with cognitive deficits and memory dysfunction in CTE as well as AD.

Synaptotagmins (SYT1, SYT4, SYT5, SYT7 and SYT13) were significantly down-regulated in CTE, CTE/AD and AD. Synaptotagmins are a Ca^{2+} binding protein that plays a pivotal role in vesicle fusion to the synaptic membrane. SYT1 and SYT7 act as the main Ca^{2+} sensors for fast and slow presynaptic vesicle exocytosis, respectively. Previous studies have shown that SYT1 and SYT7 function as redundant Ca^{2+} sensors for AMPA exocytosis during long-term potentiation (LTP) [70-72]. Therefore, we assumed that down-regulation of synaptotagmins impacts on memory function in CTE, CTE/AD and AD.

LTP process is a long-lasting strengthening of synaptic transmission and thought to be related to learning and memory. LTP process is initiated by short periods of high-frequency presynaptic stimulation. Glutamate is released from the presynaptic cell onto the post-synaptic cell. It causes depolarization of the cell through AMPA receptors and thus displacement of Mg^{2+} from the NMDA receptors. The NMDA receptors are voltage gated in the presence of Mg^{2+} and passes Ca^{2+} when opened. Ca^{2+} activates PKC and calmodulin kinase II, both of which lead to substrate level phosphorylation and insertion of additional AMPA receptors into the membrane. By adding more AMPA receptors to the membrane, post-synaptic cells respond more strongly to future release of glutamate. Thus, the synapse is strengthened and potentiation has occurred.

In our study, 4 neurotransmitters that act as a key mediators in memory function have changed in CTE, CTE/AD and AD. Down-regulation of α

(alpha) and δ (delta) chains of CaMKII (CAMK2A, CAMK2D) showed in CTE, CTE/AD and AD. CaMKII is a major synaptic protein and important mediator of LTP process [73]. CaMKII detects the uptake of Ca^{2+} and thus triggers the biochemical cascade that enhances synaptic transmission [74]. CaMKII alters glutamate susceptability by phosphorylating the AMPA receptor [75-78]. It has been reported that knock out mice of CAMK2A reduces the LTP process by half [79].

PRKACA and PRKACB, which encode catalytic subunits of PKA, were down-regulated in CTE, CTE/AD and AD. PKA is a cAMP-dependent protein kinase and involved in the induction and maintenance of LTP process [80]. PKA regulates the synaptic incorporation of AMPA receptors by phosphorylating the GluA4 and GluA1 subunits.

PRKCG, one of isozymes of the PKC, was significantly down-regulated in CTE, CTE/AD and AD. PKC is involved in neuronal functions such as regulation of ion channel activity and synaptic transmission [81-83]. PKC enhances NMDA receptors response by increasing channel open time and reducing the voltage-dependent Mg^{2+} block of the NMDA receptors channel [84, 85]. PKC phosphorylates GluA1 and GluA4 subunit of AMPA receptor to alter glutamate sensitivity [86]. Especially, PRKCG modulates GluA4 subunit of AMPA receptors by binding directly to GluA4 [87]. Previous study demonstrated that PKCγ (PRKCG) mutant mice showed impaired LTP

process [88, 89].

AMPA receptors are composed of 4 subunits (GRIA1-4). Dysregulation of GRIA2, GRIA3 and GRIA4 gene expression showed in CTE, CTE/AD and AD. AMPA receptors regulate the majority of excitatory synaptic transmission [90]. AMPA receptors are phosphorylated by protein kinases including PKA, PKC and CaMKII. Phosphorylation of AMPA receptors potentiates their function. Among the AMPA receptors, GluA1 and GluA4 mainly act on LTP process [91].

Notably, unique transcriptome signatures of CTE were associated with CAMs. CAMs regulate interactions between cells and the surrounding extracellular matrix, that are essential for the process of controlling cell survival, activation, migration, and proliferation [92]. In the brain, CAMs are important for neural network formation like axon-axon contacts, axon-astrocyte contacts, synapse formation and regulation of synaptic structure [93, 94]. In addition, MHC class I molecules are expressed on neurons and showed remarkable expression changes in CTE. MHC class I molecules regulate neuronal differentiation and affect synaptic plasticity, axonal regeneration and T cell mediated response [95-97].

In summary, we identified alterations of common and unique transcriptome signatures in head-trauma related diseases (Figure 1-32). Deregulation of synaptic transmission and memory function-associated transcriptomes were

commonly affected in CTE, CTE/AD and AD. On the other hand, up-regulation of CAMs-associated transcriptome signatures was found to be unique in CTE. Thus, altered transcriptome signatures provide insights to understand molecular mechanisms of head-trauma related disorders and these signatures may be new biological markers of CTE. Taking the results together, we found down-regulation of synaptotagmins and essential neurotransmitters of LTP process, including CaMKII, PKA, PKC and AMPA receptors. We identified that these expression changes affect synaptic transmission and memory function in CTE, CTE/AD and AD [60, 68]. It will be helpful to understand molecular mechanisms of head-trauma related disorders and provide a new approach to the understanding of the pathogenesis of neurodegenerative diseases.

Part 2

Alteration of tauopathy-associated transcriptome signatures and molecular mechanisms in CTE, CTE/AD and AD

-Imparied protein phosphatase expression

Abstract

Tauopathy is one of most common pathology that associates with TBI-related neurodegenerative disorders such as chronic traumatic encephalopathy (CTE) and Alzheimer's disease (AD). Tau protein undergoes intra-molecular alterations and some modified forms promote the production of hyperphosphorylated tau and assemble into neurofibrillary tangles (NFTs), known as tauopathy. Many studies indicated that tauopathy is a risk factor for neurodegenerative diseases. However, the precise molecular mechanisms of tauopathy in TBI-related neurodegenerative diseases remain unknown. Here we identified the mechanisms by next-generation sequencing of post-mortem human brain tissues. We performed RNA sequencing of post-mortem brain tissue from 8 CTE, 6 CTE/AD, 10 AD patients compared to 10 normal controls. The gene expression of protein phosphatase genes such as PP2B subunits (PPP3CA, PPP3CB and PPP3R1) are markedly decreased in CTE brains. Recent study showed that PP2B is related to dephosphorylation of tau in Huntington's disease. The elevation of p-tau is inversely correlated with PP2B activity in both cellular and animal model. Using *in vitro* cell lines and *in vivo* animal models, we confirmed that reduced PPP3CA/PP2B activity is directly associated with increases in phosphorylated tau (p-tau) proteins. Our study provides a transcriptional mechanism of protein phosphatase dependent tauopathy in CTE, CTE/AD and AD and it may lead to novel therapeutic

approaches to decrease the tauopathy associated with TBI-related neurodegenerative diseases.

Student number: 2014-25074

Introduction

Tauopathy is a common pathology of TBI-related neurodegenerative diseases that are caused or associated with pathological tau protein. Tau is an abbreviated or alternative term for the microtubule-associated protein tau (MAPT). Microtubules are essential for the normal trafficking of cellular cargo in neuronal axonal projections. Under normal conditions, MAPT is a soluble protein that facilitates microtubule stabilization in cells, and is found in particular high concentrations in neurons. In pathological conditions, tau can be more phosphorylated than normal. Hyperphosphorylated tau dissociated from microtubules in the axon, translocate to the cell body and proximal dendrities, and aggregate into intracellular inclusions termed neurofibrillary tangles (NFTs), leading to impair axonal function. Tau hyperphosphorylation decreases tau binding to microtubules and promotes tau fibrillization.

In CTE, hyperphosphorylated tau pathology begin focally, as perivascular neurofibrillary tangles and neurites at the depths of the cerebral sulci, and then spread to a superficial layers of adjacent cortex before becoming a widespread degeneration affecting brain stem and medial temporal lobe structures.

In AD, tau pathology is first discovered in the brainstem and entorhinal cortex. Afterward, it was also observed in the hippocampus and medial temporal lobe

and was finally widespread in the neocortex. However, how tau protein and its dynamic changes affect the pathogenesis of various neurodegenerative diseases is still a mystery.

In this study, we focused on the mechanism of how brain injury leads to neuropathological sequelae of tauopathy in CTE and AD through NGS technologies. We performed RNA sequencing analysis of post-mortem brain tissue from CTE, CTE/AD, AD patients and normal subjects. We further applied an *in vitro* cell line and *in vivo* mouse model to validate how transcriptional changes lead to neuropathological changes in CTE and AD.

Materials and methods

Differentially expressed genes analysis

To discover significant differentially expressed genes (DEGs) in CTE, CTE/AD and AD, we applied to DESeq2 [55]. We selected DEGs with p-value < 0.001 and |FoldChange| > 1.5. FPKM (fragments per kilo base of exon per million mapped reads) for each gene was calculated with edgeR and used for analyses. The DEGs selected above were applied to the Molecular Signatures Database of Gene Set Enrichment Analysis (GSEA) [98]. We selected KEGG gene sets of MSigDB to analyze up- and down-regulated genes in CTE, CTE/AD and AD.

Gene set enrichment analysis

Functional annotation analysis was performed to assign biological relevance to the gene network modules using Gene Set Enrichment Analysis (GSEA) with Kyoto Encyclopedia of Genes and Genome (KEGG) pathway [56]. The enrichment of the KEGG terms in each module was evaluated based on the hypergeometric test. The output from GSEA is and enrichment score that describes the imbalance in the distribution of ranks of gene expression in each gene set. The number of genes in the overlatp (k) was set at ≥ 3. The enrichment score was normalized according to the size of the gene sets, which were subsequently ranked according to the normalized enrichment score.

KEGG categories with a false-positive rate (FDR) q-value < 0.05 were reported.

Tau BiFC cell lines and culture

The establishment of the HEK293/tau-BiFC cell line was previously described [99]. Venus fluorescence protein amino-terminal fragment (VN 173) and carboxyl-terminal fragment (VC 155), which are independently non-fluorescent, were fused to full-length tau proteins. For neuronal cell expression, tau-BiFC constructs (pCMV6-hTau40-VN173 and pCMV6-hTau-VC155) were transfected into SH-SY5Y. SH-SY5Y/tau-BiFC stable cells were selected using Geneticin (200 µg ml^{-1}). The phosphorylation of tau resulted in the assembly, or aggregation, of two tau molecules, which enabled the maturation of the Venus protein to emit a fluorescence signal. All established cell lines were grown in Dulbecco's modified eagle medium containing 10% fetal bovine serum, 10,000 units per ml penicillin, 10,000µg ml^{-1} streptomycin and 1 µg ml^{-1} of geneticin at 37°C in a humidified atmosphere containing 5% CO_2.

Live cell imaging and analysis

For microscopic image analysis, HEK293 tau-BiFC and SH-SY5Y tau-BiFC cells were plated onto a black 384-well plate. The next day, tau-BiFC cells were treated with okadaic acid (O8010, Sigma, St Louis, MO, USA), cyclosporine A (C3662, Sigma) or deltamethrin (D9315, Sigma) at various concentrations. After incubation for 29 h, the plate was imaged using the Operetta high contents imaging system (PerkinElmer). The cellular intensities of tau-BiFC

fluorescence were analyzed using the Harmony 3.1 analysis software. Each experiment was performed in triplicate. The bar graphs for BiFC intensity indicate the means ±s.e.m. from three independent experiments.

Confocal microscopy

Tissues and cells were immunostained for p-Tau (S199) (rabbit polyclonal, 1:200; Abcam, Cambridge, UK), p-Tau (S202/T205) (mouse monoclonal, 1:500; Thermo Scientific, Waltham, MA, USA) and PP2B/ PPP3CA (rabbit polyclonal, 1:200; SantaCruz Biotech, Dallas, TX, USA) according to a previous report [100]. For confocal microscopy, the specimens were incubated for 1 h with fluorescence (FITC)-conjugated secondary antibody (Vector, Burlingame, CA, USA) and Cy3-conjugated secondary antibody (Jackson Lab, West Grove, PA, USA) after the primary antibody incubation. The images were analyzed using a Spinning Disk Confocal microscope (IX2-DSU, Olympus, Tokyo, Japan). Pre-absorption with excess target protein or omission of primary antibody was used to demonstrate antibody specificity and determine the background generated from the detection assay

Immunohistochemistry

Immunohistochemistry was performed as previously described [58]. Paraffin-embedded tissues were sectioned in a coronal plane at 10–20 μm. The tissue sections were rehydrated, blocked with blocking solution (1% H_2O_2), and incubated with p-Tau (S202/T205) (1:200), PP2B/PPP3CA (1:200; SantaCruz

Biotech), p-Tau (S199) (1:200; Abcam) and anti-III tubulin antibody (1:500 dilutions; Sigma) for 24 h. After washing three times, the slides were processed with Vector ABC Kit (Vector Lab). The immunoreactive signals were developed with DAB chromogen (Thermo Fisher Scientific, Meridian, Rockford, IL, USA) and analyzed under a bright field microscope.

Western blot analysis

Western blot analysis was performed as previously described [101]. For the detection of p-Tau and other proteins, the blots were probed with anti-p-Tau (S199) (1:1000; Abcam), anti-p-Tau (S396) (1:1000), anti-p-Tau (AT8, S202/T205) (1:1000) and anti-β-actin (1:10,000; Sigma Aldrich, St Louis, MO, USA) antibodies, followed by treatment with the appropriate secondary antibodies conjugated to horseradish peroxidase (Pierce, 170-6515 and 170-6516). Immunoreactivity was detected using an enhanced chemiluminescence (ECL) kit (Thermo Scientific).

Quantitative real-time PCR

Total RNA was extracted from the frozen brain tissues using TRIzol reagent (MRC, TR118) as previously described [58]. Fifty nanograms of RNA was used as a template for quantitative RT-PCR amplification, using SYBR Green Real-time PCR Master Mix (Toyobo, QPK-201, Osaka, Japan). The primers were standardized in the linear range of the cycle prior to the onset of the plateau. GAPDH was used as an internal control. Real-time data acquisition was

performed using a LightCyler96 Real-Time PCR System (Roche Diagnostics, Indianapolis, IN, USA) under the following cycling conditions: 95°C for 1 min × 1 cycle, and 95°C for 15s, followed by 60°C for 1 min × 45 cycles. The relative gene expression was analyzed using the LightCyler96 software and expressed as Ct the number of cycles needed to generate a fluorescent signal above a predefined threshold.

Construction and delivery of rAAV vectors containing PPP3CA shRNA

For in vivo gene silencing, the validated mouse shRNA sequences for PPP3CA were cloned into the pSicoR vector using HpaI/XhoI sites (Addgene, Cambridge, MA, USA, #21907) and subcloned into the pAAV-MCS vector (Stratagene) using MluI/BglII sites. The high-titer rAAV vectors were produced in HEK293TN cells using a helper virus-free system. Briefly, the rAAV vectors were produced after co-transfecting with equimolar amounts of a rep/cap/helper plasmid. After incubation for 72 h, the cells were lysed, treated with benzonase (Sigma #E1014) and further purified using HiTrap heparin columns (GE Healthcare, Pittsburg, CA, USA, #17-0460-01). Amicon ultra-15 centrifugal filter units (Millipore, Billerica, MA, USA #UFC9100) were used to concentrate up to the final volume. For the delivery of rAAV-PPP3CA shRNA into the brain, the stereotactic microinjection method was used. rAAV-shControl and AAV-PPP3CA shRNA were delivered into the dentate gyrus (AP: −2, ML: 1.5, DV: −1.85) of 4-month-old wild-type mice and Tau transgenic

(P301L) mice as previously described.

Animal model of TBI

All procedures for the animal study were approved by Institutional Animal Care and Use Committee (IACUC) in the Korea Institute of Science and Technology according to international standards and guidelines. Wild-type (C57BL/6) and Tau transgenic (P301L) mice at 4 months of age were used in this study. The mice were fed a standard laboratory diet and water ad libitum in a controlled environment. The mice received three weight-drop-induced closed diffuse TBIs at 3-day intervals. We induced closed diffuse TBI by using a weight-drop device (weight 100g, fall height 75cm, angle 90°) as described previously but with a slight modification [102]. The anatomical locus of impact was adjusted to bregma -1 to ±4. All mice were initially anesthetized with 2% avertin (23μg g^{-1}) IP injection before receiving the weight-drop induced TBI. Sham-injured animals were subjected to the same protocol of anesthesia administration, but no mass was ever dropped. After TBI, the mice were placed in the supine position in a clean cage heated using a commercially available heating pad. The mice were then returned to their home cages after normal behavior (for example, grooming, walking, exploring) was recovered. We examined animal behaviors based on open field and assessed neuro-histological changes. The animals were killed at 24 h after the last impact, and sham-operated animals were killed at 24 h after the last anesthesia.

Results

The blue gene co-expression module is significantly associated with CTE, CTE/AD and AD

In part 1, the blue module contains 2,668 genes with a high correlation between the members of its module and gene significance for CTE, CTE/AD and AD (correlation coefficient of 0.78). Among them, 252 positively- and 654 negatively correlated genes are differentially expressed in CTE, CTE/AD and AD. Hierarchical clustering analysis of 904 genes showed the distinct separation of CTE, CTE/AD and AD from normal subjects (Figure 2-1).

Gene set enrichment analysis of blue module

To understand the biological relevance of the identified modules highly correlated to TBI-relate neurodegenerative diseases, we performed gene set enrichment analysis (GSEA) with KEGG pathways. In up-regulated genes, Pathways in cancer and focal adhesion pathways were enriched (Figure 2-2).

Down-regulated genes were highly enriched for specific functional pathways that are directly associated with neurobiological functions: calcium signaling pathway, MAPK signaling pathway, long-term potentiation (Figure 2-3). We focused on genes related to calcium signaling pathway and MAPK pathway [103]. Using this approach, we identified 9 genes that might affect CTE

progression: PPP3CA, PPP3CB, PRKACA, PRKACB, PRKCG, CACNA1F, CACNA1B, CACNA1G and CACNA1I (Figure 2-4). From the above-mentioned genes, we identified PPP3CA, encoding a calcium-dependent, calmodulin-stimulated protein phosphatase (PP), which was reported to be decreased in the medial temporal gyrus from AD patient brains [104]. In addition, PPP3CB, the catalytic subunits of PP2B, was also significantly decreased in CTE, CTE/AD and AD subjects.

In particular, we investigated 58 tau phosphorylation-related kinase genes in Figure 2-5. The tau phosphorylation kinase, p38 MAPK (MAPK11, MAPK12, MAPK13 and MAPK14), was not activated or associated with the blue module. Moreover, other kinases such as glycogen synthase kinase 3(GSK3A, GSK3B), cyclin-dependent kinase 5(CDK5), c-Jun N-terminal kinase (JNK), extracellular signal-regulated protein kinases 1 and 2 (ERK1/2), dual specificity tyrosine-phosphorylation-regulated kinase 1A (DYRK1A), casein kinase (CK), protein kinase A (PKA), Ca2+/calmodulin-dependent protein kinase II (CAMKII) and postsynaptic density protein 95 (PSD-95) were not also increased in CTE, CTE/AD and AD. In addition, tauopathy pathogenesis-related proteases including calpain and caspases were also not increased in CTE, CTE/AD and AD.

In addition, Other Ser/Thr phosphatase proteins were also involved in tau phosphorylation. We represented 70 Ser/Thr phosphatase proteins-related genes in Figure 2-6. Among 70 genes, 4 genes including PPP3CA, PPP3CB,

PPP3R1, PPP1R14C were significantly down-regulated in CTE, CTE/AD and AD. PPP1R14C was excluded from the candidate genes because the average FPKM level was lower than 1. We selected 3 candidate genes (PPP3CA, PPP3CB, PPP3R1) that can be associated with tauopathy in CTE, CTE/AD and AD (Figure 2-7).

Reduction of PPP3CA/PP2B activity is associated with tauopathy in CTE

We explored whether altered PPP3CA gene expression also contributes to pathological tau phosphorylation and tauopathy in CTE. First, the downregulation of PPP3CA and PPP3CB was confirmed through quantitative real-time PCR (qPCR) in the cortex of human CTE and normal subjects (Figure 2-8). Western blot and densitometry analyses subsequently showed that the levels of PPP3CA and PPP3CB were markedly decreased in CTE compared to normal subjects (Figure 2-9). Furthermore, the levels of p-tau at S199, S202/T205 and S396, which are the most common sites of tau phosphorylation in neurodegenerative disorders, were increased 3- and 30-fold in CTE. Importantly, the levels of PPP3CA protein and p-tau (S202/T205) in the frontal cortex of CTE patients were inversely correlated. To further investigate the pathological characteristics of tauopathy in CTE, we performed 3,3′-diaminobenzidine (DAB) immunohistochemical staining in the cortex of normal and CTE brains (Figure 2-10). Consistent with the qPCR and western

blot data, the immunoreactivity of PPP3CA was decreased, and tau was hyperphosphorylated (S199, S396, S205/T208) in CTE.

Reduction of PPP3CA/PP2B activity is associated with tauopathy also in AD

Because the characteristics of CTE closely overlap with AD in transcriptome analysis, we examined whether PP2B activity is likely decreased in AD, which exhibits the most prevalent tauopathy. We confirmed down-regulation of PPP3CA and PPP3CB in the AD brains through qPCR (Figure 2-11). We also observed a similar inverse correlation between the PPP3CA levels and p-tau in AD (Figure 2-12). As we expected, not only the immunoreactivity of PPP3CA was decreased but tau protein also was hyperphosphorylated (S199, S396, S205/T208) in AD (Figure 2-13). Confocal microscopy showed that the immunoreactivity of PPP3CA was reduced but that the immunoreactivity of p-tau was elevated in AD (Figure 2-14). Interestingly, we also observed the colocalization of PPP3CA with p-tau (S202/T205) in peripheral foci of neurofibrillary tangles in the cortex of AD.

Inhibition of PPP3CA/PP2B activity leads to tau phosphorylation and tau aggregation

Following the confirmation of decreased PPP3CA activity and elevated tau phosphorylation in human CTE samples, we examined whether PPP3CA inhibition would be sufficient to increase tau phosphorylation and aggregation

using in vitro cell line models of tauopathy. To this end, we used Tau-BiFC cell lines (SH-SY5Y and HEK293), which enable the conventional fluorescence imaging of tau phosphorylation and aggregation (Figure 2-15). Three different PP2A/PPP3CA inhibitors (okadaic acid, cyclosporine A and deltamethrin) increased the level of tau phosphorylation in both SH-SY5Y and HEK293 Tau-BiFC cell lines (Figure 2-16). Okadaic acid and cyclosporine A treatment elevated the level of tau phosphorylation in a dose-dependent manner, whereas deltamethrin showed a declining trend after the threshold of 3μM. Similar results were observed in the HEK 293 cell line, with a higher intensity of tau phosphorylation due to okadaic acid (Figure 2-17).

PPP3CA directly regulates tau phosphorylation

After confirming the involvement of PPP3CA catalytic activity in the dephosphorylation of tau, we further verified whether PPP3CA directly modulates tau phosphorylation. Because GSK3β is a well-known kinase of tau, we overexpressed GSK3β with PPP3CA and tau and determined the level of phosphorylated tau. Whereas the overexpression of GSK3β elevated tau phosphorylation at S202/T205 and S214, the co-transfection of PPP3CA reversed the effects of GSK3β and decreased the level of phosphorylated tau in a dose-dependent manner (Figure 2-18). Regression analyses confirmed that the level of p-tau (S202/T205) was inversely correlated with the expression of PPP3CA (R=0.892; Figure 2-19). In addition, we examined whether the catalytic subunit of PPP3CA is necessary and sufficient to phosphorylate tau

(Figure 2-20). To this end, we transfected cells with a catalytic site deletion mutant of PPP3CA (PPP3CAdeltaCAT) and verified that tau dephosphorylation did not occur with this mutant. The data showed that the catalytic activity of PPP3CA is indispensable for the dephosphorylation of p-tau.

PPP3CA/PP2B modulates tau dephosphorylation in *in vivo* animal model of CTE

To verify whether the downregulation of PPP3CA affects, the phosphorylation of tau in vivo, we transduced adeno-associated viral (AAV) vectors containing shRNA for PPP3CA into hippocampal regions of tau (P301L) transgenic mouse brains and measured the difference in tau phosphorylation compared with the control after multiple weight-drop-induced head injuries (Figure 2-21). Consistent with the cellular model, the knockdown of PPP3CA using AAV-shPPP3CA markedly reduced the immunoreactivity of PPP3CA in the hippocampal regions of mice (Figure 2-22). Furthermore, the immunoreactivity of p-tau (S202/T205) was robustly increased in the dentate gyrus after exposure to weight drop-induced head injuries (Figure 2-23). The immunoreactivity of p-tau (S202/T205) was elevated in the region of PPP3CA knockdown using AAV-shPPP3CA, whereas p-tau (Ser202/Thr205) was not detected after AAV-shRNA control transduction.
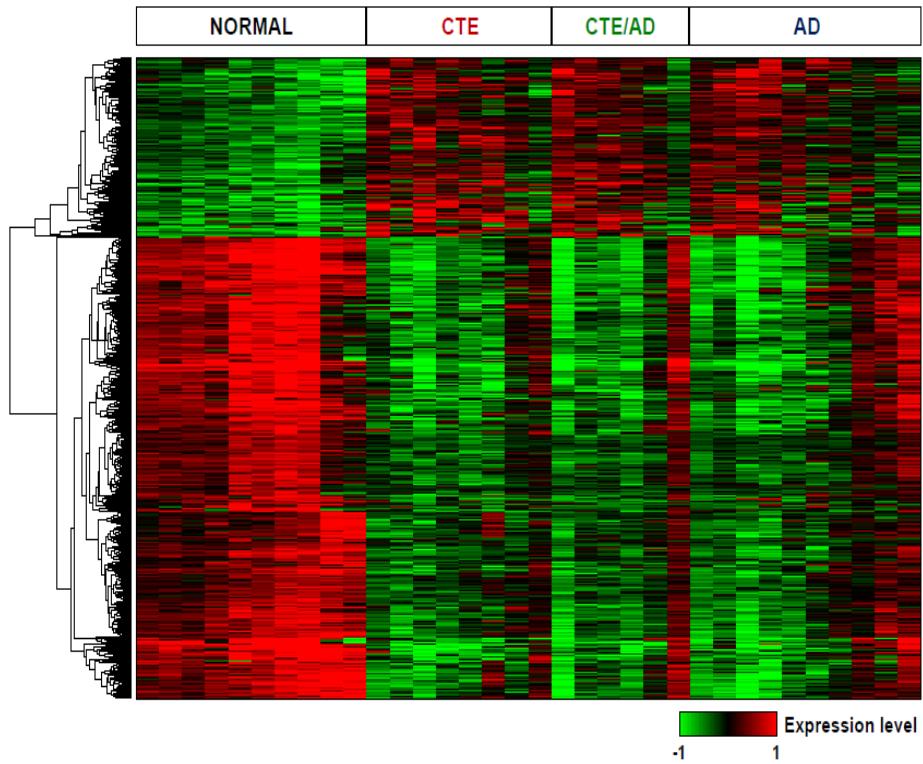
Figure 2-1. Expression patterns of 904 DEGs in blue module
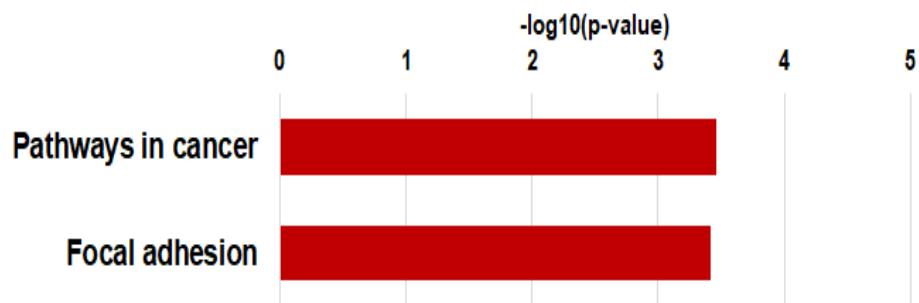
Figure 2-2. KEGG pathway analysis of up-regulated genes in blue module
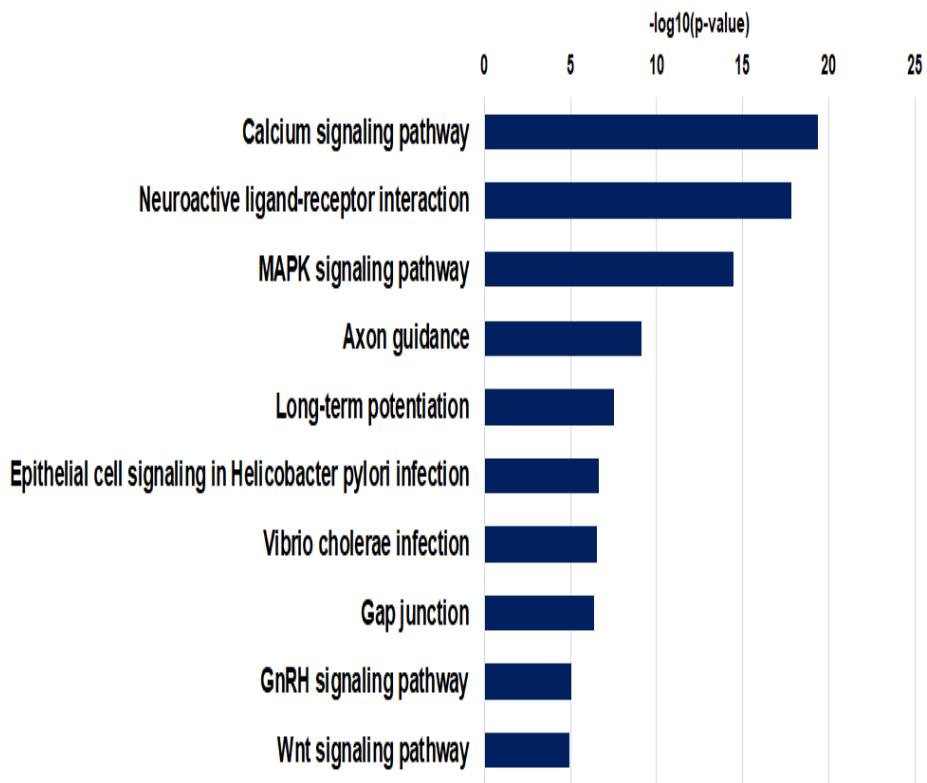
Figure 2-3. KEGG pathway analysis of down-regulated genes in blue module
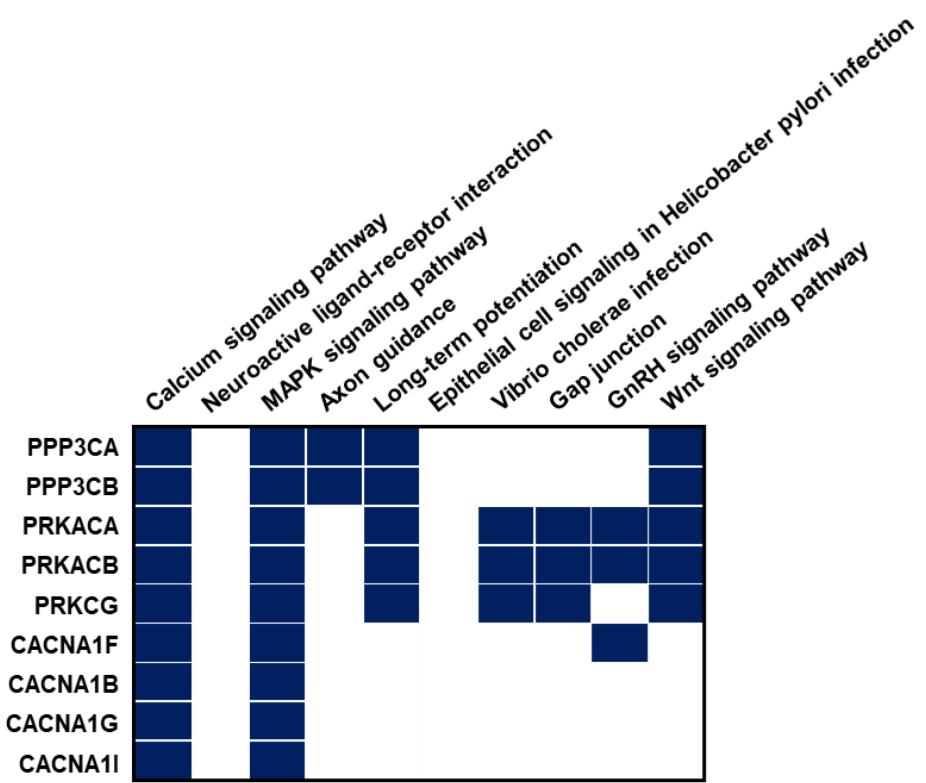
Figure 2-4. Gene list in down-regulated genes of calcium and MAPK signaling pathway in blue module
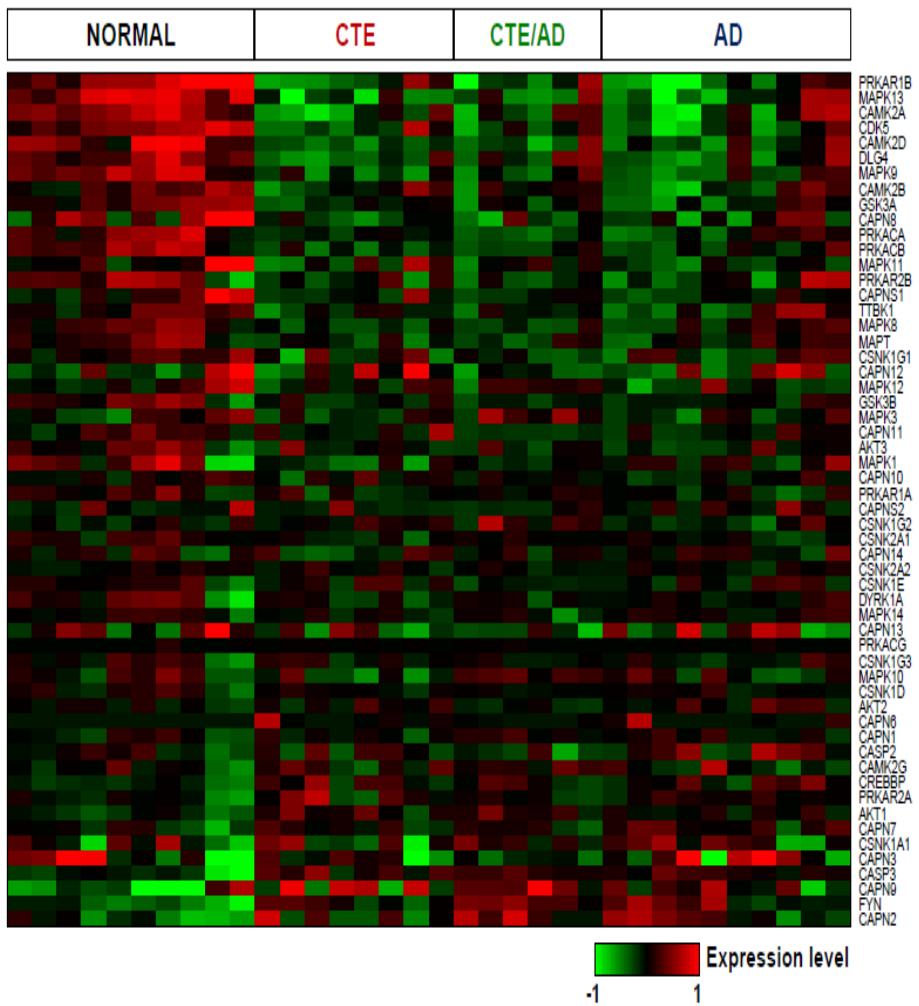
Figure 2-5. Heatpmap of tau phosphorylation-related kinase genes

Heatmap represents well-known kinase genes involved in tau phosphorylation.

Assigned module of each gene was represented by color.
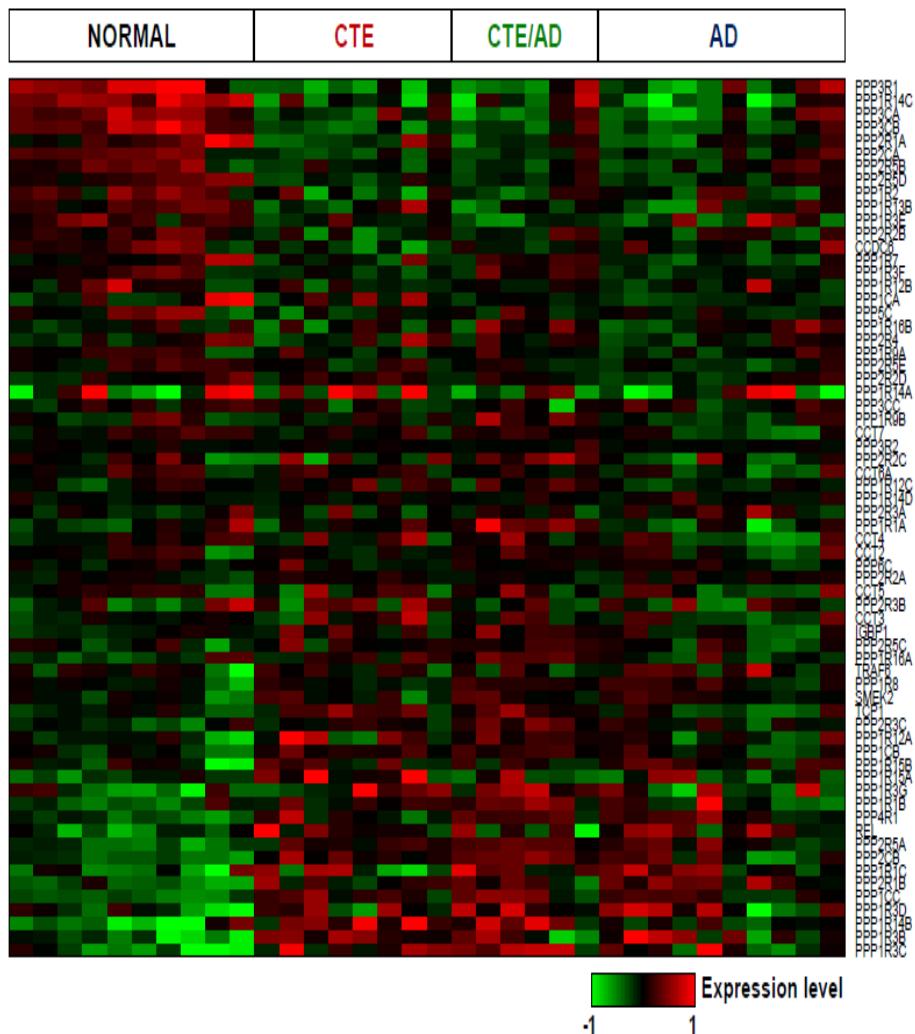
Figure 2-6. Heatpmap of tau phosphorylation –related phosphatase genes

Heatmap represents well-known phosphatase genes involved in tau phosphorylation. Assigned module of each gene was represented by color.
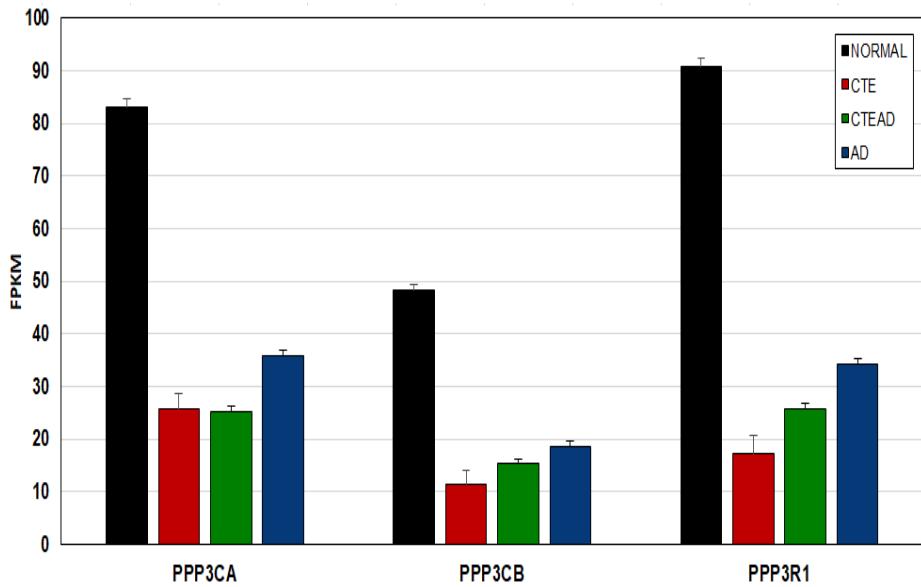
Figure 2-7. The FPKM levels of PPP3CA, PPP3CB and PPP3R1
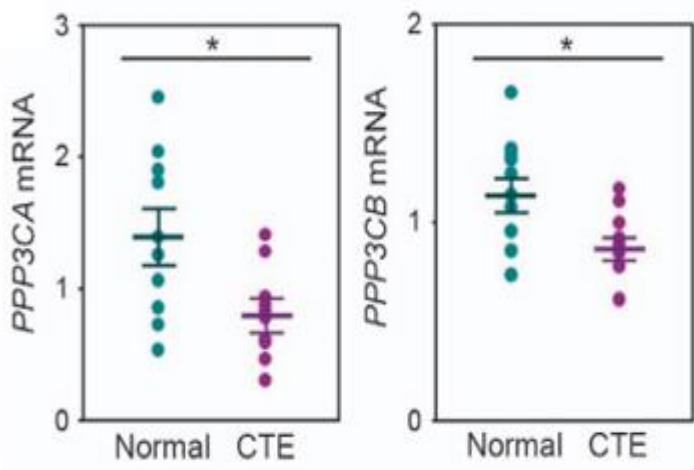
Figure 2-8. The mRNA levels of PPP3CA and PPP3CB in CTE
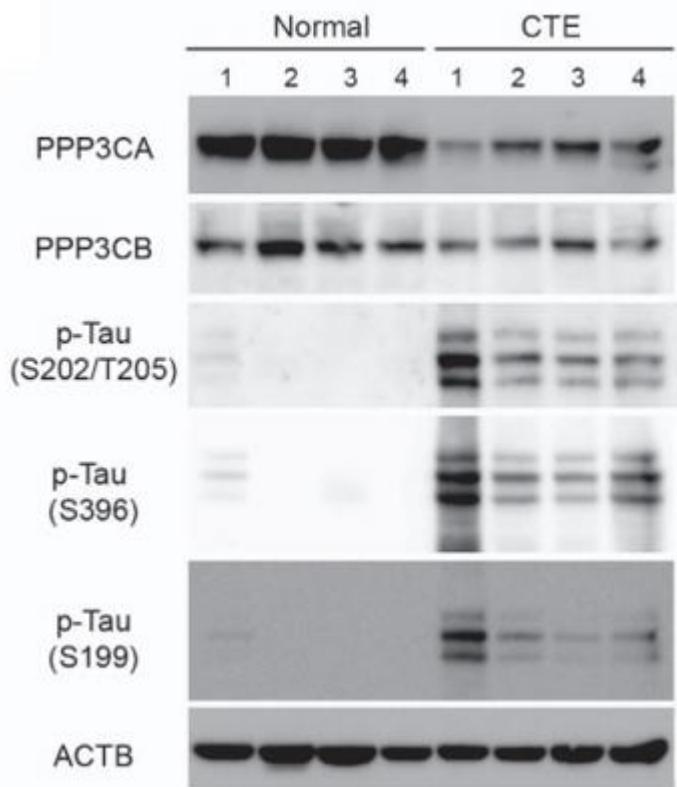
Figure 2-9. The protein levels of PPP3CA, PPP3CB and p-tau in CTE

Protein levels of PPP3CA and PPP3CB are reduced but levels of p-tau (S199, S202/T205 and S396) are elevated in CTE.
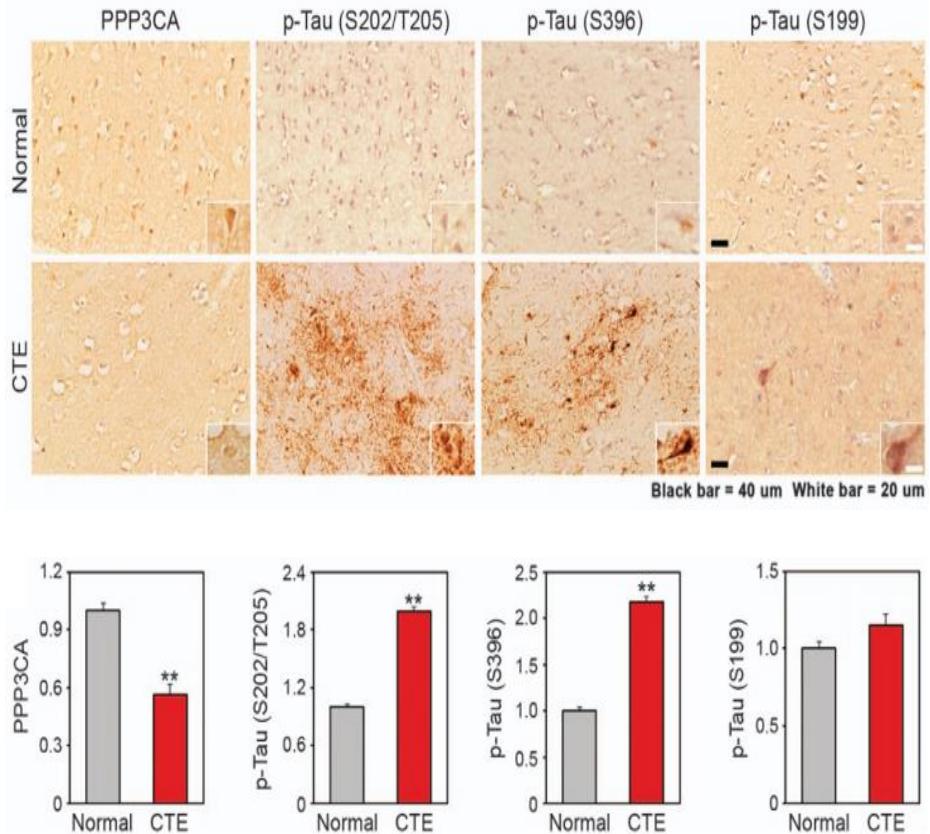
Figure 2-10. The immunoreactivity of PPP3CA and p-tau in CTE

The immunoreactivity of p-tau (Ser 396) is elevated while the immunoreactivity of PPP3CA is reduced in CTE. Scale bar: 20 μm; black, 40 μm. The densitometry analysis (of immunohistochemistry) shows that p-tau (S202/T205) is significantly increased, whereas the level of PPP3CA is reduced in CTE. Significantly different at **P < 0.001.
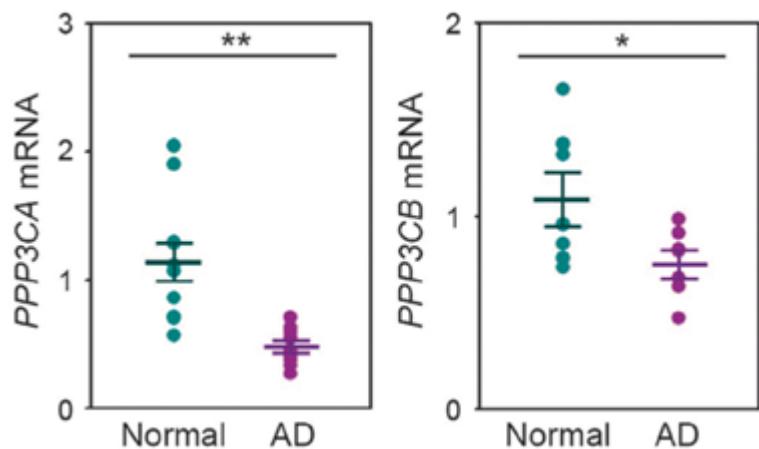
Figure 2-11. The mRNA levels of PPP3CA and PPP3CB in AD
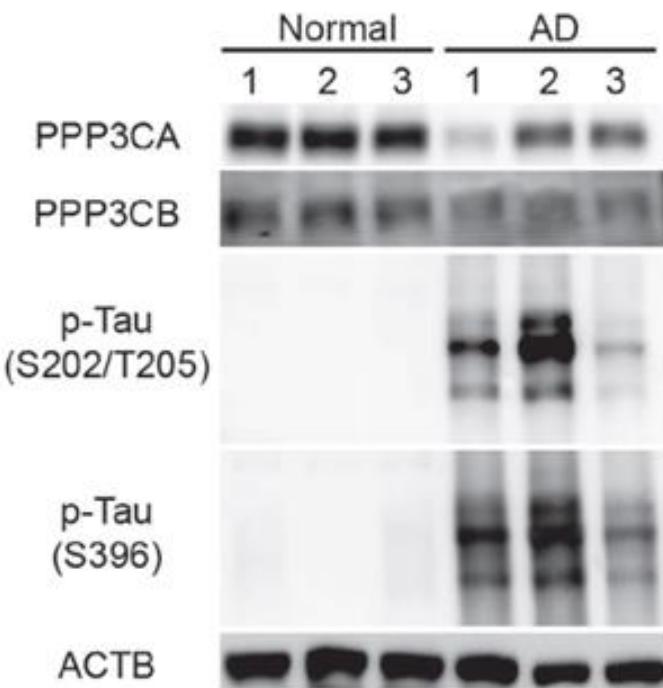
Figure 2-12. The protein levels of PPP3CA, PPP3CB and p-tau in AD

The levels of p-Tau are elevated in AD, while the protein levels of PPP3CA

and PPP3CB are reduced in AD.
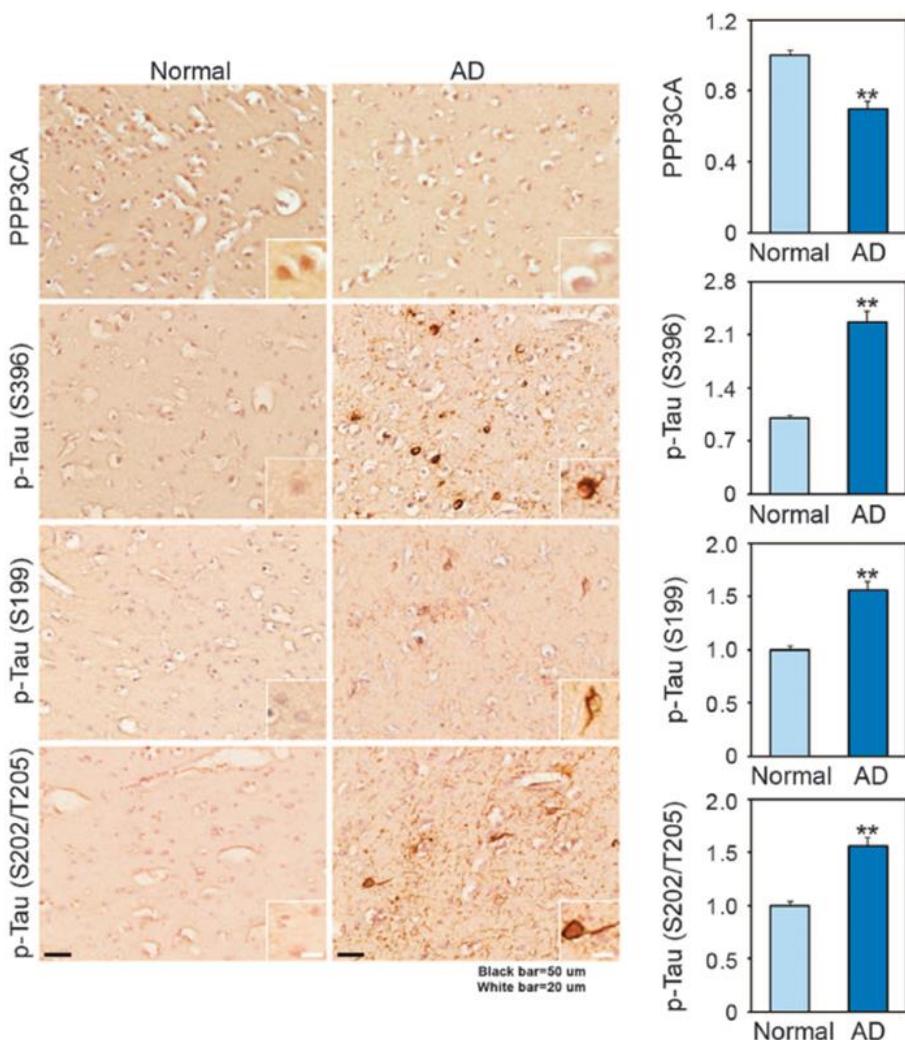
Figure 2-13. The immunoreactivity of PPP3CA and p-tau in AD

The immunoreactivity of PPP3CA is reduced in AD, while the immunoreactivity of p-Tau (S396, S199 and S202/T205) is enhanced in AD. Scale bar: 50 μm (black), 20 μm (white). The densitometry analysis (of immunohistochemistry) shows that p-tau (S202/T205) is significantly increased, whereas the level of PPP3CA is reduced in AD. Significantly different at **$P < 0.001$.
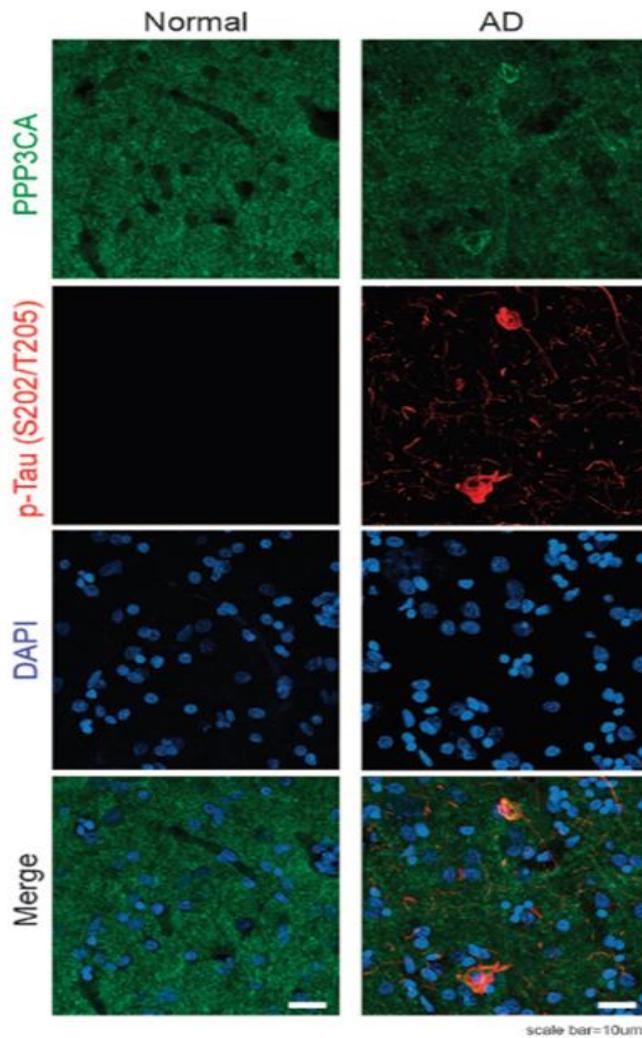
Figure 2-14. Confocal microscopy of PPP3CA and p-tau in AD

The fluorescence intensity of PPP3CA is decreased in the temporal cortex of AD, while the fluorescence intensity of p-tau (S202/T205) is increased. In part, the PPP3CA is colocalized with p-tau (S202/T205) in the peripheral foci of the p-tau tangles detected in the temporal cortex of AD. The nuclei were counterstained with DAPI. Scale bar: 10 μm (white). The PPP3CA enzyme activity is significantly reduced in AD.
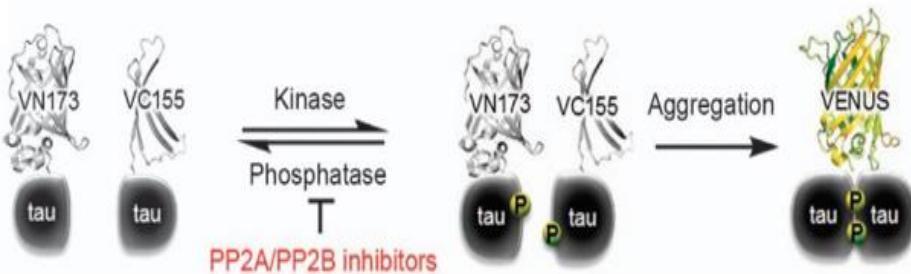
Figure 2-15. *In vitro* **cell line model of PP2B and p-tau**

Diagram of tau-BiFC maturation as an indication of tau aggregation. In tau-BiFC system, full-length tau is fused to non-fluorescent N- or C-terminal fragments of Venus fluorescence protein (VN173 or VC155), and both tau constructs were stably expressed in cells. Only when tau assembles, Venus protein could be matured, thereby activating its fluorescence signal.
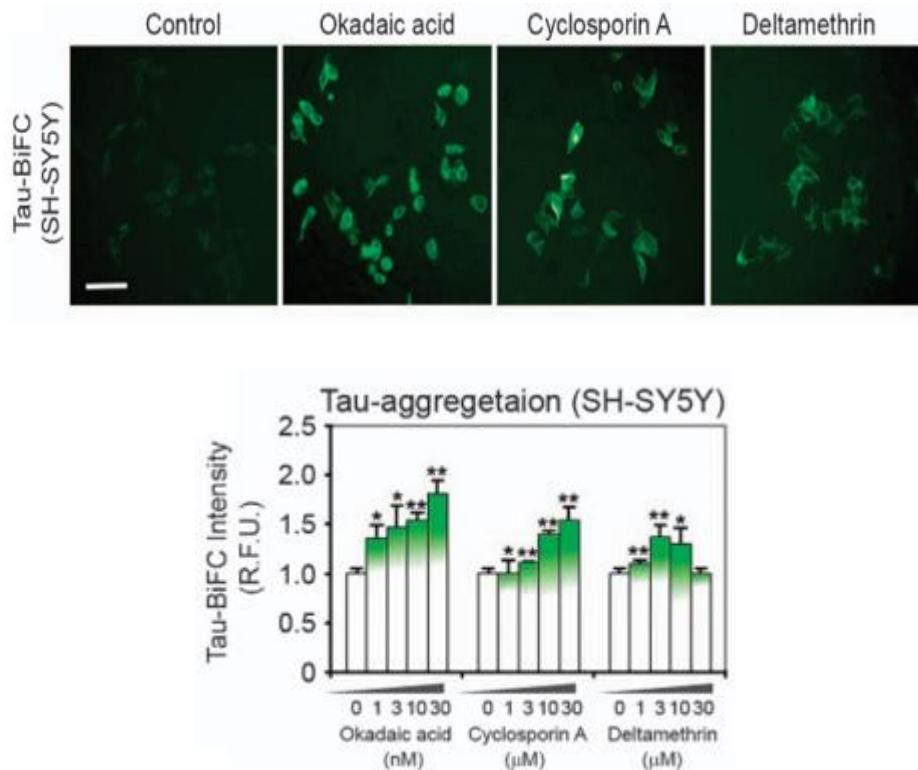
Figure 2-16. The SH-SY5Y tau-BiFC cell line analysis of PP2B and p-tau

PP2A/PP2B inhibitors induce tau aggregation in SH-SY5Y tau-BiFC cells. Cells were incubated with okadaic acid (OA; 30 nM), cyclosporine A (CsA; 30 μM) and deltamethrin (DM; 30 μM) for 29 h. Scale bar: 200 μm. Quantification of BiFC-fluorescence increases in SH-SY5Y tau-BiFC cells at various concentrations of protein phosphatase (PP) inhibitors.
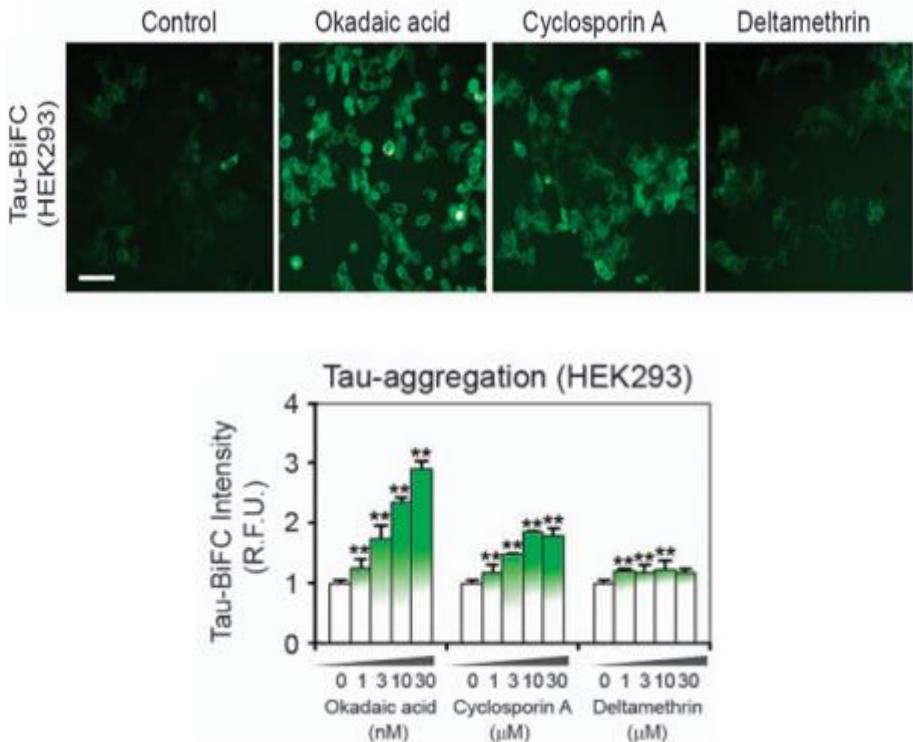
Figure 2-17. The HEK293 tau-BiFC cell line analysis of PP2B and p-tau

PP2A/PP2B inhibitors induce tau aggregation in HEK293 tau-BiFC cells. Cells were incubated with okadaic acid (OA; 30 nM), cyclosporine A (CsA; 30 μM) and deltamethrin (DM; 30 μM) for 29 h. Scale bar: 200 μm (white). Quantification of BiFC-fluorescence increases in HEK293 tau-BiFC cells at various concentrations of PP inhibitors. Significantly different at *P < 0.01; **P < 0.001.
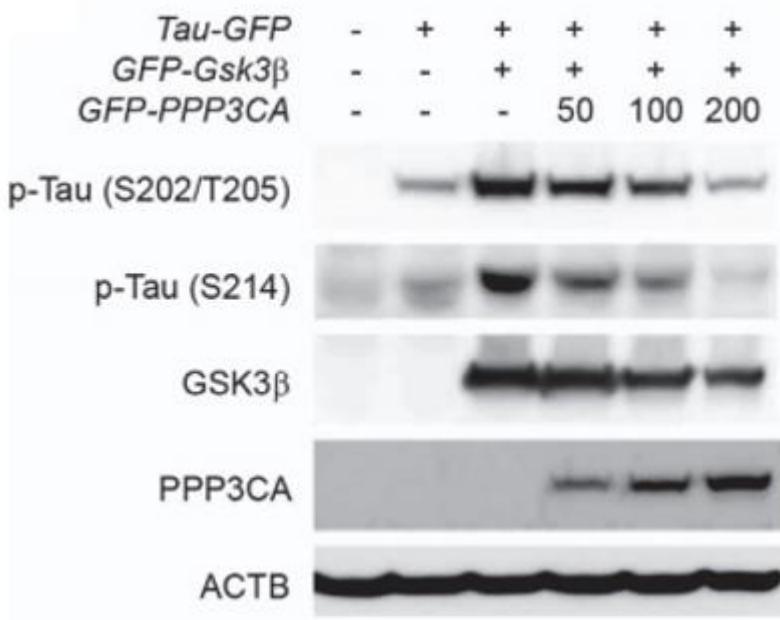
Figure 2-18. The western blot analysis of GSK3β, PPP3CA and p-tau

PPP3CA reduces the level of p-tau (Ser214, Ser202/Thr205) by through GSK3β

in a dose-dependent manner.
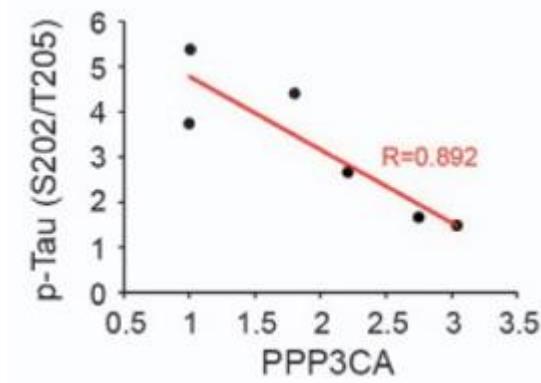
Figure 2-19. The levels of PPP3CA and p-tau

The level of phosphorylated tau is inversely correlated with the level of PPP3CA.
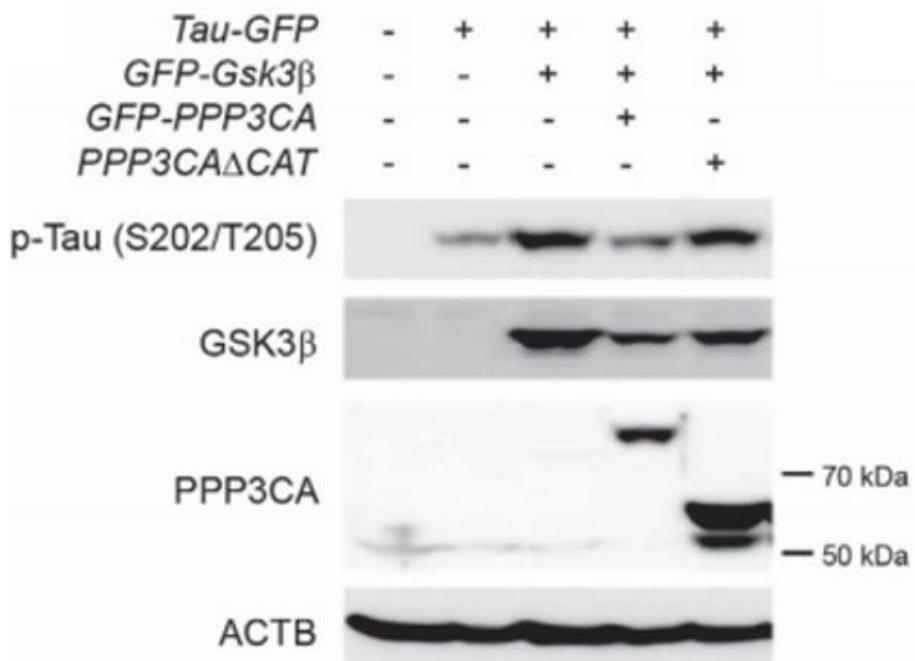
Figure 2-20. The western blot analysis of catalytic site of PPP3CA and p-tau

The catalytic site deletion mutant of PPP3CA (PPP3CAΔCat) did not reduce the level of p-tau (Ser202/Thr205
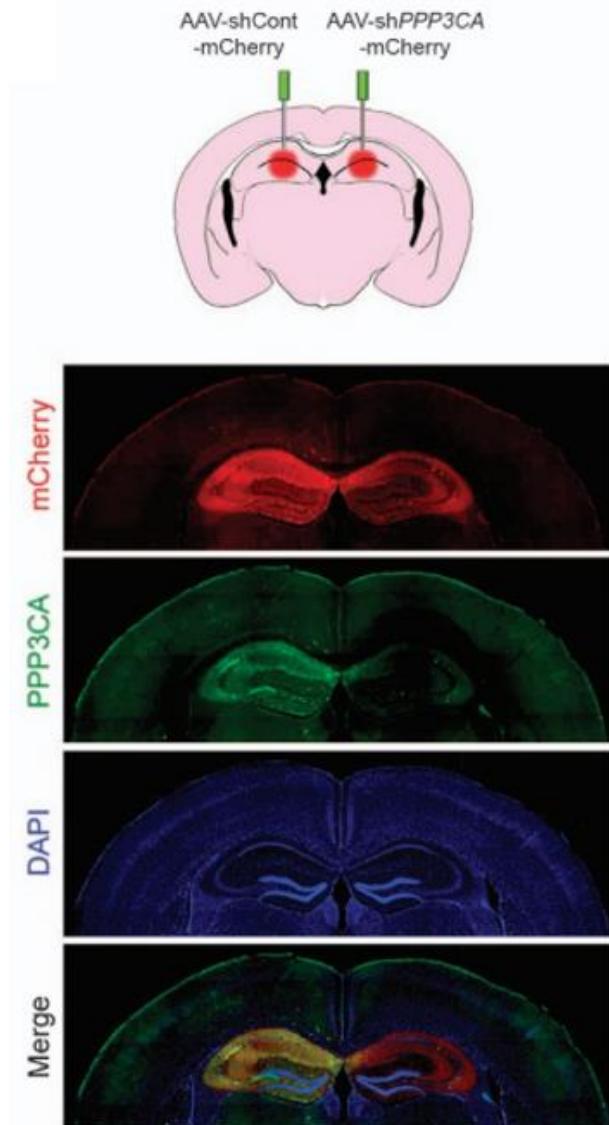
Figure 2-21. *In vivo* **animal model of AAV-shRNA injection**

The knockdown of PPP3CA/PPP3CA using shRNA increased the level of p-tau

(Ser202/Thr205).
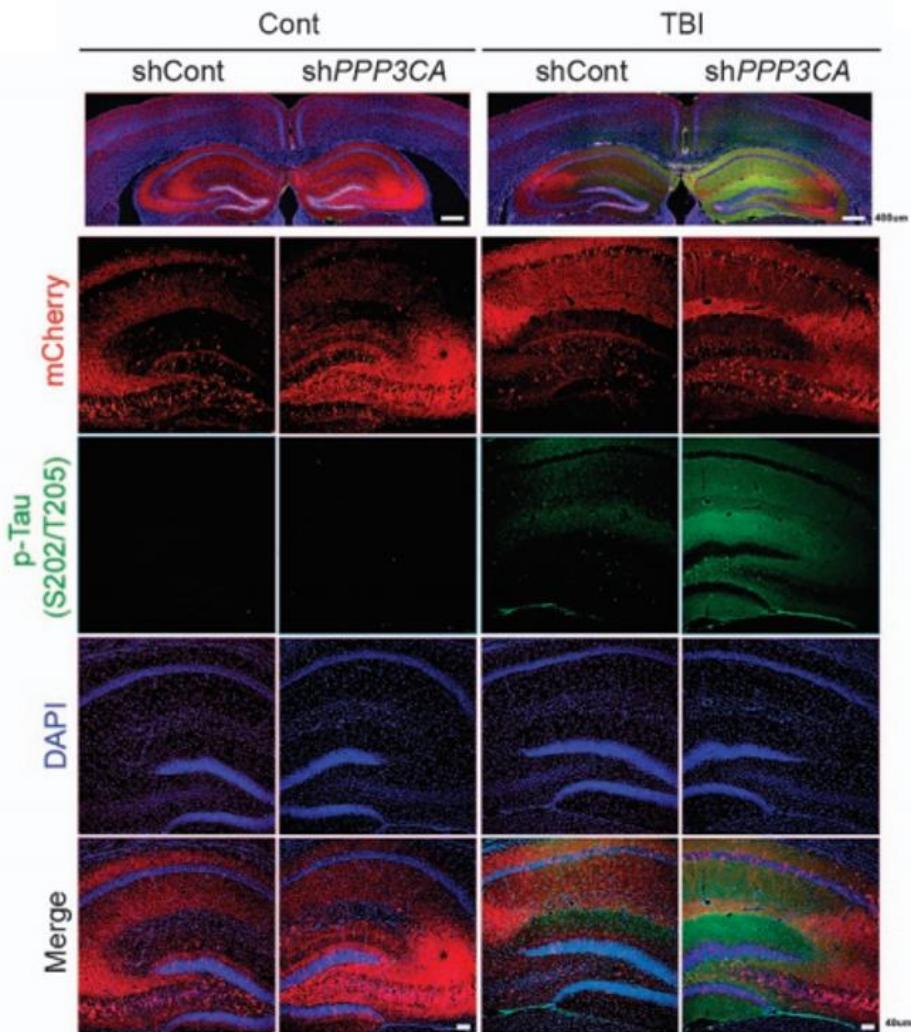
Figure 2-22. The level of p-tau in an animal model of TBI

Knock down of PPP3CA increases the level of p-tau (S202/T205) in an animal model of TBI. The level of p-tau (Ser202/Thr205) was increased by AAV-shRNA for PPP3CA in the hippocampal region of mouse brain but not by AAV-shRNA control in response to TBI.
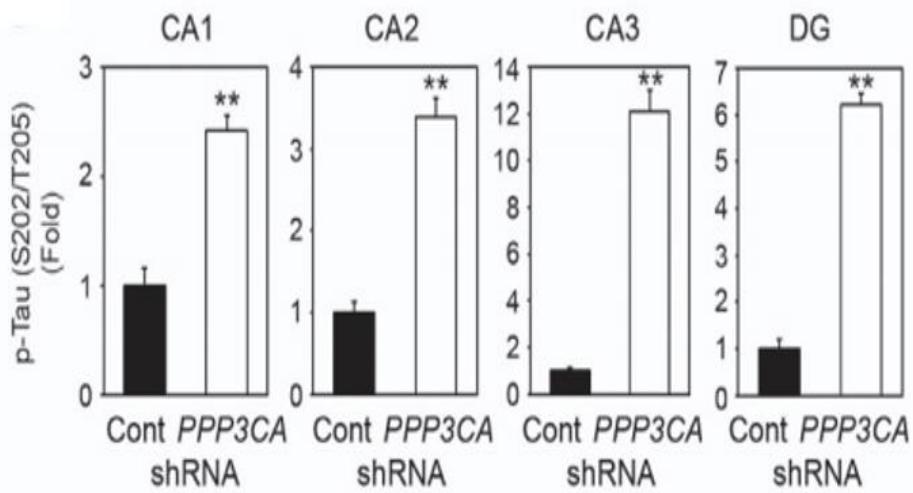
Figure 2-23. The p-tau levels of CA1, CA2, CA3 and DG

Densitometry analysis shows that the level of p-tau (Ser202/Thr205) is elevated

in CA1, CA2, CA3 and DG (dentate gyrus) upon TBI. The level of p-tau was

normalized to mCherry intensity. Significantly different at **P<0.001.
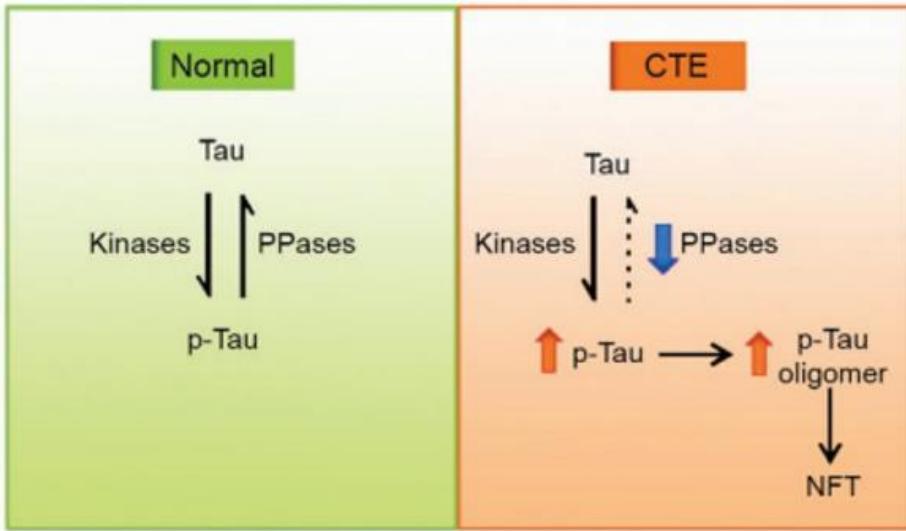
Figure 2-24. A proposed model of tauopathy promoted by deregulation of PP2B in CTE

A schematic illustrating that the deregulation of protein phosphatases increases the level of p-tau and p-tau oligomer formation and leads to pathological neurofilament tangle formation in chronic traumatic encephalopathy (CTE).

Discussion

Tau protein is a major protein constituent of neurofibrillary tangles and one of major pathological hallmarks of Alzheimer's disease (AD). Tauopathy is an aggregation of tau protein in neurofibrillary or gliofibrillary tangles in the brain, which seen in chronic traumatic encephalopathy, frontotemporal dementia, corticobasal syndrome as well as Alzheimer's diseases. In AD, tau pathology is seen as intra-neuronal neurofibrillary tangles of paired helical filaments sometimes admixed with straight filaments. Aggregates of abnormally hyperphosphorylated filaments are also seen in dystrophic neurites surrounding the β-amyloid plaque core [105].

CTE has an irregular pattern of accumulation of aberrantly phosphorylated tau in neurons and astroglia around small blood vessels at sulcal depths. In animal models, brain injury is sufficient to induce tau cleavage, acute and sustained aberrant tau phosphorylation and aggregation [106-108]. In addition, tau-based PET indicates that the temporal neocortex of most individuals over the age of 65 contain pathogenic tau [109]. In 2016, the first National Institute of Neurological Disorders and Stroke/National Institute of Biomedical Engineering and Bioengineering (NINDS/NIBIB) consensus meeting defined CTE as a clearly distinct neurodegenerative disease consisting of p-tau aggregates in neurons, astrocytes, and cell process around small vessels at the

depths of the cortical sulci [41]. However, peoples do not know what triggers the repetitive brain injury leads to CTE.

In this study, we focused on tauopathy, which is pathologically related by the accumulation of hyperphosphorylated tau and increased total tau and important pathological signs of TBI-related neurodegenerative diseases. We studied the gene expression changes of CTE, CTE/AD and AD through transcriptome sequencing analysis and shed a light on the mechanism of tauopathy.

We observed reduced expression of PPP3CA, PPP3CB, and PPP3R1 gene in post-mortem brain samples of CTE, CTE/AD and AD patients. PPP3CA is a catalytic subunit of calcineurin (PP2B), which dephosphorylates tau, whose dysfunction has been implicated in the generation of both amyloid precursor protein and hyperphosphorylated tau, the two hallmarks of AD pathology [110]. Previous studies have shown that the excitotoxin-induced dysfunction of serine/threonine PP activity induces tau phosphorylation in human neurons and that the down-regulation of calcineurin (PPP3CA) causes tau hyperphosphorylation in Huntington's disease mouse model brains [20, 111, 112].

To test whether PP2B are associated with tauopathy, we conducted three molecular experimental systems in vitro and in vivo [2]. mRNA quantification by qPCR showed that mRNA levels of PPP3CA (α isoform of PP2B catalytic subunit) and PPP3CB (β isoform of PP2B catalytic subunit) are reduced in CTE

and AD. We confirmed the protein levels of PP2B are reduced but p-tau levels are elevated in CTE and AD through western blot and immunohistochemical staining. We also found that inhibition of PP2B activity leads to tau phosphorylation and tau aggregation in *in vitro* cell line model. In weight-drop TBI animal model, multiple TBI impairs PP2B activity and results in the elevation of hyperphosphorylated tau and the formation of neurofilament tangle in neurons. We concluded that downregulation of PP2B increases the level of p-tau and p-tau oligomer formation and leads to pathological neurofilament tangle formation in CTE and AD (Figure 2-24).

Together, these findings show that alteration of protein phosphatase expression likely contribute to tauopathy in CTE and AD. This study further suggests and insight that modulation of serine/threonine protein phosphatase expression and activity could be a potential therapeutic strategy for preventing tauopathy in TBI-related neurodegenerative diseases.

General Discussion

Comprehensive transcriptome analysis of TBI-related neurodegenerative diseases
(8 CTE, 6 CTE/AD, 10 AD, 10 NORMAL)

Common transcriptome features of CTE, CTE/AD and AD

Unique transcriptome features of CTE compared with CTE/AD and AD

↓ PPP3CA, PPP3CB

-> ↑ Tau hyperphosphorylation

-> ↑ Neurofibrillary tangles

-> Tauopathy

↓ Synaptotagmin
(SYT1, SYT4, SYT5, SYT7, SYT13)

-> ↓ Synaptic transmission

-> ↓ Memory function

↑ Cell adhesion molecules
(HLA-B, HLA-C, HLA-E)

↑ Ribosome

In the first part, we found a common or unique transcriptome signature of TBI-related neurodegenerative disorders. CTE has long been recognized as sharing some similar neuropathological features with AD, mainly the presence of neurofibrillary tangles and hyperphosphorylated tau, but it also has distinct characteristics from AD including disease progression. In addition, like many neurodegenerative diseases, CTE is also often associated with comorbid pathologies [26, 40, 42, 113]. For a comprehensive understanding of CTE, we conducted transcriptome sequencing analysis of CTE and AD. We found changed expressions of synaptic transmission- and memory function-related genes in CTE, CTE/AD and AD. The unique transcriptome signature of CTE was up-regulation of cell adhesion modules. Thus, this study provides new insights to understand genetic signatures of TBI-related disorders.

In the second part, we tried to reveal the mechanisms of how TBI causes neuropathological sequelae of tauopathy in CTE, CTE/AD and AD. Previous studies of TBI-related diseases used blood samples or animal samples, which is not enough to fully understand of CTE, CTE/AD and AD. To overcome this limitation, we used gene co-expression network analysis of RNA expression data of post-mortem CTE, CTE/AD and AD samples to investigate genes known to be associated with tauopathy. We found protein phosphatase 2B (PP2B) genes, such as PP2B catalytic subunits (PPP3CA, PPP3CB) and regulatory subunits (PPP3R1), are significantly down-regulated in CTE brains. PP2B is known as calcineurin, which is activated by Ca^{2+} occupancy on B subunit and calmodulin binding to autoinhibitory domain. We confirmed that the elevation of p-tau inversely correlated with PP2B activity in both cellular and animal model of CTE and AD. This study showed that alteration in PP2B expression likely contribute to tauopathy in CTE and AD, which suggests that modulating protein phosphatase activity could be a potential therapeutic targets for preventing progressive tauopathy in TBI-related neurodegenerative diseases.

In summary, our findings suggest new diagnostic targets and biomarker candidates for TBI-related diseases diagnostic development and therapeutic intervention.

References

1. Cho, H., et al., *Alterations of transcriptome signatures in head trauma-related neurodegenerative disorders.* Sci Rep, 2020. **10**(1): p. 8811.

2. Seo, J.S., et al., *Transcriptome analyses of chronic traumatic encephalopathy show alterations in protein phosphatase expression associated with tauopathy.* Exp Mol Med, 2017. **49**(5): p. e333.

3. Reis-Filho, J.S., *Next-generation sequencing.* Breast Cancer Res, 2009. **11 Suppl 3**: p. S12.

4. Sanger, F. and A.R. Coulson, *A rapid method for determining sequences in DNA by primed synthesis with DNA polymerase.* J Mol Biol, 1975. **94**(3): p. 441-8.

5. Sanger, F., S. Nicklen, and A.R. Coulson, *DNA sequencing with chain-terminating inhibitors.* Proc Natl Acad Sci U S A, 1977. **74**(12): p. 5463-7.

6. Metzker, M.L., *Sequencing technologies - the next generation.* Nat Rev Genet, 2010. **11**(1): p. 31-46.

7. Bayes, M., S. Heath, and I.G. Gut, *Applications of second generation sequencing technologies in complex disorders.* Curr Top Behav Neurosci, 2012. **12**: p. 321-43.

8. Meynert, A.M., et al., *Variant detection sensitivity and biases in whole genome and exome sequencing.* BMC Bioinformatics, 2014. **15**: p. 247.

9.   Ozsolak, F. and P.M. Milos, *RNA sequencing: advances, challenges and opportunities.* Nat Rev Genet, 2011. **12**(2): p. 87-98.

10.   Rabbani, B., M. Tekin, and N. Mahdieh, *The promise of whole-exome sequencing in medical genetics.* J Hum Genet, 2014. **59**(1): p. 5-15.

11.   Farlik, M., et al., *Single-cell DNA methylome sequencing and bioinformatic inference of epigenomic cell-state dynamics.* Cell Rep, 2015. **10**(8): p. 1386-97.

12.   Hirst, M., *Epigenomics: sequencing the methylome.* Methods Mol Biol, 2013. **973**: p. 39-54.

13.   Buee, L., et al., *Tau protein isoforms, phosphorylation and role in neurodegenerative disorders.* Brain Res Brain Res Rev, 2000. **33**(1): p. 95-130.

14.   Cripps, D., et al., *Alzheimer disease-specific conformation of hyperphosphorylated paired helical filament-Tau is polyubiquitinated through Lys-48, Lys-11, and Lys-6 ubiquitin conjugation.* J Biol Chem, 2006. **281**(16): p. 10825-38.

15.   Lee, V.M., M. Goedert, and J.Q. Trojanowski, *Neurodegenerative tauopathies.* Annu Rev Neurosci, 2001. **24**: p. 1121-59.

16.   Lee, G. and C.J. Leugers, *Tau and tauopathies.* Prog Mol Biol Transl Sci, 2012. **107**: p. 263-93.

17.   Povova, J., et al., *Epidemiological of and risk factors for Alzheimer's disease: a review.* Biomed Pap Med Fac Univ Palacky Olomouc Czech Repub, 2012. **156**(2): p. 108-14.

18.   Hanger, D.P., B.H. Anderton, and W. Noble, *Tau phosphorylation: the*

therapeutic challenge for neurodegenerative disease. Trends Mol Med, 2009. **15**(3): p. 112-9.

19.   Martin, L., X. Latypova, and F. Terro, *Post-translational modifications of tau protein: implications for Alzheimer's disease.* Neurochem Int, 2011. **58**(4): p. 458-71.

20.   Liu, F., et al., *Contributions of protein phosphatases PP1, PP2A, PP2B and PP5 to the regulation of tau phosphorylation.* Eur J Neurosci, 2005. **22**(8): p. 1942-50.

21.   Liu, F., et al., *Dephosphorylation of tau by protein phosphatase 5: impairment in Alzheimer's disease.* J Biol Chem, 2005. **280**(3): p. 1790-6.

22.   Stein, T.D., V.E. Alvarez, and A.C. McKee, *Concussion in Chronic Traumatic Encephalopathy.* Curr Pain Headache Rep, 2015. **19**(10): p. 47.

23.   Tartaglia, M.C., et al., *Chronic traumatic encephalopathy and other neurodegenerative proteinopathies.* Front Hum Neurosci, 2014. **8**: p. 30.

24.   Thurman, D.J., C.M. Branche, and J.E. Sniezek, *The epidemiology of sports-related traumatic brain injuries in the United States: recent developments.* J Head Trauma Rehabil, 1998. **13**(2): p. 1-8.

25.   Hof, P.R., et al., *Neuropathological observations in a case of autism presenting with self-injury behavior.* Acta Neuropathol, 1991. **82**(4): p. 321-6.

26.   McKee, A.C., et al., *The spectrum of disease in chronic traumatic*

encephalopathy. Brain, 2013. **136**(Pt 1): p. 43-64.

27.   McKee, A.C., et al., *The neuropathology of chronic traumatic encephalopathy.* Brain Pathol, 2015. **25**(3): p. 350-64.

28.   Gavett, B.E., R.A. Stern, and A.C. McKee, *Chronic traumatic encephalopathy: a potential late effect of sport-related concussive and subconcussive head trauma.* Clin Sports Med, 2011. **30**(1): p. 179-88, xi.

29.   McKee, A.C., et al., *Chronic traumatic encephalopathy in athletes: progressive tauopathy after repetitive head injury.* J Neuropathol Exp Neurol, 2009. **68**(7): p. 709-35.

30.   Braak, H. and E. Braak, *Staging of Alzheimer-related cortical destruction.* Int Psychogeriatr, 1997. **9 Suppl 1**: p. 257-61; discussion 269-72.

31.   Stern, R.A., et al., *Long-term consequences of repetitive brain trauma: chronic traumatic encephalopathy.* PM R, 2011. **3**(10 Suppl 2): p. S460-7.

32.   Prince, M., et al., *The global prevalence of dementia: a systematic review and metaanalysis.* Alzheimers Dement, 2013. **9**(1): p. 63-75 e2.

33.   Korolev, I.O., *Alzheimer's disease : a clinical and basic review.* Medical Student Research Journal, 2014.

34.   Forstl, H. and A. Kurz, *Clinical features of Alzheimer's disease.* Eur Arch Psychiatry Clin Neurosci, 1999. **249**(6): p. 288-90.

35.   Bendlin, B.B., et al., *Midlife predictors of Alzheimer's disease.* Maturitas, 2010. **65**(2): p. 131-7.

36. Head, E., et al., *Alzheimer's Disease in Down Syndrome.* Eur J Neurodegener Dis, 2012. **1**(3): p. 353-364.

37. Sivanandam, T.M. and M.K. Thakur, *Traumatic brain injury: a risk factor for Alzheimer's disease.* Neurosci Biobehav Rev, 2012. **36**(5): p. 1376-81.

38. Loane, D.J., et al., *Amyloid precursor protein secretases as therapeutic targets for traumatic brain injury.* Nat Med, 2009. **15**(4): p. 377-9.

39. Johnson, V.E., W. Stewart, and D.H. Smith, *Traumatic brain injury and amyloid-beta pathology: a link to Alzheimer's disease?* Nat Rev Neurosci, 2010. **11**(5): p. 361-70.

40. Mez, J., et al., *Clinicopathological Evaluation of Chronic Traumatic Encephalopathy in Players of American Football.* JAMA, 2017. **318**(4): p. 360-370.

41. McKee, A.C., et al., *The first NINDS/NIBIB consensus meeting to define neuropathological criteria for the diagnosis of chronic traumatic encephalopathy.* Acta Neuropathol, 2016. **131**(1): p. 75-86.

42. Stein, T.D., V.E. Alvarez, and A.C. McKee, *Chronic traumatic encephalopathy: a spectrum of neuropathological changes following repetitive brain trauma in athletes and military personnel.* Alzheimers Res Ther, 2014. **6**(1): p. 4.

43. Tokuda, T., et al., *Re-examination of ex-boxers' brains using immunohistochemistry with antibodies to amyloid beta-protein and tau protein.* Acta Neuropathol, 1991. **82**(4): p. 280-5.

44. Hof, P.R., et al., *Differential distribution of neurofibrillary tangles in*

the cerebral cortex of dementia pugilistica and Alzheimer's disease cases. Acta Neuropathol, 1992. **85**(1): p. 23-30.

45.   Baugh, C.M., et al., *Current understanding of chronic traumatic encephalopathy.* Curr Treat Options Neurol, 2014. **16**(9): p. 306.

46.   Iverson, G.L., et al., *A critical review of chronic traumatic encephalopathy.* Neurosci Biobehav Rev, 2015. **56**: p. 276-93.

47.   McKee, A.C., et al., *The neuropathology of sport.* Acta Neuropathol, 2014. **127**(1): p. 29-51.

48.   Baugh, C.M., et al., *Chronic traumatic encephalopathy: neurodegeneration following repetitive concussive and subconcussive brain trauma.* Brain Imaging Behav, 2012. **6**(2): p. 244-54.

49.   Turner, R.C., et al., *Alzheimer's disease and chronic traumatic encephalopathy: Distinct but possibly overlapping disease entities.* Brain Inj, 2016. **30**(11): p. 1279-1292.

50.   Schmidt, M.L., et al., *Tau isoform profile and phosphorylation state in dementia pugilistica recapitulate Alzheimer's disease.* Acta Neuropathol, 2001. **101**(5): p. 518-24.

51.   Dobin, A., et al., *STAR: ultrafast universal RNA-seq aligner.* Bioinformatics, 2013. **29**(1): p. 15-21.

52.   Anders, S., P.T. Pyl, and W. Huber, *HTSeq--a Python framework to work with high-throughput sequencing data.* Bioinformatics, 2015. **31**(2): p. 166-9.

53.   Darmanis, S., et al., *A survey of human brain transcriptome diversity at the single cell level.* Proc Natl Acad Sci U S A, 2015. **112**(23): p.

7285-90.

54.   Wang, M., et al., *Integrative network analysis of nineteen brain regions identifies molecular signatures and networks underlying selective regional vulnerability to Alzheimer's disease.* Genome Med, 2016. **8**(1): p. 104.

55.   Love, M.I., W. Huber, and S. Anders, *Moderated estimation of fold change and dispersion for RNA-seq data with DESeq2.* Genome Biol, 2014. **15**(12): p. 550.

56.   Subramanian, A., et al., *Gene set enrichment analysis: a knowledge-based approach for interpreting genome-wide expression profiles.* Proc Natl Acad Sci U S A, 2005. **102**(43): p. 15545-50.

57.   Langfelder, P. and S. Horvath, *WGCNA: an R package for weighted correlation network analysis.* BMC Bioinformatics, 2008. **9**: p. 559.

58.   Lee, J., et al., *Epigenetic regulation of cholinergic receptor M1 (CHRM1) by histone H3K9me3 impairs Ca(2+) signaling in Huntington's disease.* Acta Neuropathol, 2013. **125**(5): p. 727-39.

59.   Jo, S., et al., *GABA from reactive astrocytes impairs memory in mouse models of Alzheimer's disease.* Nat Med, 2014. **20**(8): p. 886-96.

60.   Mukhin, V.N., Pavlov, K.I. & Klimenko, V.M., *Mechanisms of Neuron Loss in Alzheimer's Disease.* Neurosci Behav Physi, 2017. **47**(5): p. 508-516.

61.   Verkhratsky, A., et al., *Astrocytes in Alzheimer's disease.* Neurotherapeutics, 2010. **7**(4): p. 399-412.

62.   Cai, Z. and M. Xiao, *Oligodendrocytes and Alzheimer's disease.* Int J

Neurosci, 2016. **126**(2): p. 97-104.

63.   Li, Q. and B.A. Barres, *Microglia and macrophages in brain homeostasis and disease.* Nat Rev Immunol, 2018. **18**(4): p. 225-242.

64.   Salter, M.W. and B. Stevens, *Microglia emerge as central players in brain disease.* Nat Med, 2017. **23**(9): p. 1018-1027.

65.   Mandrekar-Colucci, S. and G.E. Landreth, *Microglia and inflammation in Alzheimer's disease.* CNS Neurol Disord Drug Targets, 2010. **9**(2): p. 156-67.

66.   Hansen, D.V., J.E. Hanson, and M. Sheng, *Microglia in Alzheimer's disease.* J Cell Biol, 2018. **217**(2): p. 459-472.

67.   Bomboi, G., et al., *Alzheimer's disease and endothelial dysfunction.* Neurol Sci, 2010. **31**(1): p. 1-8.

68.   Tampellini, D., *Synaptic activity and Alzheimer's disease: a critical update.* Front Neurosci, 2015. **9**: p. 423.

69.   Marcello, E., et al., *Synaptic dysfunction in Alzheimer's disease.* Adv Exp Med Biol, 2012. **970**: p. 573-601.

70.   Ahmad, M., et al., *Postsynaptic complexin controls AMPA receptor exocytosis during LTP.* Neuron, 2012. **73**(2): p. 260-7.

71.   Wu, D., et al., *Postsynaptic synaptotagmins mediate AMPA receptor exocytosis during LTP.* Nature, 2017. **544**(7650): p. 316-321.

72.   Dean, C., et al., *Synaptotagmin-IV modulates synaptic function and long-term potentiation by regulating BDNF release.* Nat Neurosci, 2009. **12**(6): p. 767-76.

73.   Lisman, J., R. Yasuda, and S. Raghavachari, *Mechanisms of CaMKII*

action in long-term potentiation. Nat Rev Neurosci, 2012. **13**(3): p. 169-82.

74.   Lisman, J., H. Schulman, and H. Cline, *The molecular basis of CaMKII function in synaptic and behavioural memory.* Nat Rev Neurosci, 2002. **3**(3): p. 175-90.

75.   Barria, A., V. Derkach, and T. Soderling, *Identification of the Ca2+/calmodulin-dependent protein kinase II regulatory phosphorylation site in the alpha-amino-3-hydroxyl-5-methyl-4-isoxazole-propionate-type glutamate receptor.* J Biol Chem, 1997. **272**(52): p. 32727-30.

76.   Giese, K.P., et al., *Autophosphorylation at Thr286 of the alpha calcium-calmodulin kinase II in LTP and learning.* Science, 1998. **279**(5352): p. 870-3.

77.   Mammen, A.L., et al., *Phosphorylation of the alpha-amino-3-hydroxy-5-methylisoxazole4-propionic acid receptor GluR1 subunit by calcium/calmodulin-dependent kinase II.* J Biol Chem, 1997. **272**(51): p. 32528-33.

78.   Lu, W., et al., *Synaptic targeting of AMPA receptors is regulated by a CaMKII site in the first intracellular loop of GluA1.* Proc Natl Acad Sci U S A, 2010. **107**(51): p. 22266-71.

79.   Silva, A.J., et al., *Deficient hippocampal long-term potentiation in alpha-calcium-calmodulin kinase II mutant mice.* Science, 1992. **257**(5067): p. 201-6.

80.   Yang, H.W., et al., *Roles of CaMKII, PKA, and PKC in the induction*

and maintenance of LTP of C-fiber-evoked field potentials in rat spinal dorsal horn. J Neurophysiol, 2004. **91**(3): p. 1122-33.

81.   Chakravarthy, B., P. Morley, and J. Whitfield, *Ca2+-calmodulin and protein kinase Cs: a hypothetical synthesis of their conflicting convergences on shared substrate domains.* Trends Neurosci, 1999. **22**(1): p. 12-6.

82.   Colley, P.A., F.S. Sheu, and A. Routtenberg, *Inhibition of protein kinase C blocks two components of LTP persistence, leaving initial potentiation intact.* J Neurosci, 1990. **10**(10): p. 3353-60.

83.   Linden, D.J. and A. Routtenberg, *The role of protein kinase C in long-term potentiation: a testable model.* Brain Res Brain Res Rev, 1989. **14**(3): p. 279-96.

84.   Chen, L. and L.Y. Huang, *Protein kinase C reduces Mg2+ block of NMDA-receptor channels as a mechanism of modulation.* Nature, 1992. **356**(6369): p. 521-3.

85.   MacDonald, J.F., et al., *Convergence of PKC-dependent kinase signal cascades on NMDA receptors.* Curr Drug Targets, 2001. **2**(3): p. 299-312.

86.   Roche, K.W., et al., *Characterization of multiple phosphorylation sites on the AMPA receptor GluR1 subunit.* Neuron, 1996. **16**(6): p. 1179-88.

87.   Correia, S.S., et al., *Protein kinase C gamma associates directly with the GluR4 alpha-amino-3-hydroxy-5-methyl-4-isoxazole propionate receptor subunit. Effect on receptor phosphorylation.* J Biol Chem, 2003. **278**(8): p. 6307-13.

88.   Abeliovich, A., et al., *Modified hippocampal long-term potentiation in PKC gamma-mutant mice.* Cell, 1993. **75**(7): p. 1253-62.

89.   Abeliovich, A., et al., *PKC gamma mutant mice exhibit mild deficits in spatial and contextual learning.* Cell, 1993. **75**(7): p. 1263-71.

90.   Chater, T.E. and Y. Goda, *The role of AMPA receptors in postsynaptic mechanisms of synaptic plasticity.* Front Cell Neurosci, 2014. **8**: p. 401.

91.   Esteban, J.A., et al., *PKA phosphorylation of AMPA receptor subunits controls synaptic trafficking underlying plasticity.* Nat Neurosci, 2003. **6**(2): p. 136-43.

92.   Murray, P., G. Frampton, and P.N. Nelson, *Cell adhesion molecules. Sticky moments in the clinic.* BMJ, 1999. **319**(7206): p. 332-4.

93.   Sakisaka, T. and Y. Takai, *Cell adhesion molecules in the CNS.* J Cell Sci, 2005. **118**(Pt 23): p. 5407-10.

94.   Togashi, H., T. Sakisaka, and Y. Takai, *Cell adhesion molecules in the central nervous system.* Cell Adh Migr, 2009. **3**(1): p. 29-35.

95.   Cebrian, C., J.D. Loike, and D. Sulzer, *Neuronal MHC-I expression and its implications in synaptic function, axonal regeneration and Parkinson's and other brain diseases.* Front Neuroanat, 2014. **8**: p. 114.

96.   Tyler, C.M.a.B., L. M., *New Roles for MHC Class I Immune Molecules in the Healthy and Diseased Nervous System.* eLS, 2014.

97.   McAllister, A.K., *Major histocompatibility complex I in brain development and schizophrenia.* Biol Psychiatry, 2014. **75**(4): p. 262-8.

98.   Liberzon, A., et al., *Molecular signatures database (MSigDB) 3.0.*

Bioinformatics, 2011. **27**(12): p. 1739-40.

99.   Tak, H., et al., *Bimolecular fluorescence complementation; lighting-up tau-tau interaction in living cells.* PLoS One, 2013. **8**(12): p. e81682.

100.   Rahman, A., I. Grundke-Iqbal, and K. Iqbal, *PP2B isolated from human brain preferentially dephosphorylates Ser-262 and Ser-396 of the Alzheimer disease abnormally hyperphosphorylated tau.* J Neural Transm (Vienna), 2006. **113**(2): p. 219-30.

101.   Rahman, A., et al., *The excitotoxin quinolinic acid induces tau phosphorylation in human neurons.* PLoS One, 2009. **4**(7): p. e6344.

102.   Mychasiuk, R., et al., *A novel model of mild traumatic brain injury for juvenile rats.* J Vis Exp, 2014(94).

103.   Weber, J.T., *Altered calcium signaling following traumatic brain injury.* Front Pharmacol, 2012. **3**: p. 60.

104.   Chiocco, M.J., et al., *Fine mapping of calcineurin (PPP3CA) gene reveals novel alternative splicing patterns, association of 5'UTR trinucleotide repeat with addiction vulnerability, and differential isoform expression in Alzheimer's disease.* Subst Use Misuse, 2010. **45**(11): p. 1809-26.

105.   Braak, H., et al., *Occurrence of neuropil threads in the senile human brain and in Alzheimer's disease: a third location of paired helical filaments outside of neurofibrillary tangles and neuritic plaques.* Neurosci Lett, 1986. **65**(3): p. 351-5.

106.   Gabbita, S.P., et al., *Cleaved-tau: a biomarker of neuronal damage after traumatic brain injury.* J Neurotrauma, 2005. **22**(1): p. 83-94.

107.   Arun, P., et al., *Acute decrease in alkaline phosphatase after brain injury: A potential mechanism for tauopathy.* Neurosci Lett, 2015. **609**: p. 152-8.

108.   Thomsen, G.M., et al., *A model of recurrent concussion that leads to long-term motor deficits, CTE-like tauopathy and exacerbation of an ALS phenotype.* J Trauma Acute Care Surg, 2016. **81**(6): p. 1070-1079.

109.   Scholl, M., et al., *PET Imaging of Tau Deposition in the Aging Human Brain.* Neuron, 2016. **89**(5): p. 971-982.

110.   Braithwaite, S.P., et al., *Protein phosphatases and Alzheimer's disease.* Prog Mol Biol Transl Sci, 2012. **106**: p. 343-79.

111.   Gratuze, M., et al., *Tau hyperphosphorylation and deregulation of calcineurin in mouse models of Huntington's disease.* Hum Mol Genet, 2015. **24**(1): p. 86-99.

112.   Qian, W., et al., *Activation of protein phosphatase 2B and hyperphosphorylation of Tau in Alzheimer's disease.* J Alzheimers Dis, 2011. **23**(4): p. 617-27.

113.   Stein, T.D., et al., *Beta-amyloid deposition in chronic traumatic encephalopathy.* Acta Neuropathol, 2015. **130**(1): p. 21-34.

국문초록

외상성 뇌손상과 관련된
신경퇴행성질환들의
종합적인 전사체 분석 연구

서울대학교 대학원 의과학과 의과학전공

조 혜 선

만성외상성뇌병증 (CTE) 은 외상성 뇌손상 (TBI) 에 의해 나타나는 신경퇴행성질환으로 주로 복싱선수, 미식축구선수, 레슬링 선수 등에서 나타난다. 만성외상성뇌병증의 주요 증상으로는 두통, 기억상실, 공격성, 무관심, 불안, 우울증 등이 있다. 만성외상성뇌병증은 다른 신경퇴행성질환과 마찬가지로 아직까지 특별한 치료법이 없으며, 사후에 부검을 통해서만 진단이 가능하다. 그리고 만성외상성뇌병증을 유발하는 유전적 위험 요인에 대한 연구도 아직 미흡하다. 그래서, 만성외상성뇌병증의 분자유전학적 특성을 좀 더 이해하기 위해, 우리는 인간의 뇌 표본을 활용하여 전사체 분석을 수행하였다.

첫번째 연구에서는, 만성외상성뇌병증과 알츠하이머병을 비교 분석하였다. 만성외상성뇌병증은 알츠하이머병 (AD) 과 임상 양상이 매우 유사하다. 만성외상성뇌병증과 알츠하이머병은 과인산화된 타우단백질이 축적되어 있고 신경세포섬유매듭 (NFTs) 이 있다는 공통점이 있으며, 신경세포섬유매듭의 분포 경향이 다르다는 차이점이 있다. 그래서 만성외상성뇌병증과 알츠하이머병의 전사체 비교분석을 통해 만성외상성뇌병증의 특징을 보다 명확히 밝히려고 노력했다. 흥미롭게도, 시냅스 전달과 기억 기능에 관련된 유전자들의 변화가 만성외상성뇌병증과 알츠하이머병의 공통점으로 나타났으며, 그 중에서도 시냅토테그민 이라고 하는 시냅스에서 신호전달에 관여하는 유전자가 두드러지게 변화하였다. 그리고, 세포부착과 관련된 유전자의 변화는 만성외상성뇌병증에서만 나타나, 이것이 만성외상성뇌병증과 알츠하이머병의 차이점임을 알 수 있었다.

두번째 연구에서는, 외상성 뇌손상이 어떤 메커니즘에 의해 만성 외상성뇌병증으로 이어지는지 타우 단백질에 초점을 맞춰 연구하였다. 타우병증(Tauopathy) 은 만성외상성뇌병증과 알츠하이머병을 포함한 외상성 뇌손상과 관련된 신경퇴행성질환의 가장 주요한 병리학적 특징이다. 만성외상성뇌병증에서는 뉴런과

136

별아교 세포에 인산화된 타우 단백질이 불규칙적인 패턴으로 분포한다. 양전자방출 단층촬영술로 65 세 이상 사람들의 측두엽을 관찰한 결과, 대부분의 사람들이 타우병증을 가지고 있는 것으로 나타났다. 그러나, 어떤 분자적 메커니즘에 의해 타우 단백질이 신경퇴행성질환을 일으키는 지에 대해서는 아직 밝혀지지 않았다. 그래서 만성외상성뇌병증, 알츠하이머병의 유전자 발현 변화를 분석하였다. 단백질 인산가수분해효소 (PPs) 유전자들이 만성외상성뇌병증, 만성 외상성뇌병증/알츠하이머병 그리고 알츠하이머병에서 공통적으로 변화하였다. 그리고 생체 외 세포와 생체 내 동물 모델을 활용하여, 단백질 인산가수분해효소와 인산화된 타우단백질이 반대로 작용한다는 것을 확인하였다.

만성외상성뇌병증과 알츠하이머병의 공통적인 특징은 시냅스 전달과 기억 상실에 관여하는 유전자의 변화였으며, 만성외상성뇌병증만이 가지고 있는 특징은 세포부착과 리보솜과 관련된 유전자의 변화였다. 또한, 만성외상성뇌병증과 알츠하이머병에서 타우병증을 일으키는 원인 유전자는 단백질 인산가수분해효소였다. 이 두 연구를 통해, 만성외상성뇌병증과 알츠하이머병을 좀 더 이해할 수 있었으며, 이를 통해 신경 퇴행성 질환들의 새로운 진단 기준과 치료법을 찾을 수 있을 것이라고 기대한다.